Characterization of persister-cell derived ovarian cancer cells and methods for advanced 3D cell and tissue culture

Von der Fakultät für Energie-, Verfahrens- und Biotechnik der Universität Stuttgart
zur Erlangung der Würde eines
Doktors der Naturwissenschaften (Dr. rer. nat.) genehmigte Abhandlung

Vorgelegt von
Kathrin Böpple
aus Tübingen

Hauptberichter:	Professor Dr. Roland Kontermann
Mitberichter:	Professor Dr. Walter E. Aulitzky
Tag der mündlichen Prüfung:	24.02.2021

Dr. Margarete Fischer-Bosch-Institut
für klinische Pharmakologie Stuttgart und Universität Tübingen
und
Institut für Zellbiologie und Immunologie
der Universität Stuttgart
2021

Die vorliegende Dissertation wurde am Dr. Margarete Fischer-Bosch-Institut für klinische Pharmakologie und Universität Tübingen (Stuttgart) unter der Anleitung von Prof. Dr. Walter E. Aulitzky angefertigt. Teile der vorliegenden Arbeit wurden am Weizmann Institute of Science (Rehovot, Israel) unter der Betreuung von Prof. Dr. Moshe Oren erarbeitet. Die Promotion wurde durch ein Stipendium der Robert-Bosch-Stiftung gefördert.

Hiermit erkläre ich, dass ich die vorliegende Dissertation selbstständig und unter ausschließlicher Verwendung der angegebenen Hilfsmittel und der Ratschläge von jeweils namentlich aufgeführten Personen angefertigt habe.

Stuttgart, den 05.10.2020

Kathrin Böpple

Table of contents

Abbreviations

ABB	Annexin binding buffer	FL	floating
ATP	adenosine triphosphate	γH2AX	phospho-Histone H2A.X
BSA	bovine serum albumin	GMNN	Geminin
CAF	cancer-associated fibroblast	h	hour
CC3	cleaved caspase 3	HE	Hematoxylin and eosin
CD	cluster of differentiation	HEPES	4-(2-hydroxyethyl)-1-piperazineethanesulfonic acid
CDX	cell line-derived xenograft	HR	homologous recombination
3D	3 dimensional/dimensionality	Ig	immunoglobulin
DMEM	Dulbecco's Modified Eagle Medium	IHC	immunohistochemistry
DMSO	dimethylsulfoxide	IL	interleukin
DNA	deoxyribonucleic acid	kPa	kilo Pascal
DSB	double-strand break	m	meter
DTP	drug-tolerant persisters / persister cells	M	molar
EC_{50}	half-maximal effective concentration	MCL	mantle cell lymphoma
EDTA	ethylenediaminetetraacetic acid	MF	Millipore filter
EpCAM	epithelial cell adhesion molecule	min	minute
ER	endoplasmic reticulum	mRNA	messenger ribonucleic acid
FACS	fluorescence-activated cell sorter	MTT	(3-(4,5-Dimethylthiazol-2-yl)-2,5)-diphenyltetrazolium bromide
FBS	fetal bovine serum	MACS	magnetic cell separation
FFPE	Formalin-fixed Paraffin-embedded	MCL	mantle cell lymphoma
FITC	fluorescein isothiocyanate	MF	Millipore filter

NGS	Next-generation sequencing	RNA-seq	RNA sequencing
O_2	oxygen	ROS	reactive oxygen species
PAC	Perfused air culture	RPMI	Roswell Park Memorial Institute
PARPi	poly(ADP-ribose)polymerase inhibitors	RT	room temperature
PBS	phosphate-buffered saline	SD	standard deviation
PCA	principal component analysis	SF	surviving fraction
PCR	polymerase chain reaction	s	second
PE	plating efficiency	STR	short tandem repeats
PI	propidium iodide	TBST	TRIS-buffered saline with Tween 20
qPCR	quantitative real time polymerase chain reaction	TME	tumor microenvironment
qRT-PCR	quantitative real time polymerase chain reaction	TMRM	tetramethylrhodamine methyl ester perchlorate
RIN	RNA integrity number	v/v	volume/volume
RNA	ribonucleic acid	w/v	weight/volume

Summary

Ovarian cancer is often diagnosed at late stages due to a lack of prognostic markers. Successive cycles of chemotherapy give rise to so-called drug-tolerant persister cells (DTP) which play an integral role in the evolution of highly aggressive ovarian cancer, and also for dynamic, non-mutation-related drug resistance mechanisms. In the first part, the generated ovarian cancer DTP indicated filopodia-like structures on the cell surface and were compared to control cells without such structures. A significantly increased ER stress expression pattern, including *ATF3* was observed from the three most aggressive DTP clones when individual clones were studied. The patient survival data corroborated the finding that high *ATF3* expression was not beneficial for survival. It is known that *in vivo* tumor cells are mainly growing as 3D, the cell-cell communication and differentiated cellular function are more relevant in 3D systems. However, results in DTP were generated by using arbitrary cell lines and may not represent the *in vivo* situation. Therefore, the second project focused on the optimization and cultivation of advanced 3D cancer models including a 3D hydrogel-based model and a tissue slice model. To evaluate the influence of the cultivation methods on 3D cancer models, three different cultivation methods were tested for culturing the 3D cancer models: the floating (FL), the Millipore filter (MF) and the novel perfusion air culture (PAC) systems. For the 3D hydrogel-based model, alginate showed a better property than agarose on the handling process and the cultivation systems influenced the cell viability and proliferation. Precision-cut tumor tissue slices from solid tumors containing native tumor microenvironment were cultured in MF and PAC system and further investigated for the anti-cancer drug efficiency. Tissue slices from cell line-derived xenografts (CDX) and human ovarian cancer were cultured and compared to their *in vivo* origin tissues using immunohistochemistry for morphology, proliferation, DNA damage, apoptosis, and gene expression of p53- and stress-related genes. With the PAC system, the viability and morphology of the tissue slices were preserved for more than 7 days and the intra-slice gradients in MF system were avoided. In these systems, the detection of cytokines from culture medium and analysis of single cell viability of dissociated tissue slices were possible.

In conclusion, the results of the first part of this work revealed an ER stress-related phenotype of DTP-derived clones, exemplified by *ATF3*, which was associated with the aggressiveness of ovarian cancer and might be a potential biomarker in the future. In the second part of this work, methods were established to use 3D hydrogel-based models and the tumor tissue slice as a powerful platform to perform patient specific tests and thus allow personalized therapy adaption.

Zusammenfassung

Ovarialkarzinome werden aufgrund fehlender prognostischer Marker meist erst in späten Stadien diagnostiziert. In aufeinanderfolgenden Zyklen der Chemotherapie entstehen so genannte arzneimitteltolerante, persistente Zellen (DTP), die eine Schlüsselrolle bei der Entstehung hochaggressiver Ovarialkarzinome und auch bei dynamischen, nicht-mutationsbedingten Arzneimittelresistenzmechanismen spielen. Im ersten Teil zeigten die erzeugten Ovarialkarzinom-DTP Filopodien-ähnliche Strukturen auf der Zelloberfläche und wurden mit Kontrollzellen ohne solche Strukturen verglichen. Bei den drei aggressivsten DTP-Klonen wurde bei der Untersuchung der einzelnen Klone ein signifikant erhöhtes Endoplasmatisches Retikulum (ER)-Stress-Expressionsmuster, einschließlich *ATF3*, beobachtet. Die Überlebensdaten der Patientinnen bestätigten den Befund, dass eine hohe *ATF3*-Expression nicht überlebensfördernd war. Es ist bekannt, dass *in vivo*-Tumorzellen hauptsächlich in 3D wachsen, wobei die Zell-Zell-Kommunikation und die differenzierte zelluläre Funktion in den 3D-Systemen von großer Bedeutung sind. Die Ergebnisse in DTP wurden jedoch unter Verwendung beliebiger Zelllinien generiert und entsprechen möglicherweise nicht der *in vivo*-Situation. Daher konzentrierte sich das zweite Projekt auf die Optimierung und Kultivierung von fortgeschrittenen 3D-Krebsmodellen, darunter ein 3D-Hydrogel-basiertes Modell und ein Gewebeschnittmodell. Um den Einfluss der Kultivierungsmethoden auf die 3D-Krebsmodelle zu evaluieren, wurden drei verschiedene Kultivierungsmethoden getestet, nämlich das Floating (FL)-, das Millipore-Filter (MF)- und das neuartige Perfusions-Luft-Kultur (PAC)-System. Für das 3D-Hydrogel-basierte Modell zeigte Alginat bessere Eigenschaften als Agarose bezüglich des Handhabungsprozesses und die Kultivierungssysteme beeinflussten die Zellviabilität und -proliferation. Präzisionsgeschnittene Tumorgewebeschnitte aus soliden Tumoren mit nativer Tumormikroumgebung wurden im MF- und PAC-System kultiviert und weiter auf die Wirksamkeit von Krebsmedikamenten untersucht. Gewebeschnitte von zelllinienentwickelten Xenotransplantaten (CDX) und menschlichem Ovarialkarzinom wurden kultiviert und mit ihren *in vivo*-Ursprungsgeweben verglichen, wobei immunhistochemische Untersuchungen zur Morphologie, Proliferation, DNA-Schädigung, Apoptose und Genexpression von p53- und stressverwandten Genen durchgeführt wurden. Mit dem PAC-System wurden die Lebensfähigkeit und Morphologie der Gewebeschnitte für mehr als 7 Tage erhalten und die Intra-Slice-Gradienten im MF-System vermieden. In diesen Systemen war der Nachweis von Zytokinen aus dem

Kulturmedium und die Analyse der Einzelzell-Lebensfähigkeit von dissoziierten Gewebeschnitten ebenfalls möglich.

Zusammenfassend lässt sich sagen, dass die Ergebnisse des ersten Teils dieser Arbeit einen ER-Stress-bezogenen Phänotyp von DTP-abgeleiteten Klonen zeigten, am Beispiel *ATF3*, der mit der Aggressivität des Ovarialkarzinoms assoziiert war und in Zukunft ein potenzieller Biomarker sein könnte. Im zweiten Teil dieser Arbeit wurden Methoden etabliert, um 3D-Hydrogel-basierte Modelle und den Tumorgewebsschnitt als leistungsfähige Plattformen für die Durchführung patientenspezifischer Tests zu nutzen und so eine personalisierte Therapieanpassung zu ermöglichen.

1 Introduction

1.1 Cancer

The Center for Cancer Registry Data in Germany estimated 233,570 new cases of malignant neoplasms including lymphomas and leukemias in women and 258,520 in men in 2019, with a relative 5-year survival rate of 65% (women) versus 59% (men) (Robert Koch-Institute, 2019). The US National Center for Health Statistics published in 2019 891,480 new cancer cases in women and 870,970 new cases in men (Siegel et al., 2019). Since the number of inhabitants in the US is about 4 times higher than in Germany, the rate of new cancer cases in women is similar and a slightly lower rate for US men results. In women, the most common malignant neoplasm is breast cancer, while in men prostate cancer is most frequent. The second and third most frequent cancer types, irrespective of gender, are lung and colon cancer. In the biomedical database Pubmed (https://pubmed.ncbi.nlm.nih.gov/) in 2016, more than 16% annual entries (out of >26 million total entries) dealt with cancer, compared to 6% in 1950 (Reyes-Aldasoro, 2017), supporting the assumption that the interest in cancer research has increased.

Although malignant neoplasms can originate from almost any cell type (except non-dividing cells, such as erythrocytes) in any organ of the body, most commonly, epithelia give rise to the development of cancer. Approximately 70% of these malignant neoplasms develop in glandular tissue and are called adenocarcinomas. A further 15% are squamous cell carcinomas, malignant tumors of the transitional epithelium (urothelial carcinomas) and small cell carcinomas of the lung. The remaining entities are constituted by e.g. leukemia and lymphoma that develop in the hematopoietic bone marrow and lymphatic tissue. Also, malignant tumors can originate in the connective and supporting tissue (such as sarcomas), in the supporting cells of the nervous system (gliomas) or the pigment-forming cells (melanomas) (Robert Koch-Institute, 2019).

Technical innovations, i.e. primarily next-generation sequencing (NGS), and the resulting decline of costs for DNA sequencing allowed the analysis of a high number of tumor samples and the identification of a vast number of mutations in various cancer entities. Researchers have started to identify so-called driver mutations that underlie the development of cancer (Tomasetti et al., 2015). Mutations either are germline

inherited or occur somatically. Germline mutations can be passed to some or all offspring, while somatic mutations are not inherited. Commonly, driver mutation in tumors affect the regulation of cell survival, cell fate, and genome (Vogelstein et al., 2013).

Three types of driver mutations, i.e. a mutation that provides the cell with a selective growth advantage (Haber, Settleman, 2007), are described: i) Proto-oncogene mutations result in the activation of oncogenes, ii) mutations of tumor suppressor genes, and iii) non-coding driver mutations that alter cis-regulatory elements, for example by removing transcription factor binding sites (Poulos, Wong, 2019). Proto-oncogenes, such as *MYC* (Evan et al., 1985) and *FOS* (Sassone-Corsi et al., 1988), become oncogenes due to a mutation in the regulatory area of gene expression. Alternatively, mutations in coding regions can alter the protein function, as observed in *RAS* mutated cells (Bos, 1989). Oncogenes are causally involved in the pathogenesis of malignant neoplasia, which leads to cancer (Evan et al., 1985).

Tumor suppressor genes, especially the prototypic representative *TP53*, often carry driver mutations. Due to its important functions in maintaining genomic integrity, the gene product of TP53, the tumor suppressor protein p53, is known as the “guardian of the genome“ (Lane, 1992). The protein p53 accumulates in response to cell-damaging processes such as oncogene activation, DNA damage or oxidative stress (Aylon, Oren, 2007) resulting in cell cycle arrest or apoptosis of the cell. Various proteins that detect these cellular stresses transmit the information to p53 (Riley et al., 2008) and these mechanisms ultimately prevent damaged cells from passing their tumorigenic capacity to daughter cells. Initially, transient cell cycle arrest allows repair mechanisms to remove DNA-damage and re-instate proper cellular function (Vousden, Prives, 2009). Since p53 is a transcription factor, the regulation of the processes takes place mainly at the transcriptional level. Although it should be noted that p53 additionally has transcription-independent functions, such as induction of autophagy (Green, Kroemer, 2009, Riley et al., 2008). Overexpression of a p53 mutant that is missing most of the DNA binding domain and completely lacks the transactivation function, still induces apoptosis (Haupt et al., 1995). Furthermore, it was found that activation of p53 induces apoptosis even in cells lacking a nucleus (Chipuk et al., 2003). These observations support the idea that a cytoplasmic pool of p53 can induce apoptosis via a transactivation-independent mechanism (Green, Kroemer, 2009).

In breast cancer, mutations of the genes *BRCA1* (breast cancer 1) and *BRCA2* have been identified as driver mutations. BRCA proteins are importantly involved in DNA damage repair (Venkitaraman, 2002). Loss of function mutations of BRCA1 and BRCA2 result in chromosomal instability due to improper DNA double-strand break repair (Venkitaraman, 2002). *BRCA1* and *BRCA2* has been described as responsible for the occurrence of breast and ovarian cancer, and cumulate in families due to hereditary germline mutations (Bouwman et al., 2010).

1.1.1 Ovarian cancer

Ovarian cancer is estimated to be the fifth most deadly cancer in women in the USA in 2019. It has the fourth highest incidence of approximately 62,000 new gynecological cases and nearly 14,000 annual ovarian cancer deaths (Siegel et al., 2019). Ovarian cancer is also in Germany the fifth most common and deadly cancer in women which causes more than 7,000 new cases and 5,000 annual deaths and the 5-year-survival rate is 43% (Robert Koch-Institute, 2019). Of the 5 different ovarian cancer subtypes i) endometrioid, ii) mucosal, iii) clear cell, iv) low-grade and v) high-grade serous ovarian cancer (HGSOC), the latter is most frequent and usually diagnosed at advanced stage (Torre et al., 2018). Reasons for late diagnosis of ovarian cancer are that the symptoms are non-specific and more likely emerge in late stages of the disease. Furthermore, there is a lack of reliable diagnostic options, as in the case of the biomarker CA125, which has a low specificity and sensitivity (Sölétormos et al., 2016). Prognostic biomarkers relate to a measurement variable (e.g. gene expression) that is associated with the likely cancer outcome (Ballman, 2015).

Studies propose that ovarian cancer originates from cells of the ovarian surface epithelium (Bell, 2005, Feeley, Wells, 2001, Scully, 1995) or the serous tubular intra-epithelium that emerges in the distal fallopian epithelium (Crum et al., 2007, Kurman, Shih, 2010, Tone et al., 2012). The original tissue that gives rise to ovarian cancer is not yet been conclusively identified.

Ovarian cancer diagnosis in the late stage as well as in relapse is very often associated with tumor cell invasion into adjacent tissue and metastases formation, which are accepted hallmarks of cancer. Further hallmarks of cancer are dysregulation of proliferation, DNA repair, angiogenesis, and apoptosis. These aberrations and genome instability promote tumor development and accumulate in cancer cells. Cancer cells

can have a variety of genetic alterations that promote the progression of cancer (Hanahan, Weinberg, 2011).

With a proportion of 96%, nearly all HGSOC share a mutation of the tumor suppressor p53, which leads to uncontrolled cell proliferation and reduced apoptosis (Bell, 2011, Patch et al., 2015). The p53 mutation can occur dichotomously. On the one hand, a point mutation in the DNA binding domain leads to loss of the tumor suppressor function (Bouaoun et al., 2016, Olivier et al., 2010), and on the other hand, in certain cases, tumor progression can be supported, which is referred to as gain of function (Weisz et al., 2007). It is also known that mutations in the genes *BRCA1* and *BRCA2* can occur in HGSOC (Bell, 2011). This was especially shown in several publications in the case with inherited HGSOC (Friedman et al., 1994, King et al., 2003, Miki et al., 1994, Wooster et al., 1995).

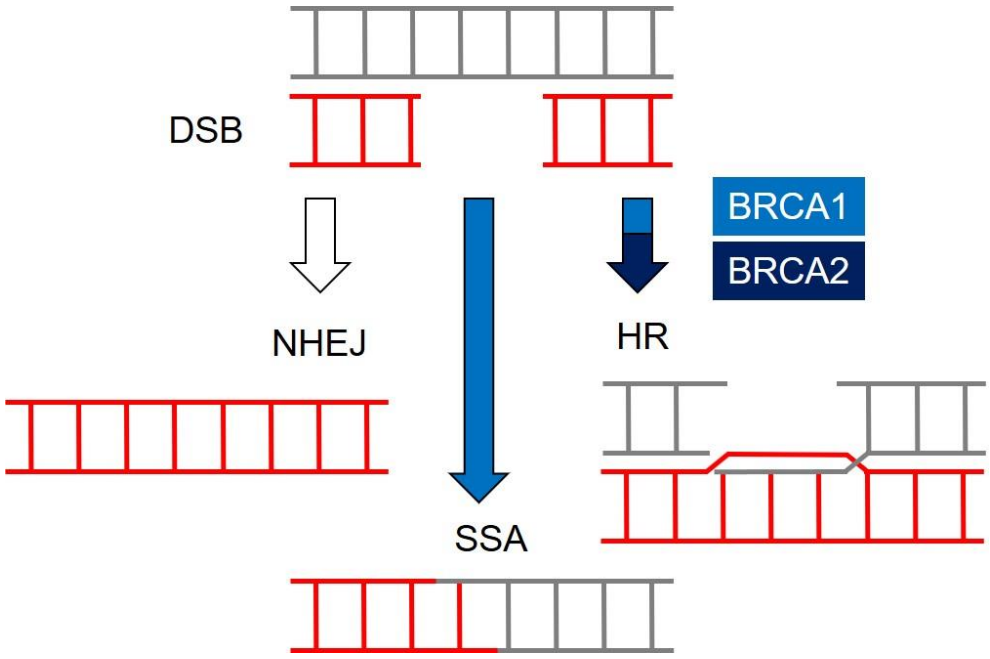

Figure 1: ***Schematic illustration of DNA repair mechanisms for double-strand breaks (DSB).*** *Non-homologous end-joining (NHEJ), single-strand annealing (SSA) and homologous recombination (HR) are illustrated. Due to loss of function mutation of BRCA1 or BRCA2, the mechanisms of HR are no longer effective. BRCA1 deficiency results in additional disturbed SSA. (Adapted from (Venkitaraman, 2002))*

DNA double-strand breaks (DBS) are normally corrected by the DNA damage repair machinery. The BRCA genes are involved in DNA repair by homologous recombination (HR) (Aymard et al., 2014, Moynahan, Jasin, 2010) (Figure 1). Including HR, the five most common DNA repair pathways - base excision repair, nucleotide excision repair, mismatch repair, non-homologous end joining - become active depending on the type

of damage and enable DNA damage to be repaired in a normal cell (Chatterjee, Walker, 2017). Mutations of the BRCA genes often lead to loss of function, leading to dysfunctional DNA repair and therefore the risk of developing ovarian cancer increases to 40% for mutations in BRCA1 and 11-18% in case of BRCA2 mutations (Antoniou et al., 2003, Chen, Parmigiani, 2007).

1.1.1.1 *Ovarian Cancer Therapy*

In ovarian cancer, no uniform drug target has been identified. Thus, the standard therapy for ovarian tumors is radical resection and platinum-based chemotherapy with cisplatin or carboplatin, which can be supplemented by the administration of taxane. However, after an initial response to chemotherapy tumor relapse is frequent in ovarian cancer. A major step towards a more successful therapy was achieved by using poly(ADP-ribose)polymerase inhibitors (PARPi) that are described as promising treatment option for BRCA-mutation-associated ovarian cancer (Bryant et al., 2005, Farmer et al., 2005): DSB are normally efficiently repaired by HR, which is a DNA damage repair strategy of the cell that affects both DNA strands (Wright et al., 2018). Damage is signaled by the recruitment and activation of ATM or ATR protein kinases. This is followed by phosphorylation of various proteins, such as BRCA1 and BRCA2, which causes cell cycle arrest and induces DSB repair. (Andreassen et al., 2006, Bernstein, 2002). Loss of the wild-type BRCA1 or BRCA2 allele in tumors promotes cancer progression by enhancing genome instability and gene mutation (Gudmundsdottir, Ashworth, 2006). Thus, in tumor cells carrying BRCA mutation, PARPi further decrease DNA damage repair and therefore cells show increased cell death (Bowman et al., 1998, Tentori, Graziani, 2005). The U.S. Food and Drug Administration approved the prescription of the PARPi Olaparib (AZD2281) (Kim et al., 2015) in 2015 and Niraparib (MK-4827) (Ison et al., 2018) in 2017.

1.1.1.2 *Chemopersistence versus chemoresistance*

Patients with ovarian cancer often suffer from metastasis and develop a highly aggressive and non-responsive recurrence of ovarian cancer. A source for recurrent HGSOC cancer are drug-tolerant persister cells (DTP) that appear at the beginning of treatment and develop into resistant cells during therapy. Originally, persistence was described in the context of microbiology as the survival of bacteria in the presence of penicillin (Bigger, 1944). Currently, it is described that persistent cells randomly arise

from stochastic events. Stochasticity provides the cells with an advantage by allowing flexible adaptation to a changing environment. This is also seen in dormant and non-dividing subpopulations (Kaern et al., 2005, Lewis, 2007, 2010). The concept of persistence was applied to further biological domains: Fungi (LaFleur et al., 2006) and infectious diseases (Lewis, 2007). Not surprisingly, “persistence” is also applicable to cancer cells. Here, persistence describes a non-mutational, dynamic mechanism of survival in the presence of anti-cancer drugs that protects the cancer cell population (Sharma et al., 2010).

In contrast to persistence, therapy resistance in ovarian cancer can be intrinsic, e.g. germline mutations leading to inherited protection of the tumor cells, or acquired resistance during drug treatment (Abdullah, Chow, 2013, Ling et al., 2005, Tapia, Diaz-Padill, 2013). An example of intrinsic resistance is the upregulation of drug efflux pumps that prevents efficient toxification of the tumor cells (Gottesman, Pastan, 2015). A decreased drug concentration in tumor cells may also be caused by poor vascularization (Saggar et al., 2013). Besides, the interacting cells of the tumor microenvironment, e.g. cancer-associated fibroblasts (CAF), can support the proliferation and survival of cancer and thereby promote drug resistance (Straussman et al., 2012). These intrinsic resistance mechanisms crucially affect the initial therapy response and influence later outcomes of therapy. Acquired resistance develops through the adaption and survival advantage of individual tumor cells. For instance, gene expression can increase anti-apoptotic signaling, e.g. BCL-2, BCL-XL, MCL-1 expression, and thereby suppress apoptosis (Gottesman, 2002).

In many types of cancer, DTP are present with a very low frequency but accumulate during successive therapeutic episodes. Mutational intra-tumoral heterogeneity is provoked by the chemotherapeutic intervention (Gerlinger et al., 2012) as well as the development of different drug tolerance mechanisms (Ramirez et al., 2016). From small and probably temporarily drug-tolerant populations of the cell lineage at the beginning of therapy, therapy-resistant tumor cells eventually develop (Ramirez et al., 2016). To prevent recurrence and to cure ovarian cancer, eradication of these DTP is prerequisite and therefore the characterization of DTP is essential. Novel and appropriate cancer cells models are required to characterize DTP in individual tumors. To mimic the situation that is actually happening in the tumor, 3D models are useful tools.

1.2 Advanced 3D cancer models

For pre-clinical models, reproducible and transferable results have the highest priority. In cancer research, the aim has been to understand the diseases as closely as possible to the patient and to test new promising active substances. It is therefore essential that the results of *in vitro* experiments are generated in pre-clinical models that reflect the *in vivo* situation in patients. Only if the results can be translated in humans, or if the investigated mechanisms operate in the same way, conclusions can be drawn (Kamb, 2005). For decades, 2D culture as monolayer of transformed cell lines has been used for this purpose (Figure 2A). Cell culture has existed since the 1950s and has been used to study promising active substances. At that time, cells were cultivated on glass with pasteurized medium (Eagle, Foley, 1958, Hirschberg, 1958). However, the correlation of *in vitro* results to *in vivo* data from mouse experiments and clinical results was not conclusive. In the past, this was seen as a chance to compare the various models (Hirschberg, 1958). The current gold standard is cell culture in disposable cell culture flasks or Petri dish made of plastic with a special cell culture surface treatment for adherent cells. Co-culture of two or more cell types and studying the cell communication between them is also possible in 2D cell systems.

Alternative models are necessary to find sophisticated solutions and to imitate the heterogeneous 3D tumor microenvironment in the best possible way. It is well known that *in vivo* tumor cells are mainly growing as three-dimensional in extracellular matrix (ECM) which consists of a complex fibrous meshwork. Therefore, 3D systems are biologically more relevant. Until nowadays, many *in vitro* 3D cancer models have been used for pharmacology and cancer cell biology (Hickman et al., 2014). Several different techniques have been developed for construction of 3D cancer models. They can mainly be classified into three categories: spheroids, 3D hydrogel/matrix and tissue slice.

Aggregated cells of cell lines are often cultured as spheroids (Figure 2B). This technique prevents attachment of the cells to the cell culture vessel surface by means of a special non-adherent surface coat (e.g. poly-HEMA), round bottom wells in a 96-well format (Friedrich et al., 2009, Lee et al., 2013, Vinci et al., 2012) or as “hanging drops” (Kelm et al., 2003) (Figure 2B). The aggregated cells secrete components of the extracellular matrix and can upregulate proteins that mediate cell-cell interactions, such as the adhesion protein E-CADHERIN, thus creating tight cell-cell contacts in many cell types (Lin et al., 2008).

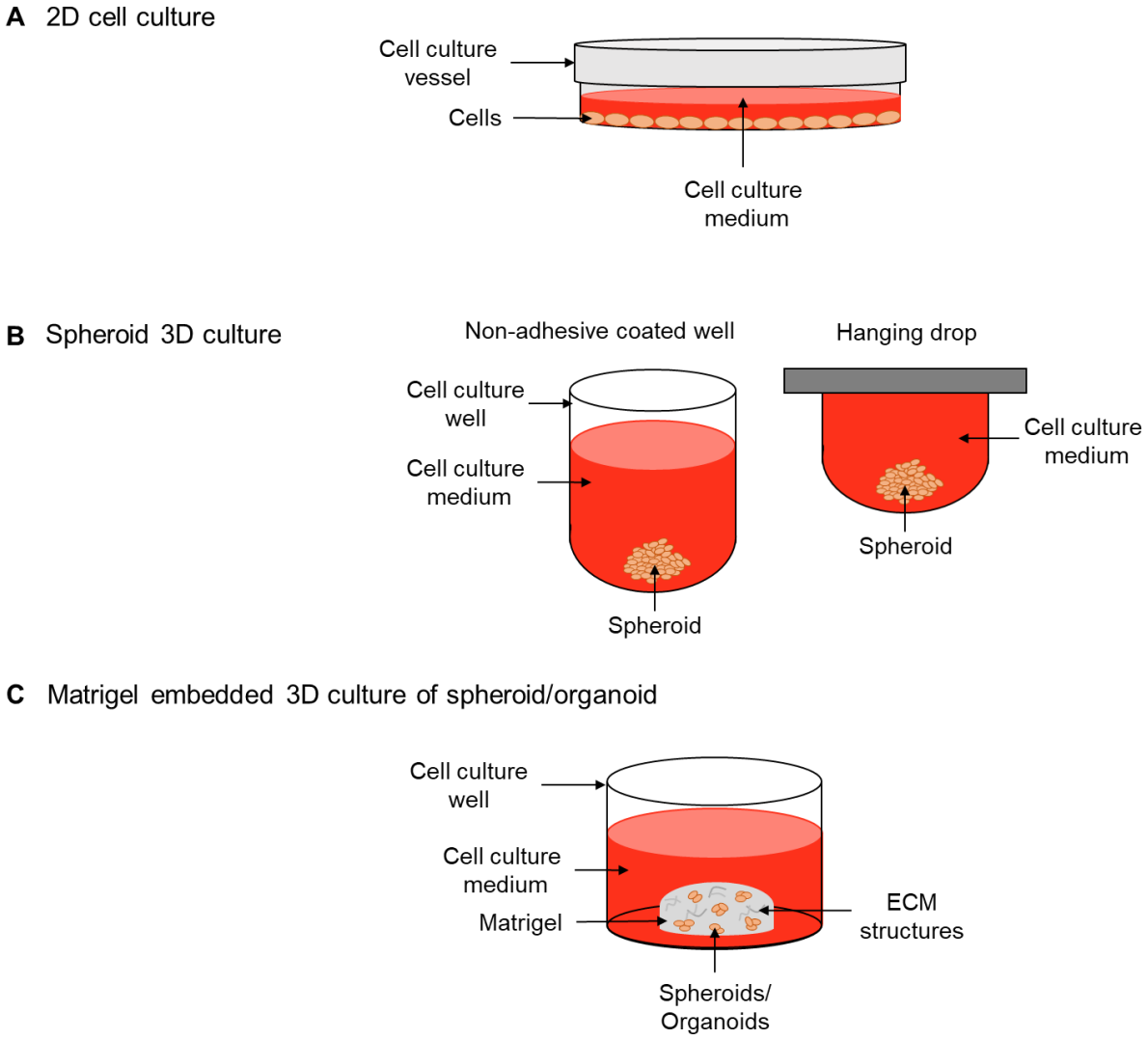

Figure 2: ***Schematic illustration of cell culture in vitro methods****. (A) 2D monolayer cell culture of adherent cells growing on the surface of cell culture vessel. (B) 3D culture of spheroids in a non-adhesive coated well or as hanging drop. (C) Cell line cells or isolated tumor cells from primary tissue are cultured in Matrigel as spheroids or patient-derived organoids. Cells embedded in Matrigel are covered by cell culture medium growing in a well of a microtiter plate.*

These solid 3D spheroids have a gradient, with higher proliferation, higher oxygen content and better nutrient supply in outer areas (Kunz-Schughart, 1999, Lee et al., 2013, Lin et al., 2006, Vinci et al., 2012). Interestingly, these features are similar to those of small metastases and vascularized regions of larger solid tumors (Sutherland, 1988).

However, physiology of cell lines is less similar to patient derived primary cells that are cultured directly after surgery. In addition, cell lines lack the stroma cells and the microenvironment surrounding. In addition to its supporting function, the extracellular matrix (ECM) plays an essential role in the differentiation and preservation of tissues.

It further provides drug resistance and survival signals in cancer (Correia, Bissell, 2012). Therefore, the techniques of 3D hydrogel/matrix containing biomaterial to embed spheroids or cells into the hydrogel or matrix and form the 3D structure of the tumor ECM, were developed very fast in recent years.

1.2.1 Cell culture in hydrogels/matrix

Many methods have been developed to form 3D tumor models using hydrogel, for example encapsulating cells in agarose or alginate hydrogel droplets/beads, organoid culture in Matrigel (Sato et al., 2011) and the most advanced 3D printing technology.

1.2.1.1 *Encapsulating cells in agarose or alginate hydrogels*

Commonly used hydrogels to embed cells are agarose (Dimicco et al., 2007, Dupuy et al., 1988, Smith et al., 2011) and alginate (Cai et al., 1988, Clayton et al., 1991).
Agarose is a polysaccharide obtained from red seaweed (Jeppsson et al., 1979). It is a thermally reversible hydrogel, but in cell culture the thermal requirements for gel formation are higher than the temperature the cells could withstand. By heating up to 90°C, a polymer solution can be formed from an agarose gel. Low melting agarose has a melting point of <66°C, which is nevertheless too warm for cells. The gelation takes place during cooling down to room temperature. Therefore, embedding of cells in agarose is irreversibly. This linear polymer consists of the repeating unit of agarobiose, consisting of a disaccharide of D-galactose and 3,6-anhydro-L-galactose (Figure 3) (Jeppsson et al., 1979).

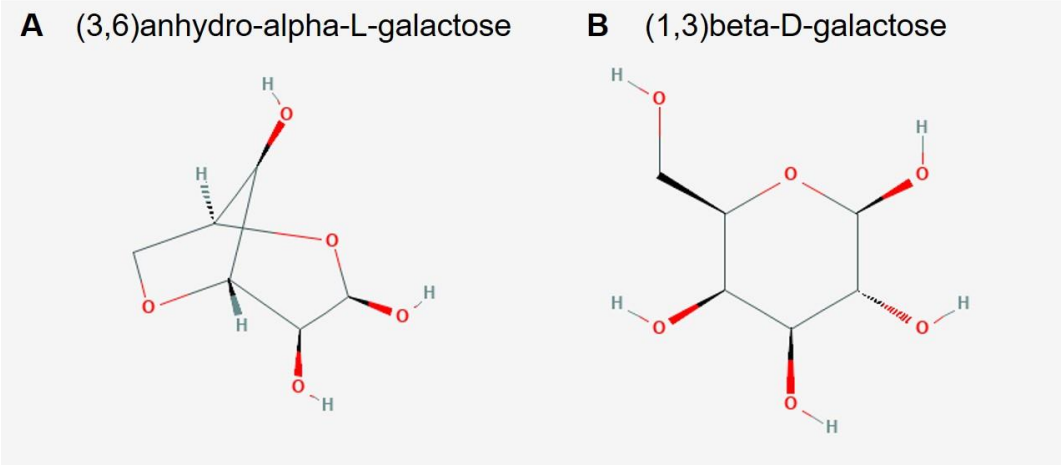

Figure 3: ***Chemical structure depiction of anhydro-alpha-L-galactose and beta-D-galactose****. (Adapted from (National Center for Biotechnology Information, National Center for Biotechnology Information))*

Agarose is used in biomedical research, especially in cell culture systems, due to its many useful properties: It is generally bioinert, does not adsorb to proteins or adhere to cells, it can be easily functionalized with cell adhesion or other signaling molecules, and its mechanical properties can be adjusted by varying the agarose concentration (Agudelo et al., 2009, Iwata et al., 1994, Kumachev et al., 2011, Lahooti, Sefton, 2000, Pelaez et al., 2009). Agarose is a suitable material for cell culture, but it is not biodegradable under physiological conditions (Hunt, Grover, 2010, Pelaez et al., 2009). This limits its applications, for example as a scaffolding material in tissue engineering, because the material should degrade over short time to make room for newly formed tissue (Hunt, Grover, 2010).

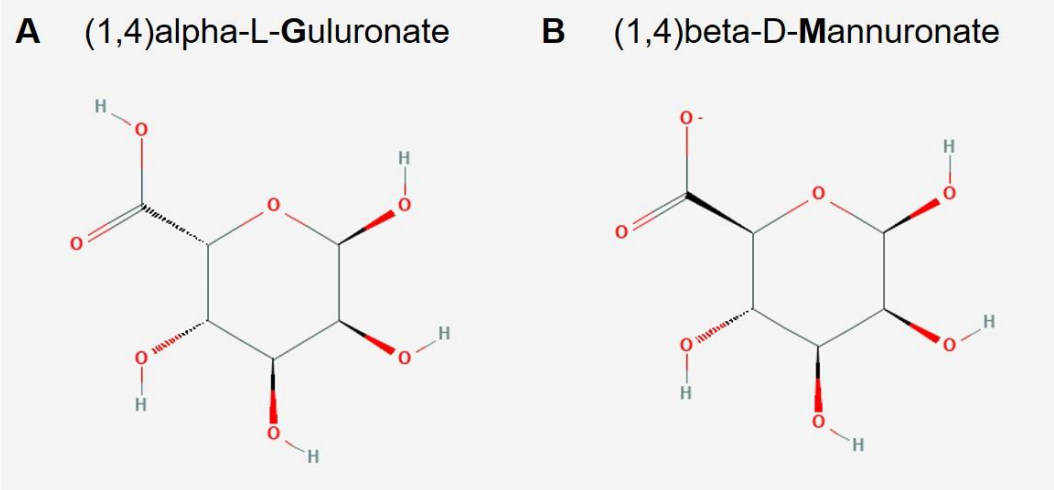

Figure 4: ***Chemical structure depiction of alpha-L-Guluronate (G) and beta-D-Mannuronate (M)****. (Adapted from (National Center for Biotechnology Information, National Center for Biotechnology Information))*

Alginate is extracted from brown algae and is a water-soluble biopolymer. This polysaccharide consists of two uronate sugars, which are converted at harvest into linear copolymers containing blocks of (1,4)alpha-L-guluronate (G) and (1,4)beta-D-mannuronate (M) residues (Figure 4). The G-blocks participate in intermolecular cross-linking with divalent cations (except Mg^{2+}) and junction zones are formed, leading to gelation. Since G-blocks are the key structural elements in the alginate hydrogels, the M/G block ratio, the G-block length, content and molecular weight are the critical factors that influence the properties of alginate hydrogels (Lee, Mooney, 2012). The affinity for divalent cations of alginates increase as $Ca^{2+}<Sr^{2+}<Ba^{2+}$ (Andersen et al., 2015). Type and amount of gel forming ion influences the properties of the resulting hydrogel, therefore this can be utilized to optimize elasticity, swelling and stability. The

cross-linked alginate hydrogel can be dissolved by exchange of divalent for monovalent cations such as sodium ions (Andersen et al., 2015, Lee, Mooney, 2012). This facilitates the release and analysis of embedded cells after cultivation in contrast to cultivation with agarose.

1.2.1.2 *Organoids culture in Matrigel*

A further 3D culture method that adds ECM properties to the culture system, is the cell culture in Matrigel (Figure 2C). Matrigel is a LAMININ-rich basement membrane extract from mice (Kibbey, 1994). The basement membrane connects epithelial, endothelial, fat, and smooth muscle cells (Benton et al., 2011). Matrigel is biologically highly active, promotes cell differentiation (Kleinman, Martin, 2005) and is used to measure the invasiveness of tumor cells (Even-Ram, Yamada, 2005, Hotary et al., 2006). Its *in vivo* application is often applied to examine angiogenic inhibitors and stimulators, to repair damaged tissue and to increase tumor growth (Kleinman, Martin, 2005). Matrigel culture has become a widely applied technique in recent years by the culture of patient-derived organoids (Figure 2C). It was established in 2009 using mouse stem cells from intestine in the Clever's Lab (Sato et al., 2009). One or a few cells from a tissue are embedded in Matrigel and covered with cell culture medium with the addition of various growth factors (e.g. Noggin, R-spondin). The intestine stem cells grow in a 3D orientation and build crypt and villi-like structures by cell differentiation, similar to the *in vivo* situation in mouse intestines. Furthermore, organoids were successfully generated from normal and colon cancer patient tissue and *ex vivo* expanded in long-term (Sato et al., 2011), representing a useful tool and providing a variety of applications of personalized medicine (Takahashi, 2019). Besides cancer, organoid models have been established for e.g. liver (Sugimoto et al., 2005), lung (Wu et al., 2011) and gastrointestinal tract diseases (Barker et al., 2010, Sato et al., 2009, Sato et al., 2011). This reflects the wide range of applications of this 3D model. Organoids enable high-throughput screening of a large number of anti-cancer drugs and evaluation via common *in vitro* assays or sequencing (Czerniecki et al., 2018, Hou et al., 2018). A notable limitation of the organoid system is the lack of the tumor microenvironment (TME), as co-culture is only possible after the addition of cells (Neal et al., 2018, Yuki et al., 2020). Today, it is possible to choose from more than 1000 established and characterized organoid cultures, e.g. at the HUB Organoid Biobank,

representing different organs and disease models and acquire them commercially (HUB Organoids).

1.2.1.3 *3D printing technology*

The encapsulated alginate beads or organoid Matrigel culture are limited with the shape and format of the 3D structure of the model. This limitation can be overcome by 3D print technique. 3D printing, also called additive manufacturing is a technique which was developed very fast in the last years. The term "3D printing" can be used to cover a broad range of computer-controlled processes in which materials are applied, combined or solidified to generate 3D objects (Hinton et al., 2015), by joining materials together layer after layer (e.g. fusing liquids or powder particles).

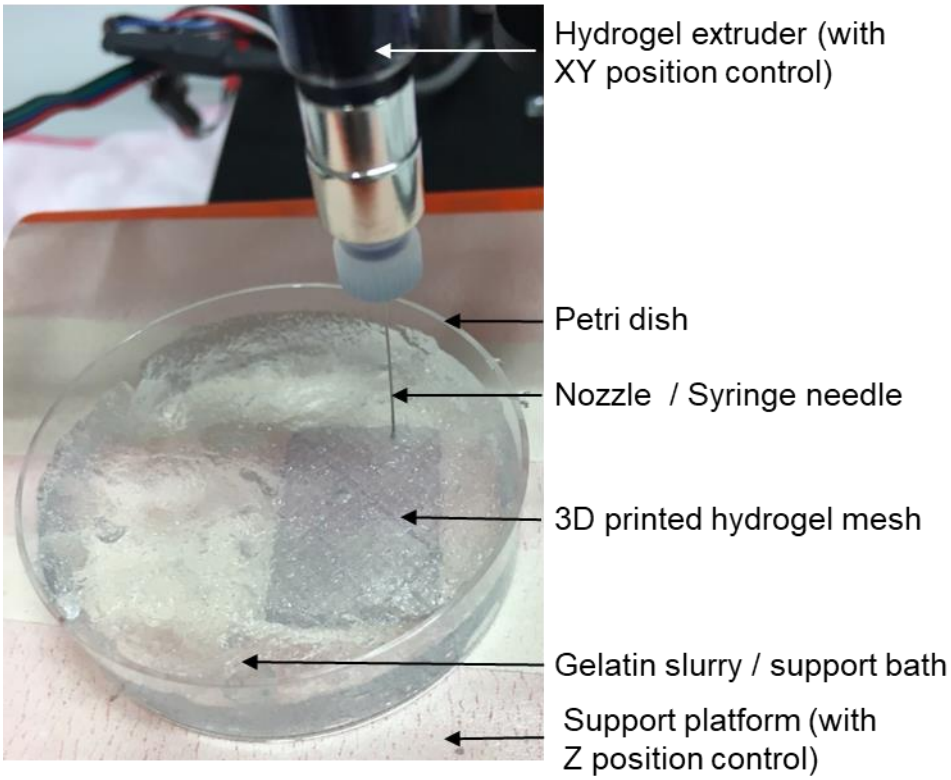

Figure 5: ***Hydrogel mesh printing using a 3D printer.*** *Printing of hydrogel in a gelatin slurry support bath to maintain structure and prevent collapsing of the 3D object.*

Different materials can be used for 3D printing including biomaterials such as hydrogels. Current approaches for the 3D printing of biological hydrogels have achieved important advances. Using conventional manufacturing approaches, soft protein and polysaccharide hydrogels are difficult to produce. To avoid collapsing of these soft structures during the printing process, the hydrogels can be printed between

a support bath that enables to maintain the 3D orientation (Figure 5). This process is called reversible free-form embedding of suspended hydrogels (Hinton et al., 2015). It enables 3D printing of hydrated materials, e.g. alginate, collagen and fibrin, with a modulus of elasticity <500 kPa. The hydrogel structures are built as filaments layer after layer and fused with adjacent filaments to form the 3D print structures. In recent years, 3D bioprinting of hydrogels together with cells have been used to form *in vitro* tumor models. Mostly a grid structure with or without cells was manufactured in a layer-by-layer manner (Zhao et al., 2014).

1.2.2 Tissue slices as 3D *ex vivo* cultivation model

A further step to approach the complexity of 3D cancer models are tissue slices from mouse xenograft or patient tumor tissue. In addition to the 3D structure, this model contains the patient-specific tumor microenvironment. Solid tumors are precision-cut into slices and cultivated in appropriate systems. As early as the 1920s, "organotypic tissue sections" were cultivated, long before the first immortalized cell lines were used in the laboratory. The metabolism of carcinomas from rats and humans were investigated (Warburg, 1923, Warburg et al., 1924). In further studies, human tumors were cultivated in cell culture medium surrogate solutions (Röller et al., 1966) or in “hanging drops” (Kredel, 1928). The aim of this and various more studies was to investigate and predict the response to therapy, as it is often mentioned today under the name "personalized medicine". However, after the well-known HeLa cell line was established in 1952 (Gey et al., 1952), research has mainly focused on immortalized cell lines. Still, cell lines represent the most intensively studied model system of basic cancer research in the world.

Tissue slice culture became popular again after the development of high-precision tissue cutting devices (Krumdieck et al., 1980). With these devices, slices of constant thickness can be cut thus improving reproducibility of the tissue slice experiments.

Studies in recent decades have investigated precision-cut tumor tissue slices of patient tumors from breast (Holliday et al., 2013, Milani et al., 2010, Mira-y-Lopez, Ossowski, 1990, Séveno et al., 2012, Sonnenberg et al., 2008, van der Kuip et al., 2006), lung (Dong et al., 2011, Schmid et al., 2012, Vaira et al., 2010), brain (Liu et al., 2011, Merz et al., 2010), ovaries (Estes et al., 2007, Meijer et al., 2013), cervix (Kendrick et al., 2008), kidney (Weissinger et al., 2013) and prostate (Kiviharju-af Hällström et al., 2007). Tumor tissue slices were primarily used to analyze the general drug response

to e.g. cytotoxic chemotherapeutic agents (Dong et al., 2011, Estes et al., 2007, Frederick et al., 2009, Gerlach et al., 2014, Grosso et al., 2013, Holliday et al., 2013, Kendrick et al., 2008, Kern et al., 2006, Merz et al., 2013, Milani et al., 2010, Schmid et al., 2012, Sonnenberg et al., 2008, van der Kuip et al., 2006). Drug uptake, proliferation, and induction of cell death up to changes in protein and gene expression were investigated. In addition to the response to drugs of the tumor cells, the influence of CAF on the tumor cells during drug administration (Schmid et al., 2012, Sonnenberg et al., 2008) and tumoral immune cell infiltration was also examined (Salmon et al., 2012). The tumor tissue slices were also used to validate 2D cell line experiments of different entities (Meijer et al., 2013, Séveno et al., 2012, Weissinger et al., 2013). In the meantime, drug tests based on tumor tissue slices obtained from patients can also be purchased (Indivumed GmbH, 2020).

Although tumor tissue slices are now more frequently used in cancer research, the possible alterations in the cultured samples compared to the original tumor has not been sufficiently investigated. Previous investigations are limited to parameters viability (Estes et al., 2007, Vaira et al., 2010, van der Kuip et al., 2006), cell proliferation (Davies et al., 2015, Schmid et al., 2012, Vaira et al., 2010), biomarker expression (Davies et al., 2015, Vaira et al., 2010) and apoptosis (Davies et al., 2015, Vaira et al., 2010, van der Kuip et al., 2006) to examine the slices. The consensus of these studies is that tumor tissue slices can be cultivated without significantly changing of the investigated parameters compared to the control tissue.

However, the transfer of tumor tissue from the operating table to the laboratory for tissue slice cultivation is partly beyond the control of the researcher and depends on many factors. Therefore, it would be optimal to define generally applicable standards, that each hospital and institute stick to and implement in their organizational structures (Davies et al., 2015). Further, uncontrollability must be prevented, and the tissue transported should be conducted as quickly as possible, surrounded by optimal preservation solution to prevent external influences before the laboratory part begins. These external influence factors can be mechanical stress, temperature shifts, altered oxygen and nutrition availability, which can affect the quality of the tissue slices as well as the tumor cell response to applied drugs. The inter- and intra-tumoral heterogeneity (Swanton, 2012), consistency variability (Holliday et al., 2013, Vaira et al., 2010, van der Kuip et al., 2006) and necrotic or proliferative areas (Schmid et al., 2012, Vaira et al., 2010), as well as the composition of the cells in the tissue (Schmid et al., 2012)

must be taken into account. Therefore, non-cultured controls and biological replicates are essential for evaluating the data obtained with this methodology and a sufficient number of controls to obtain meaningful results.

Various instruments can be used for producing tissue slices, such as the Krumdieck (Estes et al., 2007, Frederick et al., 2009, Sonnenberg et al., 2008, Stoff-Khalili et al., 2005, van der Kuip et al., 2006, Zimmermann et al., 2009), manual choppers (Gerlach et al., 2014, Merz et al., 2013) and vibratomes (Gerlach et al., 2014, Merz et al., 2013, Vaira et al., 2010, Zimmermann et al., 2009). The vibratome from Leica is the newest technique to make tissue slices, it can cut the tissue slices with a defined thickness very precisely and the sequential of the slices can be followed. The section range can be from 1 to 1000 µm according to the user requirements (Leica product information). The precision-cut tumor tissue slice from mouse xenograft or patient tumor tissue with 150-300 µm thickness maintains both, the three-dimensional architecture and tumor heterogeneity. During culture, the native microenvironment is preserved including cell types that surround and infiltrate the tumor such as stromal cells, immune cells, and extracellular matrix (Davies, 2015; Hickman, 2013). The tumor environment influences drug sensitivity and other aspects of tumor biology (Junttila, Sauvage, 2013). Therefore, it is crucial that a 3D cancer model reflects the complexity and heterogeneity of tumor biology *ex vivo* to individually predict *in vivo* therapy response of tumors. Furthermore, the tissue slice culture has the potential to represent the entire clinical spectrum of solid tumors (subtype, stage, grade, differentiation) in a person-specific manner, whereas the tumor cells represented by cell lines is limited (Masters, 2000). Thus, short-term tumor tissue slice cultivation captures the inter- and intra-tumor heterogeneity of tumor tissue that is typically observed *in vivo*. In addition, it enables the investigation of *in vivo* mimicking cell proliferation and drug response.

1.2.3 Cultivation systems for 3D cancer models

Over the past decade, the most used culture system for 3D cancer models is the floating system. In this system, the 3D hydrogel based models or tissues slices are floating in the cell culture medium (Benzoni et al., 2005, Schneider et al., 2003) (Figure 6A). The filter-supported culture systems were often used for tissue slice culture, such as the Millipore filter culture system (MF) (Davies et al., 2015, Gerlach et al., 2014, Merz et al., 2013, Vaira et al., 2010, Weissinger et al., 2013) and rotating cultivation (Kiviharju-af Hällström et al., 2007), but seldom tested for the 3D hydrogel

based models. Therefore, it is interesting to evaluate if the MF culture system is also suitable for 3D hydrogel-based models.

Davies et al. compared tissue slice culture methods, i.e. the floating (Figure 6A) and the MF system (Figure 6B) using mouse xenografts and patient tumors (Davies et al., 2015).

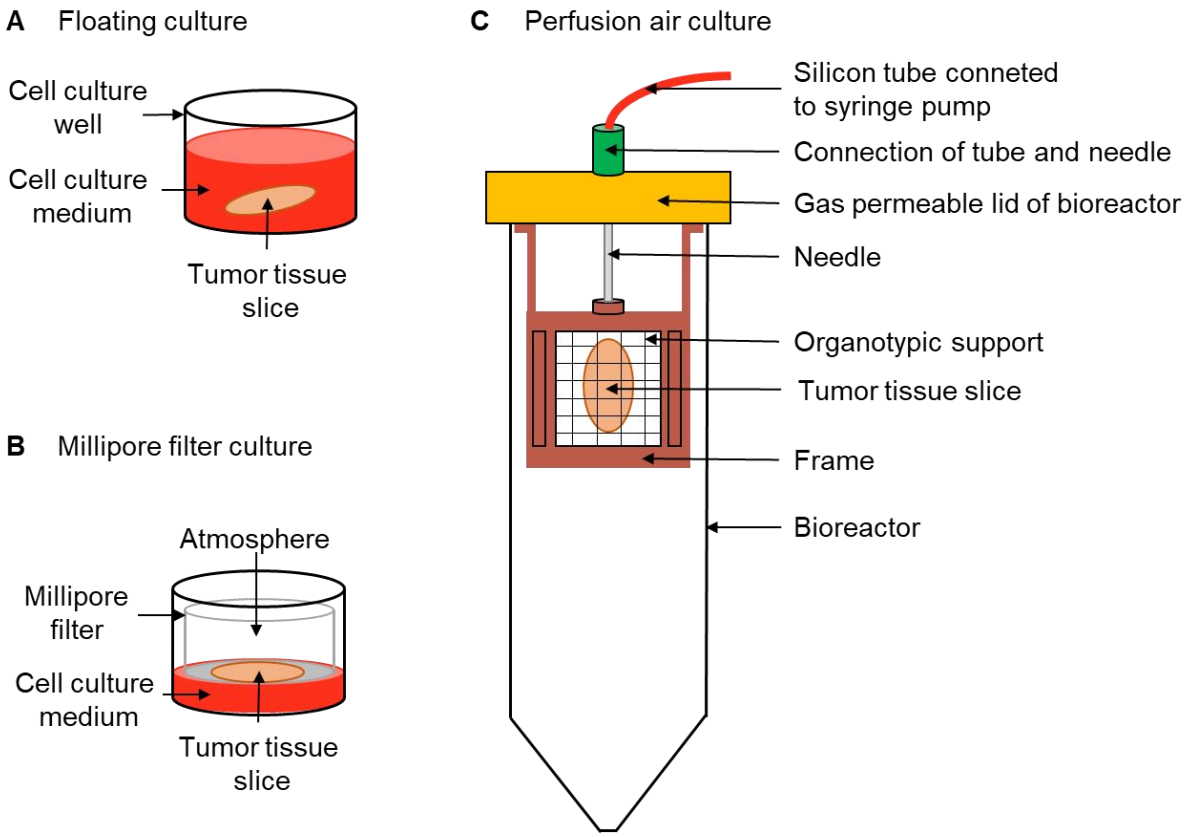

Figure 6: ***Schematic illustration of 3D cancer model cultivation systems.*** *Common methods for the cultivation of tissue slices are (A) the floating system, in which the slice is cultivated in a well of a microtiter plate submersed in cell culture medium, and (B) a filter-supported culture system, e.g. on a Millipore filter, in which the slice is supplied with medium from below and with the atmospheric side facing upwards. (C) The perfusion air culture system cultivates the tissue slices in a vertical direction between two organotypic supports within a patented frame holder. All is placed in a bioreactor with a gas-permeable lid with septum. The syringes are filled with the medium and/or drugs to be applied and inserted into an external syringe pump connected by a silicone tube which is attached to the frame holder by a needle. The tumor tissue slice is continuously perfused along the force of gravity.*

The cultured tumor tissue slices were compared to their *in vivo* source tissue regarding biomarker expression. The comparison was based on immunohistochemically (IHC) analysis and transcription of biomarkers, particularly those involved in cellular stress. They described a standardized workflow to systematically compare different tumor slice cultivation methods. They concluded that cultivation of tumor slices required organotypic support materials and atmospheric oxygen to maintain the integrity of

tissue slices. The authors further concluded that the MF culture induces loco-regional changes of protein expression in the tissue slice. The MF system produced an intra-slice gradient regarding proliferation, biomarker expression and oxygen supply. The IHC analysis of MF cultured tissue slices that were horizontally embedded in paraffin changed with distance from the tissue slice surface. Ideally, IHC analysis of sections must not be influenced by distance from tissue slice surface and the assessment of the drug treatment of the tissue sections. Therefore, the slices were sectioned vertically for analysis of morphology and protein expression for IHC staining.

To facilitate homogenous supply with nutrients and oxygen, the perfusion air culture (PAC) system (Figure 6C) with a frame holder (Dong, M.; Schwab, M.; van der Kuip, H. Device for cultivating tissue sections (patented)) was developed to further improve the tumor tissue slice culture. In the PAC system, the precision-cut tissue slices are placed in-between two organotypic supports and all is fixed in a frame holder allowing continuous perfusion with medium and supplements. The frame is settled vertically inside a 50 mL tube with capacity of air exchange and connected to a syringe pump by a silicon tube. The system is cultured in a standard cell culture incubator. Cotton meshes were used as organotypic supports to cover opposite sides of the tissue slice in the system. The cotton fibers can work as capillaries to supply the medium containing nutrients and drugs to the tissue slice. Meanwhile the big open pores of the cotton mesh allow the oxygen to be easily diffused into the tissue slice from both sides during cultivation. The PAC system can provide continuous and precisely controlled oxygen, medium and drug supply during the tissue slice cultivation.

1.2.4 Potential of 3D *ex vivo* slice culture for personalized medicine in cancer

The main reasons for the failure of cancer therapy are tumor heterogeneity (Marusyk, Polyak, 2010) resulting in resistance (Ramos, Bentires-Alj, 2015), metastasis and recurrence (Niibe, Hayakawa, 2010). In anti-cancer therapy, individual drugs or drug combinations can only be applied sequentially. Cell line and mouse experiments recapitulate the 3D *in vivo* situation in the patient only very limited (Mak et al., 2014, Wilding, Bodmer, 2014), since the interplay of tumor cells and cells constituting the TME is complex and produce a tumor specific and dynamic milieu (McMillin et al., 2013, Pietras, Ostman, 2010). The preserved and patient specific TME plays a key role in tumor development, progression, and response to therapy (Bian et al., 2019,

Quail, Joyce, 2013). Interestingly, tumors have been described as "organs" with a dynamic TME (Egeblad et al., 2010). Therefore, the question arises how cell lines growing in 2D culture or tumor cells transplanted in mice (which often lack the human stroma) can represent tumors.

Tumor tissue slice cultivation represents a preclinical *ex vivo* model system that captures the complex tumor biology (Davies et al., 2015). It is therefore suggested for assessing the response of cancer drugs to tumor cells (Gerlach et al., 2014, Merz et al., 2013). Nevertheless, the assertion that fresh tumor tissue slices reflect the in situ tumor and thus allow the programs of personalized medicine must be carefully evaluated (Hickman et al., 2014).

1.3 Aims of the work

The lack of therapeutic options in HGSOC treatment underlines the urgency to identify new targets for ovarian cancer. Due to persistent and resistant cells, the treatment options are very limited. Many studies on chemoresistance have already been carried out, but persistence of cells is not yet fully understood and must be addressed in the future. In addition, it is known that current cell culture models as the basis of drug research should be tailored more closely to the *in vivo* patient situation and 3D cancer cultivation models offer possibilities for such adaptations. These models can lead to more physiologically relevant and likely more predictive pre-clinical models, such as tissue morphology, tumor heterogeneity, TME, drug response, and reduced animal use. Different cultivation methods should also be evaluated to culture 3D cancer models. The physical and chemical properties of hydrogel materials also affect the gelation process and handling difficulties of 3D hydrogel-based cancer models. Precision-cut tumor tissue slices maintain the 3D architecture, heterogeneity of the tumor and the native TME concerning different cell types and the ECM. It has been reported that the cultivation of tumor tissue slices require organotypic supports and atmospheric oxygen for maintenance of tissue integrity. The commonly used MF system fulfilled these criteria, but MF culture can induce intra-slice gradients of biomarker expressions during the culture process. The novel developed PAC system facilitates the cultivation of tumor tissue slices due to its flexibility and adjustability of culture conditions such as choice of organotypic supports, continuous and precisely controlled oxygen, medium and drug supply.

The aims of this work are:

i) Generation and characterization of ovarian cancer DTP and identification of new biomarkers.

ii) Development of 3D hydrogel-based cancer models with different hydrogels and evaluation of the influence of different culture methods to the 3D hydrogel-based models.

iii) Comparison of the PAC system with the commonly used tissue slice cultivation methods for the culture and drug treatment of the tissue slices.

iv) Optimization of the organotypic supports for the PAC system and their further applications.

2 Materials and methods

The following solutions, consumables and instruments were used for the experiments. Further materials are mentioned in the methods.

2.1 Solutions

Table 1: List of solutions and substances used and manufacturer.

Solution/substance/reagent	**Manufacturer**
Mayer‘s Hematoxylin	Merck, Darmstadt, Germany
FACS Flow	Becton Dickinson, Franklin Lakes, USA
4% Formaldehyde Histofix	Carl Roth, Karlsruhe, Germany
Cisplatin (1 mg/mL)	Teva GmbH, Ulm, Germany

2.2 Consumables

Table 2: List of consumables used and manufacturer.

Consumable	**Manufacturer**
Cell scraper, 25 cm	Sarsted AG & Co. KG, Corning, Inc.
FACS tubes	Multimed Biotechnologiekontor GmbH, Giengen an der Brenz, Germany Ref# 9480708
Embedding cassettes	Carl Roth, Karlsruhe, Germany
Cell culture microplate 384-/96-/48-/24-/12-/6-well, Cellstar	Greiner Bio One, Frickenhausen, Germany
Cell culture microplate 96-well Cellstar, white	Greiner Bio One, Frickenhausen
Petri dish Cellstar, cell culture dish, Ø 10 cm	Greiner Bio One, Frickenhausen
Petri dish 60x15 mm with cams	Sarsted AG & Co. KG
Petri dish 35x10 mm with cams	Sarsted AG & Co. KG
Microscope slides SUPERFROST PLUS	Thermo Scientific, USA
Cover slips	Hecht, Sondheim v. d. Röhn, Germany
Test membrane A: Gore BIO-A Tissue Reinforcement	Gore-Tex, Newark, Delaware, USA

Test membrane B: Gore Dualmesh Biomaterial	Gore-Tex
Test membrane C: Polycaprolactone scaffold	T&R Biofab, Siheung-si, South Korea
Test membrane D: Lumox foil	Sarsted AG & Co. KG

2.3 Instruments

Table 3: List of devices used and manufacturer.

Instrument	**Manufacturer**
2300 EnSpire Multimode Reader	PerkinElmer, Hamburg, Germany
Inverse transmitted light microscope CKX41	Olympus Life Science, München
Fluorescence Activated Cell Analyzer "FACS Calibur"	Becton Dickinson, Ranklin Lakes, USA
Slide Scanner VS-120	Olympus Deutschland GmbH, Hamburg, Germany
Inverted microscope CKX41	Olympus Deutschland GmbH
Rotary Microtome, Leica RM2255	Leica Biosystems Nussloch GmbH, Nussloch, Germany
Leica TCS SP8 Confocal Laser Scanning Microscope	Leica Microsystems CMS GmbH, Mannheim, Germany
IFC Controller MX	Fluidigm, USA
IFC Controller HX	Fluidigm, USA
BioMark-HD-System	Fluidigm, USA
PHD 22/2000 Syringe Pump Series	Harvard Apparatus, Holliston, MA, USA

2.4 Hydrogels for 3D cancer models

Alginates, agarose and Matrigel from different manufactures (Table 4) were used in the process of cell embedding (3D hydrogel).

Table 4: Hydrogels used.

Hydrogel	Information	Manufacturer
Alginate 1	Lot# GQ9109901	FMC Protanal
Alginate 2	CAS# 9005383	Sigma
Alginate 3	Lot# B3006523	Nova Matrix
Agarose (low melt)	Catalog #1613111	Bio-Rad
Matrigel	Catalog #356231	BD Biosciences

2.5 Cell culture

2.5.1 Cell lines

Human tumor cell lines from different entities were used (Table 5), regularly tested for mycoplasm and authenticated by short tandem repeats (STR) profile analysis.

Table 5: Tumor cell lines used.

Cell line	Entity	Source
OVCAR-3	Ovarian cancer	ATCC NCI-60
A2780	Ovarian cancer	ATCC NCI-60
MCF-7	Breast cancer	ATCC NCI-60
Calu-1	Lung cancer	ATCC
Mino	Mantle cell lymphoma	German Collection of Microorganisms and Cell Cultures GmbH, Germany
Jeko-1	Mantle cell lymphoma	German Collection of Microorganisms and Cell Cultures GmbH, Germany

2.5.2 Culture media and culture conditions

Ovarian cancer cell lines were cultured in RPMI-1640 (Biochrom, Berlin, Germany) and supplements as listed in Table 6. Calu-1 cells were cultured in McCoy's 5A medium (Thermo Fisher Scientific, Waltham, MA, USA) supplemented with 10% fetal bovine

serum (FBS; Gibco, Germany), 0.1 g/L penicillin-streptomycin (Gibco) and 2 mM L-glutamine (Biochrom). MCF-7 cells were cultivated in DMEM (Gibco), H1437 CDX and primary ovarian cancer slices were cultivated in RPMI 1640. The medium was supplemented with 10% FBS, 2 mM L-glutamine and 0.1 g/L penicillin-streptomycin. MCL cell lines were cultivated in RPMI-1640 supplemented with 20% fetal bovine serum, 0.1 g/L penicillin-streptomycin, and 2 mM L-glutamine.

Table 6: Supplements in 500 mL cell culture medium.

Supplement	**Manufacturer**
10% (v/v) fetal bovine serum (FBS)	Sigma-Aldrich, Steinheim, Germany
0.1 g/L penicillin/streptomycin	Thermo Fisher Scientific
10 mM HEPES (2-(4-hdroxyethyl)-1-piperazinyl-ethanolsulfonacid); pH 7.4	Merck
2 mM L-glutamine	Biochrom
0.13 mM L-asparagine	Serva
0.05 mM ß-mercaptoethanol	Merck
1 mM sodium pyruvate	Gibco
3 mL 100x non-essential amino acids	Biochrom

2.5.3 2D Cultivation procedures

Cells were cultured in sterile cell culture flasks at 37 °C and 5% CO_2 in cell culture incubators. All cells were passaged after 2-3 days cultivation when reached confluency. The adherent cells were first washed with 1x PBS (Biochrom, Berlin), then detached by adding 0.05% Trypsin+EDTA (Gibco) and a short incubation at 37 °C. After centrifugation and resuspension in medium, a certain number of cells are then transferred into a new vessel with fresh medium.

2.5.4 3D cancer model cultivation

MCF-7 CDX slices were cultivated in DMEM (Gibco), H1437 CDX and primary ovarian cancer slices were cultivated in RPMI 1640 (Biochrom AG). The medium was supplemented with 2 mM glutamine (Gibco), 100 U/mL penicillin (Gibco), 100 µg/mL streptomycin (Gibco) and 10% fetal bovine serum (FBS; Gibco). Cultivation of tissue slices was performed at 37 °C and 5% CO_2 in a cell culture incubator under

atmospheric oxygen (21% oxygen) conditions. Three different methods were tested in this work for tissue slices cultivation.

2.5.4.1 *Floating (FL) culture*

Cell-hydrogel and tumor tissue slices were transferred into a 24-well plate well with 1 mL cell culture medium per well. Each well contains one tissue slice as shown in Figure 6A. The slice is freely floating in the medium in the well.

2.5.4.2 *Millipore filter (MF) culture*

Millipore filter (Millicell cell culture insert, PTFE, pore size 0.4 µm, Merck Millipore) is used as support in this culture system. The cell-hydrogel and tumor tissue slices are laying on top of the filter on the surface of 1.5 mL cell culture medium in a 6-well plate well as shown in Figure 6B. One drop of the medium on the top of the slices prevents the slices from drying out.

2.5.4.3 *Perfusion air culture (PAC) culture*

In the PAC system, the cell-hydrogel and tumor tissue slices are kept in-between two organotypic supports and fixed in a frame holder (Figure 6C). The sandwich of tumor slices and organotypic supports with the frame holder is held in a 50 mL tube with air exchange capacity. The culture system is placed in a conventional cell culture incubator under standard cultivation conditions. Cell culture medium was supplied to the tumor tissue slice by a syringe pump via the silicone tube. This allows continuous perfusion of the tissues slice set up with culture medium.

2.5.4.4 *Organotypic support for PAC culture*

Organotypic supports in PAC culture are crucial for the stabilization of cell-hydrogel and tumor tissue slices and the support of a homogeneous supply of nutrients, oxygen, and drugs. The membranes must meet several requirements: culture-dependent stress (e.g. shear stress) for the tissue slice must be minimized, gas permeability must be sufficient, and liquid must be conducted through the membranes. Cotton fabric (pore size 500 µm) and cell-free porcine intestine (Figure 7) showed promising results in preliminary experiments regarding the fulfilling of the criteria.

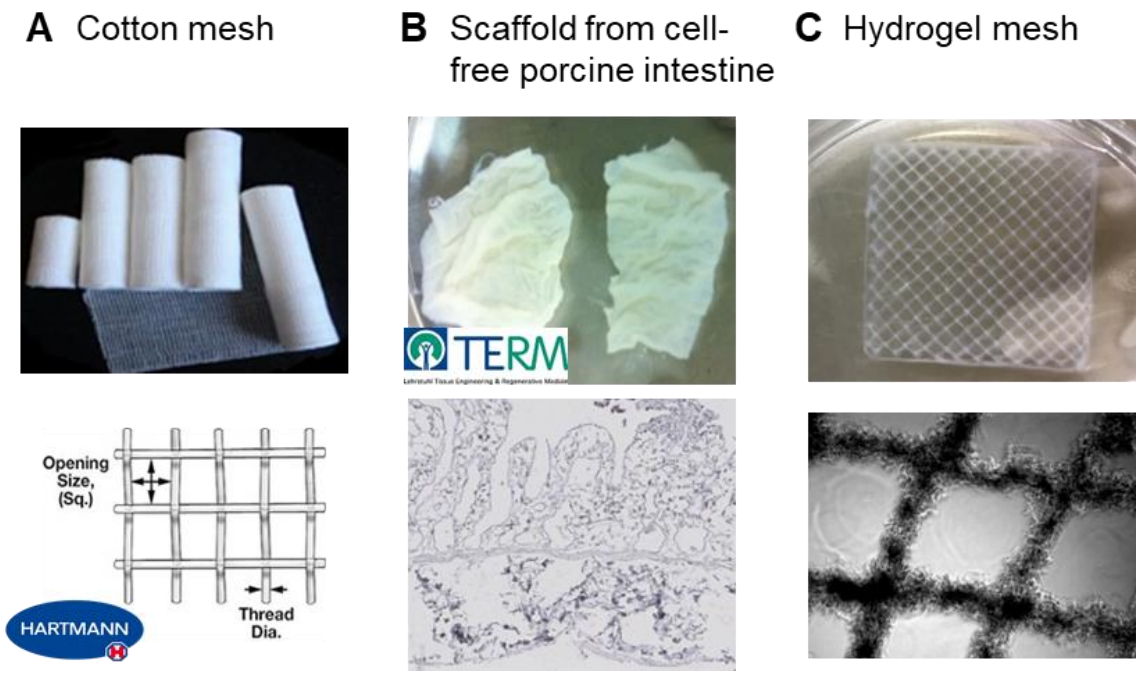

Figure 7: ***Organotypic supports used in the PAC system for cell-hydrogel and tissue slice cultivation.*** *(A) Cotton mesh with a pore size of 500 µm, (B) cell-free porcine intestine and (C) 3D printed hydrogels were used for culture in the PAC system.*

2.5.5 Cisplatin incubation of cells and tumor tissue slices

In cell culture experiments, cells were seeded until 60-70% confluence. Cisplatin was added to the cell culture medium until required concentration was obtained. The medium was changed with cisplatin containing medium and cells were pre-incubated with 13 µM cisplatin for 24-48 h. Tissue slices from both CDX and primary human ovarian tumors were treated with 13 µM cisplatin in both MF and PAC systems. In the MF system, cisplatin was applied in 1.5 mL medium in each well (6-well plate) with a drop of medium containing cisplatin on the top of the tissue slices. In the PAC system, 13 µM cisplatin in the medium was continually applied to the tissue slices through a syringe pump. The control and treated slices were always adjacent slices from the tumor in order to minimize the influence of tumor intra-heterogeneity.

2.5.6 Cryopreservation and re-cultivation of cell lines

Cell lines used for experiments were up to passage 35, to prevent the occurrence of genetic changes. For cryopreservation the cells were centrifuged (RT, 340×g, 5 min) and resuspended in ice-cold freezing medium (FBS + 10% dimethyl sulfoxide, DMSO, Sigma). Between 0.5-1×10^6 cells in 1 mL freezing medium per cryovial (Nalgene Nunc

International, Thermo Fisher Scientific) were frozen in a special freezing box (Thermo Fisher), which cooled the cell suspension by 1 °C/min to -80 °C. The vials were further stored in liquid nitrogen.

The cryopreserved cells were quickly thawed at 37 °C and immediately transferred to pre-heated 37 °C cell culture medium. After centrifugation and resuspension in fresh medium, the cells can be re-cultivated under standard conditions.

2.5.7 Generation of monoclonal OVCAR-3 cell lines

To generate OVCAR-3 control clones, 10^3 cells were seeded in a petri dish (Ø 10 cm) and individual clones were isolated. The attached cells were rinsed with PBS. For isolation, silicone cylinder (Carl Roth, Karlsruhe, Germany) were sealed with autoclaved petroleum jelly (Carl Roth) and placed around one single colony. Cells were detached with 200 µL Trypsin and transferred to a 12-well plate filled with fresh medium for monoclonal cell expansion. In parallel, 1.2×10^6 OVCAR-3 cells were bi-incubated with 13 µM of cisplatin and individual DTP-derived clones were isolated and expanded. Clones were cryo-conserved and stored in liquid nitrogen for further analysis.

2.5.8 Embedding cells with hydrogels for 3D *in vitro* cultivation models

The alginate and agarose powders were sterilized by UV light for 30 min. A 3% agarose solution was prepared and heated to ensure total dissolving of the powder. Before embedding cells, the agarose solution was cooled until 40 °C. The solution was dissolved (1:10) with the required cell suspension in cell culture medium using a pre-heated pipet tip and transferred in sterile silicon chambers (Figure 8, flexiPERM slides, Sarstedt) that are fixed on a glass slide for polymerization. To avoid air bubbles, reverse pipetting was performed. Alginate was dissolved as 1.1% (w/v) in sterile 0.9% NaCl to form alginate solution and stored at 4 °C for further usage. Cells were dissolved in the alginate solution and transferred by reverse pipetting in the chambers. The cell-hydrogel slices are then rinsed with warm 14.4 mM $CaCl_2$ or $BaCl_2$, respectively, further rinsed with culture medium and placed in the used cultivation system.

To dissolve them again, cell-alginate slices were incubated for 10 min with 55 mM Na-citrate in 0.15 M NaCl (pH 6.8), then centrifuged (3 min, 300×g) and washed twice with PBS. The alginate dissolved completely and could then be stained.

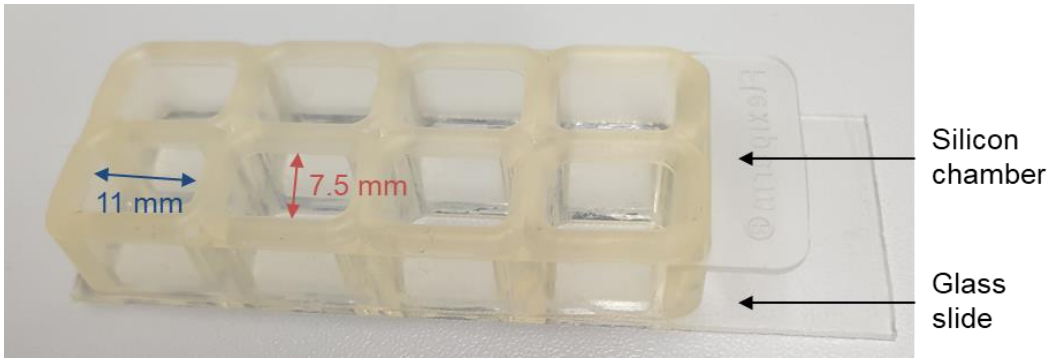

Figure 8: ***Silicon chamber for embedding cells in hydrogels.*** *Cells and hydrogel are mixed by pipetting and transferred in one chamber for polymerization.*

2.5.9 3D-cultivation of patient-derived organoids from ovarian cancer in Matrigel

In order to isolate tumor cells from ovarian cancer tissue, fresh tissue or untreated and cisplatin treated tissue slices were minced and enzymatically digested for 45 min with collagenase solution and subsequently filtered through 100 µm and 70 µm filters. The fractions 100 µm >70 µm and <70 µm were harvested in DMEM. Cells were pelleted by centrifugation and resuspended in a growth medium-Matrigel solution (1:3). Droplets of 15 µL were placed in 48-well plates and left to polymerize before overlay with culture medium supplemented with 10 mM Hepes, 1× Glutamax (Fisher Scientific), 1× penicillin/streptomycin (Fisher Scientific), 1x B27 (Fisher Scientific), 1xN2 (Fisher Scientific), 1 mM N-acetylcysteine (Sigma), 50 ng/mL human EGF (Peprotech, Rocky Hill, USA), 10 µM Y-27632 (Absource Diagnostics, München, Germany) and 1.25 µg/mL Amphotericin (Merck).

2.5.10 Cell line-derived xenograft (CDX) samples

MCF-7 and H1437 CDXs were used in this work. The experiments with mice for MCF-7 CDX (obtained from AstraZeneca) were compliant with the UK Animals (Scientific Procedures) Act, which is consistent with EU Directive 2010/63/EU and had undergone internal ethical review. Experiments carried out with mice for H1437 CDX at Charles River Discovery Research Services Germany were scrutinized by the Committee on the Ethics of Animal Experiments of the regional council (Regierungspräsidium Freiburg, Abt. Landwirtschaft, Ländlicher Raum, Veterinär- und Lebensmittelwesen).

2.5.11 Primary human ovarian tumors

Fresh tumor tissue samples from patients were obtained as surgical waste from Robert Bosch Hospital (Stuttgart, Germany) immediately after surgical resection and maintained in ice-cold MACS Tissue Storage Solution (Miltenyi Biotec) until use. The experiments were approved by the local ethics committee (397/2016BO1) and all patients agreed to an informed consent.

2.6 Tissue slice culture

2.6.1 Tissue slice preparation

Tumor tissues from primary human ovarian cancer or cell line-derived xenografts (CDX) were fixed with tissue adhesive onto the magnetic specimen holder of a Leica VT1200 vibratome (Leica Biosystems Nussloch GmbH, Nussloch, Germany). The tissue slices were cut at a thickness of 250 µm for MCF-7 and H1437 CDX and 280 µm for primary ovarian cancer tissues. Each tissue slice was carefully transferred with tweezers into a 24-well plate well prefilled with cell culture medium, preserving the order of the cut slices. The whole tissue slice workflow is illustrated in Figure 9.

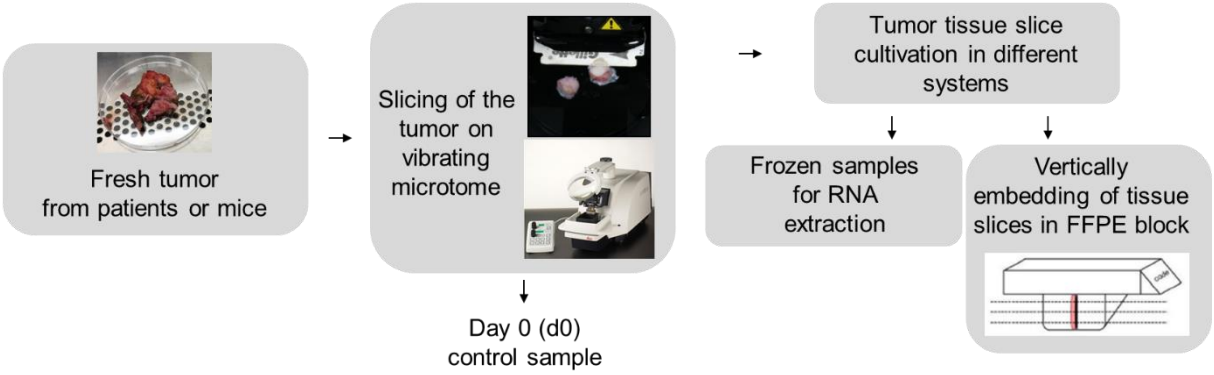

Figure 9: ***Schematic workflow of the tumor tissue slice culture.*** *Fresh tumor is processed and cultivated in different systems. (Adapted from (Davies et al., 2015))*

2.6.2 Examination of cell culture medium after tissue slice culture

The supernatants after cultivation in FL and MF or the flow-through of tissue slices cultivated in the PAC system were transferred to sterile Eppendorf vials. The media were examined using the ABL 800 flex (Radiometer GmbH, Krefeld, Germany) to

obtain a blood gas and electrolyte analysis of the medium, which in the culture systems is analogous to blood in the *in vivo* situation. In addition, the cell culture medium after culture in the different systems was analyzed by MACSplex (Miltenyi Biotec, Bergisch Gladbach, Germany) according to the manufacturer's protocol. This bead-based assay allowed the quantification of 12 commonly examined cytokines: GM-CSF, IFN-α, IFN-γ, IL-2, IL-4, IL-5, IL-6, IL-9, IL-10, IL-12, IL-17A and TNFα.

2.7 Cell cycle analysis

By measuring the DNA content, it is possible to analyze the individual cell cycle stages. The DNA content of a cell can be determined using the dye propidium iodide (PI, Sigma), which is incorporated into double-stranded nucleic acids. Apoptotic cells lose parts of the DNA fragments and therefore incorporate less PI. This state is also known as Sub-G_1. Cells were fixed with cold 70% ethanol, washed with PBS and stained with 50 µg/mL PI. Analysis of cell cycle phases was conducted using flow-cytometry.

2.8 Cell proliferation analysis

In order to determine the proliferation of the cells, the doubling time was calculated. For this purpose, 10^5 cells were seeded into the wells of a 6-well plate. Every 24 hours in following days, the cells from one well were detached using trypsin and counted with the EVE Automatic Cell Counter. Growth rate and doubling time were calculated using the following equations:

$$Growth\ rate\ (GR) = \frac{\ln(\frac{n_x}{n_{x-1}})}{t_x - t_{x-1}} \qquad [\frac{1}{h}]$$

$$Doubling\ time\ (t_d) = \frac{\ln(2)}{GR} \qquad [h]$$

n=cell number; t=time

2.9 Cell viability assays

2.9.1 Trypan blue staining

Before starting an experiment, the cell suspension in cell culture medium was stained with trypan blue (1:1, NanoEnTek, South Korea) and dead cells were counted with EVE Automated Cell Counter (NanoEnTek).

2.9.2 Flow cytometry-based AnnexinV/PI assay

Flow cytometry was used to differentiate between vital and apoptotic cells. After cell detachment with trypsin, the cells were resuspended and washed in ice-cold PBS. Then the cell pellet was resuspended in 100 µL Annexin binding buffer (ABB; 10 mM HEPES, 140 mM NaCl, 2.5 mM $CaCl_2$, pH 7.4), supplemented with AnnexinV-FITC (1:20) and propidium iodide (PI, 50 µg/mL stock solution in PBS, 1:40). The cell suspension was incubated for 10 min at RT. Next, 200 µL ABB was added and the cells were analyzed using a FACS Lyric Flow Cytometer. The proportion of stained and unstained cells were assessed using FACS Suite software V1.2.1 (Becton Dickinson GmbH, Heidelberg, Germany).

Since cells in early apoptosis show characteristic changes in their cell membrane, as switch of phosphatidylserine from the cytosolic to the outer membrane, it can be used as a marker for apoptosis. The phospholipid can be bound by the Ca^{2+}-dependent phospholipid binding protein AnnexinV. This protein-protein interaction is used to detect apoptotic cells flow cytometrically by labeling AnnexinV with a fluorophore such as fluorescein isothiocyanate (FITC). The higher fluorescence signal indicates higher proportion of apoptotic cells.

At late stages of apoptosis or necrosis, the cell membrane is permeable and AnnexinV can penetrate the cell membrane and bind phosphatidylserine on the inner sheet of the membrane. To distinguish between early and late apoptotic cells, the AnnexinV-FITC staining was combined with propidium iodide (PI) staining. PI is an intercalating fluorescent agent that is excluded from viable cells, but during late apoptosis or necrosis it can penetrate cells with damaged or already perforated membranes. Therefore, PI staining of cells is a sign of late apoptosis or necrosis, while single staining of cells with AnnexinV-FITC indicates early stages of apoptosis.

Table 7: Reagents and solutions used in flow cytometry.

Reagents	**Manufacturer**
AnnexinV-FITC	BD Pharmingen
Propidium iodide stock solution (1 mg/ml)	Sigma
AnnexinV binding buffer (10x)	BD Pharmingen
Dulbecco's PBS	Biochrom

2.9.3 Colony formation assay

In order to determine the long-term survival of drug-tolerant persister cells after incubation with a cytotoxic drug such as cisplatin, a colony formation assay is performed (Crowley et al., 2016). For the evaluation of the colony assay, the plating efficiency (PE) and the surviving fraction (SF) are calculated based on the number of colonies that are formed from adherent cells. The PE was calculated as a percentage value indicating cell proportion, which survive after seeding and are able to form colonies.

$$\mathrm{PE} = \frac{\text{no.of counted colonies}}{\text{seeded cells}} \times 100 \qquad [\%]$$

The SF is the proportion of cells that survive after cytotoxic treatment and are able to form colonies:

$$\mathrm{SF} = \frac{\text{no.of counted colonies after treatment}}{\text{seeded cells}} \times \mathrm{PE} \qquad [\%]$$

To determine the two values, the cells were seeded in two T25 culture flasks. To calculate the PE, 500 cells were seeded per culture flask and to calculate the SF, 2×10^5 cells were seeded. The latter was first treated with 13 µM cisplatin for 4 h and then further incubated for another 24 h. The media was changed after all the processes. In the flask for the determination of the PE no change of medium and no incubation with cisplatin were carried out. The cells were cultivated until colonies formed. In the cells incubated with cisplatin, medium was changed when many cells died. In order to evaluate how many colonies had formed, the cells were stained with hematoxylin. For this purpose, the cells were fixed for 5 min with ice-cold (-20 °C) 70% ethanol and then stained with Mayer's hematoxylin solution for 2 min. Afterwards the stained colonies were counted, and the PE and SF were calculated.

2.9.4 MTT assay

In a 96-well plate, 4000 cells were seeded in 100 µL cell culture medium per well. After 24 h, cells were incubated with 13 µM cisplatin for another 48 h. Then, 10 µL of MTT reagent was added to each well and incubated for 2 h, 90 µL MTT lysis buffer (15% SDS in 1:1 dimethylformamide-water, pH 4.5) were added and samples were covered with aluminum foil to avoid the light and incubated overnight on a rotating shaker at RT. Absorbance was measured at 550 nm using a 2300 EnSpire Multimode Plate Reader (Perkin Elmer, Rodgau, Germany, software version 4.10). Viable cells metabolize MTT to formazan that can be measured colorimetrically. A reduction of absorbance indicated loss of cell viability and growth.

2.9.5 Cell titer glo assay

Using a 96-well plate, 4000 cells were seeded in 80 µL cell culture medium per well. On the next day, 13 µM cisplatin was added for 48 hours and 95 µL CTG reagent (Promega, Walldorf, Germany) was added. The 96-well plate was placed on a shaker for 2 min to lyse the cells, incubated at room temperature for 10 min and luminescence was measured with the 2300 EnSpire Multimode Plate Reader (Perkin Elmer). In the presence of ATP, the luciferase converts Luciferin to luminescent Oxyluciferin. Reduction of luminescence correlates with loss of cell viability.

2.9.6 Viobility Fixable Dyes of tumor cell viability post tumor tissue slice culture

Human tumor cells from tumor tissue slices were isolated with the Tumor Cell Isolation Kit (Miltenyi Biotec) according to the manufacturer's protocol. Cell viability analysis of tumor tissue slices was conducted by flow cytometry after cultivation in the MF and PAC system in the presence and absence of cisplatin. The tissue was mechanically minced and enzymatically digested in cell rinse buffer (1 mM NaH_2PO_4, 5.4 mM KCl, 120 mM NaCl, 5.6 mM glucose, 2.5 mM $MgCl_2$, 20 mM HEPES, pH 7.2, all chemicals were purchased from Sigma-Aldrich), supplemented with 167 U/mL collagenase and 0.25 mg/mL protease. After 90 min incubation at 37 °C, the tissue suspension was filtered through a cell strainer (BD Falcon, USA) with a pore size of 70 µm to exclude cell agglutination. Two tissue slices were dissociated per approach. Cells were stained

according to the manufacturer's protocol for viability (Viobility dye, Miltenyi Biotec) and quantified with the MACSQuant Analyzer 10 Flow Cytometer (Miltenyi Biotec).

2.10 Cell migration assays

2.10.1 2D wound healing assay ("Scratch assay")

A wound healing assay can be performed to assess the motility of cells. In this assay a gap is created in a confluent cell layer which can be closed by motile cells (Liang et al., 2007).

Persister cells were seeded at a density of 1.7×10^5 cells per well in three wells of a 12-well plate. The scratch was created on the following day. To avoid that the gap is closed by cell proliferation, the cells were incubated with 30 µM proliferation inhibitor Mitomycin C for 2 h before scratching. The scratch was performed with the tip of a 200 µL pipette tip, which scratched in the monolayer of the cells. The cells were then carefully washed with PBS and incubated in culture medium for 24 h. Microscope images of the scratches were taken at 10x magnification and the closed distance was measured using ImageJ.

2.10.2 3D scaffold migration assay

Using the PAC system, cell-free porcine intestine (from University Hospital Würzburg, Department Tissue Engineering and Regenerative Medicine (TERM) and Translational Center Würzburg ´Regenerative therapies in oncology and musculoskeletal diseases` Würzburg branch of the Fraunhofer-Institute Interfacial Engineering and Biotechnology, IGB, Röntgenring 11, 97070 Würzburg, Germany) can serve as organotypic support. This matrix around the tumor tissue slice offers the cells the possibility to migrate out of the slice into the surrounding scaffold structure.

2.11 Protein and biochemical analyses

2.11.1 Immunohistochemistry (IHC)

The tissue was fixed in 10% neutral buffered formalin and after dehydration embedded in paraffin. Sections (4 µm) were cut by Rotary Microtome (Leica RM2255, Leica Biosystems) and incubated overnight at 56 °C. IHC of marker proteins (Table 8) was performed with Dako REAL EnVision Detection System (Agilent Technologies, Santa

Clara, CA, USA) according to the protocol: After 20 min incubation in Microclear, the slides were incubated in a descending alcohol series (100%, 96%, 70%) for 3 min each and rinsed briefly with water. Subsequently, incubated 30 min in hot steam with Antibody-Retrievel buffer (pH6/pH9) and cooled down for 20 min. After 2-3 rinses with TRIS-buffered saline with Tween 20 (TBST) 3 min each, a 10 min incubation with Peroxidase Blocking solution followed by 2-3x washing steps with TBST. In the next step, the required antibody was diluted with DAKO REAL Antibody dilution buffer and applied to the tissue sections for the required time (Table 8). After another 2-3 rinses with TBST, incubation with the secondary antibody was performed for 30 min and washing with TBST again (2-3x). Substrate chromogenic was then incubated on the sections for 10 min and rinsed with running tap water for 3-5 min. The counterstain was performed with Mayer's hematoxylin for 30 s and rinsed again with running tap water for 3-5 min. Then incubation was performed in an ascending alcohol series (70%, 96%, 100%) for 3 min each and 5 min in the last step. Finally, the slides were incubated in Microclear for 5 min and after drying, they were covered with mounting medium and a cover glass. Finally, the tissue sections were digitized using a slide scanner.

Table 8: Antibodies used for IHC.

Antibody	**pH**	**Antibody incubation time**	**Dilution**	**Manufacturer**
Ki67	pH6	30 min	1:75	Dako #M7240
Geminin	pH6	30 min	1:300	Proteintech #10802-1-AP
cleaved caspase 3	pH6	60 min	1:75	Cell Signaling #9661
EpCam	pH6	30 min	1:100	Dako #M 0804
gamma-H2AX	pH6	30 min	1:75	Cell Signaling #2577
Hif1-alpha	pH6	60 min	1:25	BD #610959
Estrogen receptor (ER) Clone 6F11	pH6	60 min	ready to use	Leica Bond #PA1051

2.11.2 Hematoxylin-Eosin (H&E) staining

The tissue slice was prepared and cut as for the IHC. Dehydration was performed by 20 min Microclear (Merck) and 3 min for each step in a descending alcohol series

(100%, 96%, 70%) followed by 1 min washing with deionized water. The staining was carried out in filtered Mayer's hematoxylin for 5 min and another 5 min washing with water followed by 1 min staining in 0.5% (w/v) eosin solution. After washing with deionized water, an ascending alcohol series for 3 min each (70%, 96%, 100%) and 1 min Microclear step followed.

2.11.3 Live-Dead assay with confocal laser scanning microscopy

To identify cytotoxicity of the cells embedded in hydrogels or in organoids, a three-color fluorescent viability assays adapted from (Dong et al., 2011) was used. Briefly, cells in the hydrogels or organoids were incubated simultaneously with 0.5 µM tetramethylrhodamine methyl ester perchlorate (TMRM, Sigma-Aldrich) and 5 µM DAPI for 20 min at 37 °C in the dark, followed by 0.7 µM Picogreen (Molecular Probes, Invitrogen) for additional 10 min and the samples were analyzed immediately without further washing steps using Confocal Laser Scanning Microscope (Leica TCS SP8 Confocal Laser Scanning Microscope, Leica Microsystems CMS GmbH, Mannheim, Germany). Cells that showed signals from Picogreen in the nuclei were considered as dead cells.

2.12 Gene expression analyses

2.12.1 RNA isolation

Cells from cell line were harvested with a cell scraper on ice, washed twice with ice cold PBS and centrifuged (200×g, 5 min). To obtain RNA from human tissue samples, tissue was homogenized using FastPrep-24 (MP Biomedicals, Illkirch-Graffenstaden, France). RNA was isolated with the RNeasy Mini KIT (Qiagen, Hilden, Germany) according to the manufacturer's protocol with adaptions: in the lysis step 0.14 M β-Mercaptoethanol was added to RLT buffer and final elution was performed with 40 µL nuclease-free water. Furthermore, an "on-column DNase digestion" to eliminate DNA contamination was conducted for tumor tissue RNA isolation according to the protocol.

2.12.2 RNA quantification and qualitative analysis

The isolated RNA was directly quantified by measuring the absorption in the ultraviolet spectral range with the NanoDrop Spectrophotometer Peqlab ND-100 (Biotechnologie

GmbH, Erlangen). To determine the RNA concentration, the absorbance was measured at a wavelength of 260 nm. An OD of 1 here corresponds to a concentration of 40 µg/mL RNA.
RNA quality of cells from human tissue samples was determined via the Bioanalyzer RNA 6000 Nano assay for eukaryotic cells (Agilent Technologies) according to the manufacturer's manual. RNA degradation equals a low RNA integrity number (RIN) and samples with RINs >5 were further analyzed by Fluidigm qPCRs.

2.12.3 cDNA synthesis

In the cell lines 500 ng and in cells from human tissue samples 250 ng RNA were used in 13 µL nuclease-free water for cDNA synthesis. For each sample preparation, 2 µL of 125 µg/mL Oligo dT (or random hexamers) with water was added to the sample. The sample was vortexed for 30 s, centrifuged (10 s, 100×g) and incubated at 70 °C for 5 min. After cooling the samples to RT, 10 µL master mix (Table 9) was added, the sample mixing and centrifugation steps were repeated, and the samples were incubated at 42 °C for 1 h followed by 70 °C for 10 min. Samples were stored at -20 °C until gene expression analyses.

Table 9: cDNA synthesis master mix.

Reagents	**Volume per sample [µL]**	**Manufacturer**
5x buffer	5	Promega
dNTPs	1.25	Thermo Scientific
RNasin	0.5	Promega
Water (nuclease-free)	2.25	Qiagen
M-MLV	1	Promega
∑	10	

2.12.4 TaqMan-based qPCR assays

The evaluation of the data was done by first calculating the ΔΔCt values from control and treatment samples. As reference gene the TATA box binding protein (TBP) was used. TaqMan assays were obtained from Applied Biosystems (Foster City, CA, USA),

as well as the 7500 real-time PCR system (7500 software v2.3) that was used for real-time quantitation of gene expression.

Table 10: TaqMan qPCR master mix.

Reaction numbers	**Volume per sample [µL]**	**Manufacturer**
Taqman Universal PCR Master Mix (2x)	5	Applied Biosystems
20X Taqman Gene Expression Assay	0.5	Applied Biosystems
water (nuclease-free)	2.5	Qiagen
cDNA (1:5 in water)	2	
∑	10	

2.12.5 High through-put qPCR Chips (BioMark HD system)

For gene expression analyses with the BioMark HD system, each cDNA was then mixed with a portion of the combined TaqMan Gene Expression Assays and a portion of TaqMan PreAmp Master Mix (2x) (Table 11). The following PCR program was used for the amplification reaction: First, the preparations were incubated for 10 min at 95 °C and then in 14 cycles of 15 s at 95 °C and 4 min 60 °C. Finally, gene expression analysis of patient samples was performed on the BioMark HD System (Fluidigm, San Francisco, CA, USA) according to manufacturer's instructions. This system offers the possibility to measure a variety of genes in different samples, e.g. 48 genes with 48 samples or 96 genes with 96 samples, simultaneously in nanoliter scale reactions using TaqMan gene expression assays (Appendix, A1).

Table 11: Reagents used for BioMark high through-put qPCR.

Reagent	**Manufacturer**
20x TaqMan Gene Expression Assays	Applied Biosystems, USA
TaqMan PreAmp Master Mix (2x)	Applied Biosystems, USA
2x Assay Loading Reagent	Fluidigm, USA
20x GE Sample Loading Reagent	Fluidigm, USA
TaqMan Universal PCR Master Mix (2x)	Applied Biosystems, USA
48.48 and 96.96 Dynamic Array IFC	Fluidigm, USA

2.12.6 RNA sequencing (RNA-seq)

RNA was isolated and sent to the Centre for Genomic Regulation (Barcelona, Spain) for RNA-seq. RNA library was prepared with a stranded mRNA-seq library and the sequencing was conducted with 2x75 bp paired-end reads (Illumina, San Diego, USA). FastQ-Files of all samples were obtained.

2.13 Bioinformatical analyses

2.13.1 User-friendly transcriptome analysis pipeline

RNA-seq data were analyzed using the User-friendly Transcriptome Analysis Pipeline, an open source web-based platform (Kohen et al., 2019). Analyses were conducted according to the protocol: Click “run pipeline” and choose “Transcriptome RNA-seq”, a name and an input folder for the analysis. For human samples, choose “hg38” as reference genome and annotation by “refseq”. Choose an output folder and the stranded protocol (RNA-seq protocol). Samples were grouped in treatment-naïve versus DTP-derived clones and non-aggressive control versus aggressive DTP-derived clones. Then the analysis was started. Results were available as raw data; various plots (e.g. hierarchically clustered heatmaps) are shown with default threshold $p<0.05$ and $FC>2$.

2.13.2 Principal component analysis

The web tool ClustVis (Metsalu, Vilo, 2015) was used to create principal component analysis (PCA) plots. Principle components were calculated using Pareto scaling applied to rows (genes) and the Nipals PCA algorithm.

2.13.3 Preranked gene set enrichment analyses

Preranked gene set enrichment analyses perform a Gene Set Enrichment Analysis (GSEA) based on a ranking of genes provided by the user. The analysis determines whether a priori defined gene set at either ends of the ranking list shows a statistically significant enrichment and is correlated with the user-provided ranking. The program GSEA (v4.0.1) from US San Diego and the Broad Institute (Mootha et al., 2003, Subramanian et al., 2005) was used for analysis.

2.13.4 Statistics

Data is expressed as means ± standard deviation (SD) and for statistical analyses an unpaired Student's t-test was performed using Prism (GraphPad, v5.04). Volcano plots were constructed by an adapted R script (Blighe, K. *EnhancedVolcano*, 2018). The functional annotation clustering was done online with DAVID Bioinformatics Resources (v6.8) (Huang et al. 2009, Huang et al. 2009). The Kaplan Meier-Plotter was used for the KM plots (Nagy et al., 2018). All statistical tests were two-tailed and set to the significance threshold at 5%. Where indicated, p-values were adjusted for multiple testing using Benjamini-Hochberg procedure (Thissen et al., 2002). Correlation analysis was performed using Pearson's correlation coefficient.

In results, p-values were designated as follows: * = $p \leq 0.05$, ** = $p \leq 0.01$, *** = $p \leq 0.001$, **** = $p \leq 0.0001$.

3 Results

3.1 Drug-tolerant ovarian cancer persister cells

Drug-tolerant persister cells (DTP) represent a small but distinct subpopulation of cells in cancer, e.g. HGSOC, which is tolerant to chemotherapeutic agents and thus often leads to tumor relapse and therapy failure. In order to gain a better understanding of mechanisms that underlie drug tolerance of DTP, cells were isolated from the cisplatin sensitive OVCAR-3 cell line. DTP were exposed to cisplatin and surviving drug-tolerant colonies were isolated and expanded. The resulting cell lines were designated as DTP-derived clones. In addition, single clones were generated from the parental OVCAR-3 cell line using standard cell culture conditions and the consequent cell lines were designated as treatment-naïve (naïve) cells. The 12 DTP and 8 naïve clones were then examined for molecular and functional properties to identify features that distinguish DTP from naïve clones.

3.1.1 Morphological alterations in naïve and DTP-derived clones

During the generation and expansion of DTP and naïve clones, microscopic examination revealed filopodia-like structures in DTP that were not detected in naïves and the parental OVCAR-3 (OVCAR-3 par). Systematic investigation confirmed the presence of filopodia-like structures in each of the DTP and none of the naïve clones (Figure 10).

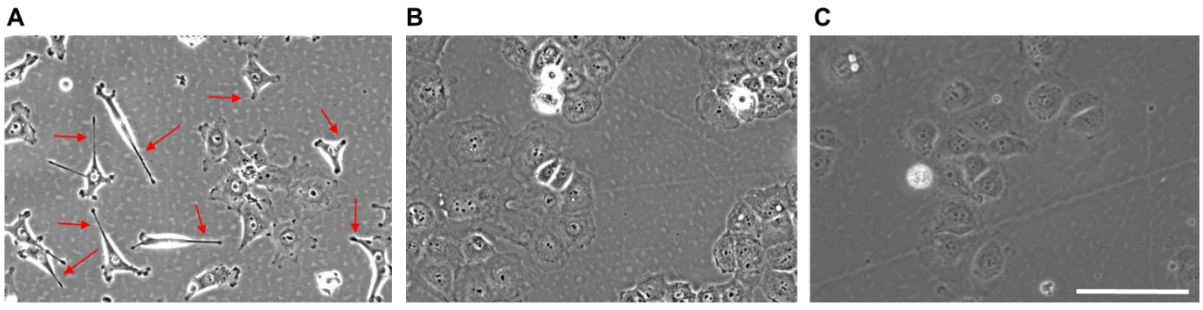

Figure 10: ***Morphologic phenotype****. Bright-field microscope images reveal pseudopodia-like structures (red arrows) in (A) DTP-derived clones that are absent in (B) naïve clones and (C) OVCAR-3 parental cells. Pictures were taken in passage 4-5 and are representatives for all generated clones of the cell model. Scale bar represents 200 µm.*

In contrast to DTP, OVCAR-3 par and naïve clones show a round morphology characteristic for epithelial cells, suggesting that the clones represent the parental cell

line. DTP showed a mesenchymal cell morphology, which is characteristic for migrating cells. The altered morphological phenotype in DTP was maintained for more than 20 passages.

3.1.2 2D migration in the wound healing assay

To analyze whether filopodia-like structures indicate altered migratory capacity DTP, a wound healing assay was performed. In this assay a scratch creates a gap in a cell monolayer and the gap-distance was measured at different time points (e.g. 0 h and 24 h). To exclude that clone-specific cell proliferation rates influenced gap-closure, the assays were performed in the presence of the proliferation inhibitor mitomycin C. Thus, the scratch assay allowed an estimation about how far the cells can migrate within 24 h. DTP-derived clones closed a larger distance (72.47 ± 9.9%) compared to naïve clones (45.25 ± 9.5%), suggesting that an altered morphology did indeed correlate with an augmented migratory capacity (Figure 11).

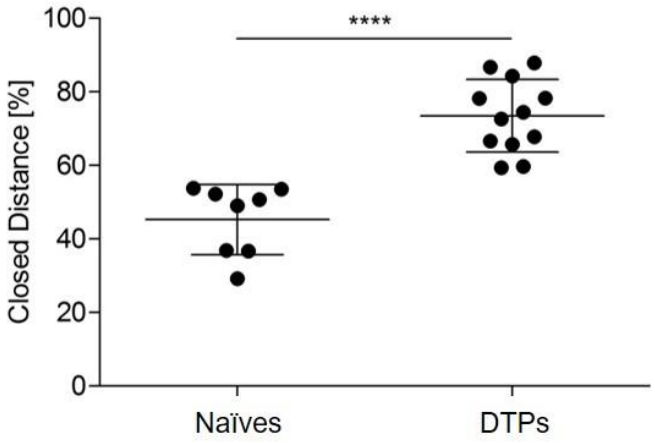

Figure 11: ***Wound healing assay****. Cells were seeded at identical density and a scratch was performed in the presence of mitomycin C. Cell migration was quantified by measuring the gap-distance after 24 h. DTP-derived clones (DTPs) show a significantly higher motility (p<0.0001) than treatment-naïve clones (naïves). Dots represent the mean of biological triplicate analyses per clone; lines represent mean ± SD of all clones. Distances were measured in ImageJ and calculated in MS Excel. The results were performed in cooperation with Andrea Gaißler. (n=3)*

3.1.3 Short- and long-term survival

In order to test whether the morphologic differences had an influence on apoptosis sensitivity to cisplatin, the short-term survival was investigated. During S-phase, cisplatin intercalates mainly with guanine and induces double-strand breaks, leading

to inhibition of cell replication and eventually to apoptosis. DTP and naïve clones were incubated in the presence of 13 µM cisplatin for 48 h, harvested and stained with AnnexinV-FITC and propidium iodide (PI) for flow cytometrical analysis. In this AnnexinV/PI assay, FITC+/PI+ indicated dead cells while living cells showed FITC-/PI-. In short-term survival experiments, the cell death of treatment-naïve (45.08 ± 19.1%) and DTP-derived clones (46.75 ± 21.6%) did not show significant differences (Figure 12A) and both groups displayed sensitive and non-sensitive clones based on the mean cell death.

Thus, on average no differences were found in short-term survival of DTP and naïve clones. To study the clonogenic survival of DTP-derived and treatment-naïve clones, a colony formation assay was further applied. Cells that enter senescence after incubation with cisplatin are detected as viable cells in the AnnexinV/PI assay. A colony formation assay is useful to determine the number of cells that can tolerate cytotoxic chemotherapy and form a colony in the presence or absence of cisplatin, i.e. these cells are theoretically capable of forming a new tumor site. The plating efficiency (PE) was determined and based on this the surviving fraction (SF) was calculated.

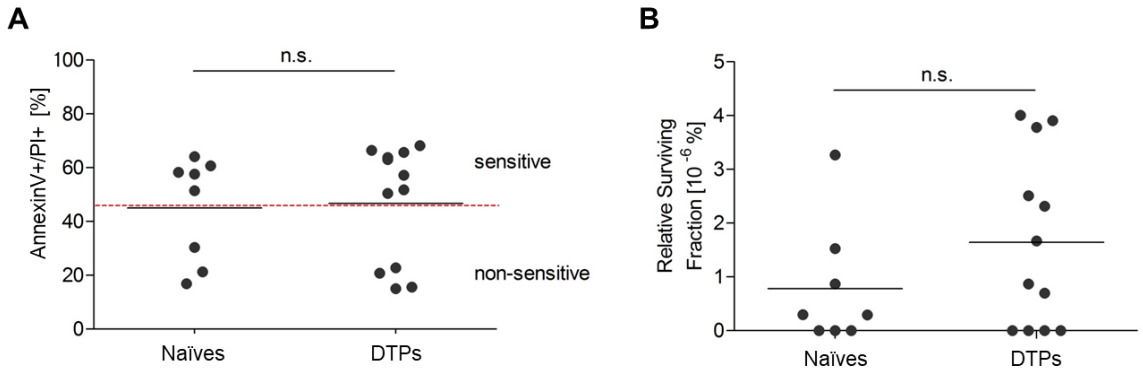

Figure 12: ***Short- and long-term survival of naïve clones and DTPs.*** *(A) To determine the short-term survival, naïve clones and DTPs were incubated in the presence of cisplatin for 48 h and cell death was analyzed by AnnexinV-FITC/PI and using flow cytometry. (B) Colony formation assay. Cells were seeded in the presence and absence of cisplatin. PE and SF were calculated for each naïve and DTP-derived clone. Dots represent the mean of biological triplicate analyses per clone, lines represent mean of all clones per group. The results were performed in cooperation with Andrea Gaißler. (n=3)*

The SF of the treatment-naïve clones ($0.78x10^{-6}$ ± $1.14x10^{-6}$%) was smaller than the SF of the DTPs ($1.65x10^{-6}$ ± $1.62x10^{-6}$%), as shown in Figure 12B. Due to a huge standard deviation, no significant difference was observed between the naïve and DTP clones (p=0.2).

In line with the results from the short-term survival assay, the two groups of treatment-naïve clones and DTPs did not show difference in long-term cisplatin survival, although DTPs tended to show a higher clonogenic survival. Both groups contained clones that were not able to survive cisplatin pulse incubation and form a new colony.

3.1.4 RNA-seq analysis of gene expression in naïve and DTP-derived clones

DTP is attributed to dynamic and non-mutational mechanisms that cause persistence. Therefore, alterations in gene expression were investigated. To study the differential gene expression of treatment-naïve and DTP-derived clones, the gene expression of each clone was analyzed by RNA sequencing (RNA-seq). All significant differentially expressed genes (DEG) (p_{adj}-values<0.05 and expression fold change (FC)>2) were marked in rows in the heatmap in Figure 13A. Columns represented the OVCAR-3 parental cell line, treatment-naïve and DTP-derived clones. RNA-seq data showed clustering of similar gene expression of treatment-naïve and parental cells. DTP-derived clones were clustered separately from the previous, suggesting that naïve clones are suitable representatives for the OVCAR-3 parental line. Interestingly, pearson clustering of the same naïves and DTP-derived clones (Figure 13B) indicated that the overall gene expression of these clones were highly similar (pearson correlation>0.998). This supports the assumption that the DTP phenotype is non-genetic.

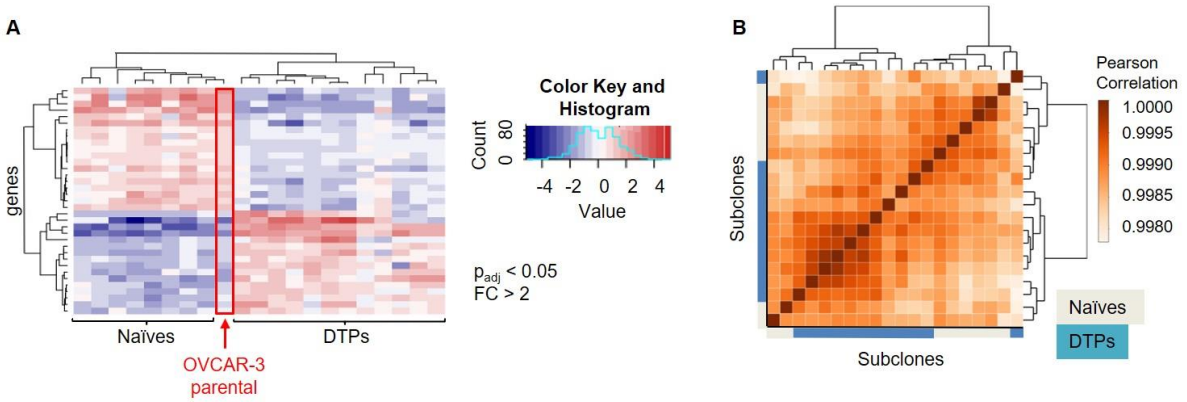

Figure 13: ***Bioinformatical results based on RNA-seq data.*** *(A) Hierarchical clustering heatmap of DEG (p_{adj}<0.05; FC>2; Appendix, A 2) in treatment-naïve and DTP-derived clones along with parental OVCAR-3 cell line. (B) Pearson correlation was calculated according to the gene expression between naïve versus DTP-derived clones indicated a high similarity of gene expression.*

The similar gene expression with the filter threshold FC>2 in comparison of treatment-naïve and DTP-derived clones resulted in 33 DEG (Appendix, A 2).

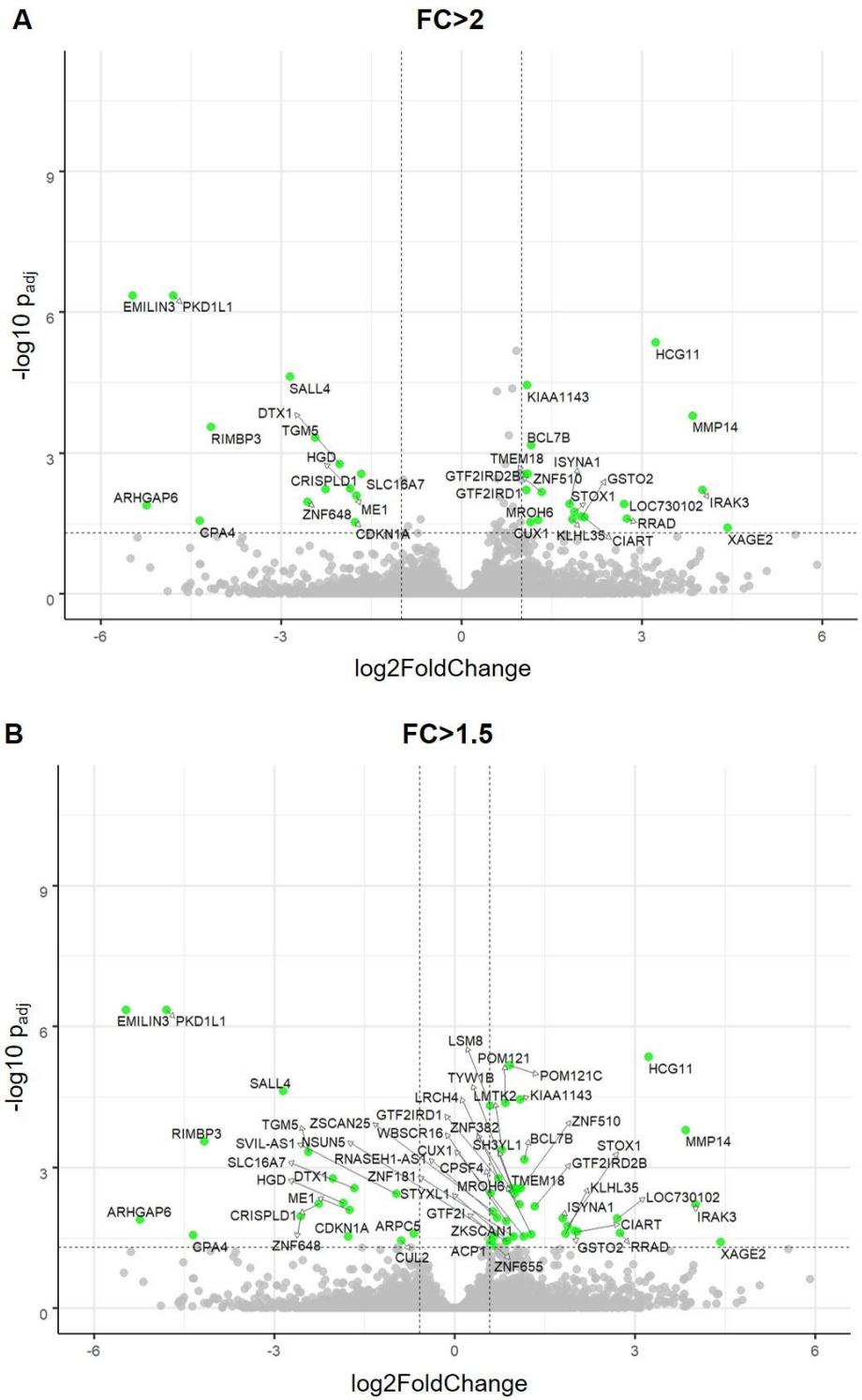

Figure 14: ***Volcano plots of genes in treatment-naïve versus DTP-derived clones****. Genes with* p_{adj}*<0.05 and (A) FC>2 (Appendix, A 2) and (B) FC>1.5 DEG (Appendix, A 3) are labeled and shown in green. Green dots indicate DEG, grey dots represent genes that failed the thresholds. Negative FC's represent upregulated genes of DTP-derived clones (naïve versus DTP). High values of* $-\log_{10} p_{adj}$ *values represent low* p_{adj} *values.*

At reduced FC threshold of 1.5, additional 22 DEG arose, resulting in 55 DEG (Appendix, A 3). Results based on both filter settings of the FC threshold values for DEG are shown in Figure 14 in two separate volcano plots. All further bioinformatics analyses will be conducted with DEG that show significant expression differences with the threshold FC>1.5 between treatment-naïve and DTP-derived clones.

In order to identify common molecular signaling pathways and relationships among genes, a functional gene-annotation clustering of the set of DEG (Figure 15) was performed. This analysis allows to examine gene lists by classifying highly related genes into functionally related groups, based on databases with published gene terms from functional annotation sources. The analyses revealed a nuclear localization and common biological function for the differentially expressed genes *ARPC5*, *HGD*, *TGM5*, *CPA4*, *DTX1*, *ZNF648*, *SALL4* and *CDKN1A* (Figure 15) that were altered (enrichment score = 0.77) in DTP-derived clones. The higher the enrichment value, the more frequently genes in similar gene function are described and thus the group of DEG is linked in its biological function.

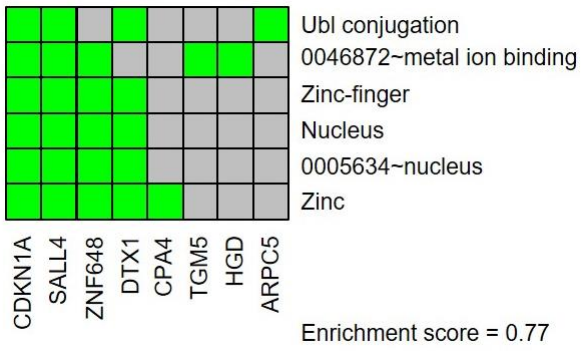

Figure 15: ***Functional gene-annotation-clustering of DEG.*** *All DEG were analyzed using Gene Functional Classification Tool (DAVID) to identify functionally related groups. A high relation of the genes ARPC5, HGD, TGM5, CPA4, DTX1, ZNF648, SALL4, and CDKN1A regarding their biological function in the cell nucleus was discovered.*

A common nuclear localization or interaction is not cancer specific and from these 8 genes, only three have been described in the context of cancer (*ARPC5*, *SALL4*, *CDKN1A*). For the remaining genes, an unknown function or other diseases have been reported so far.

Therefore, the next analysis was a gene set enrichment analysis (GSEA), using an ordered list according to their fold change of all genes detected in treatment-naïve versus DTP-derived clones. Comparing the ordered list to hallmark signature gene sets allowed to investigate if these genes were significantly enriched in upregulated or

downregulated genes. GSEA showed a significant enrichment for the Hallmark signatures angiogenesis, early estrogen response and myogenesis (Figure 16).

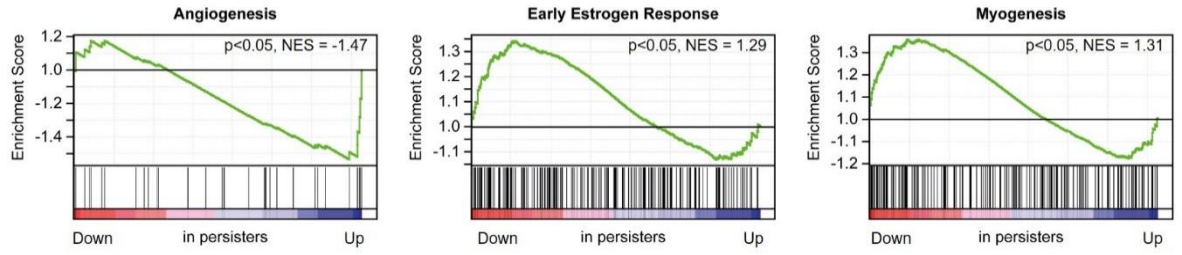

Figure 16: ***Gene set enrichment analyses of genes in treatment-naïve versus DTP-derived clones.*** *A pre-ordered gene list according to the fold change was compared to hallmark gene sets. The analyses identified enrichment for the Hallmark signatures angiogenesis, early estrogen response and myogenesis.*

This suggested that genes that are upregulated in DTP-derived clones were enriched in the hallmark pathway from the Molecular Signature Database (MSigDB) angiogenesis. Whereas downregulated genes from DTP-derived clones were enriched in early estrogen response and myogenesis. Overall, these results suggest that angiogenesis-related genes in DTPs tended to be upregulated.

3.1.5 Re-classification of treatment-naïve and DTP-derived clones

Clones within each group, regardless of origin, differed greatly in their extent of cisplatin-induced cell death and clonogenic survival (Figure 12). This phenotypic heterogeneity might have affected the ability to recognize transcriptional programs unique to DTP-derived cell populations. To identify the most aggressive clones within the entire panel and compare their gene expression profiles to those of the least aggressive clones, all clones were re-characterized (Figure 17). Aggressive clones were defined by the following criteria: i) less cisplatin-induced cell death than the mean, ii) higher clonogenic survival than the mean, and iii) higher motility than the mean. The least aggressive clones were defined as control clones that did not match any of the three criteria above. Three clones were identified that fulfilled the criteria for the aggressive phenotype. Noteworthy, all three clones were DTP-derived. In contrast, the three clones with the least aggressive phenotype were derived from the treatment-naïve controls. Therefore, the three most aggressive clones were called aggressive DTP (aDTP) and the three least aggressive clones were called non-aggressive controls (naControl). To further characterize the response of these groups to cisplatin,

naControl and aDTP clones were incubated with increasing cisplatin concentrations and analyzed for cell viability.

A

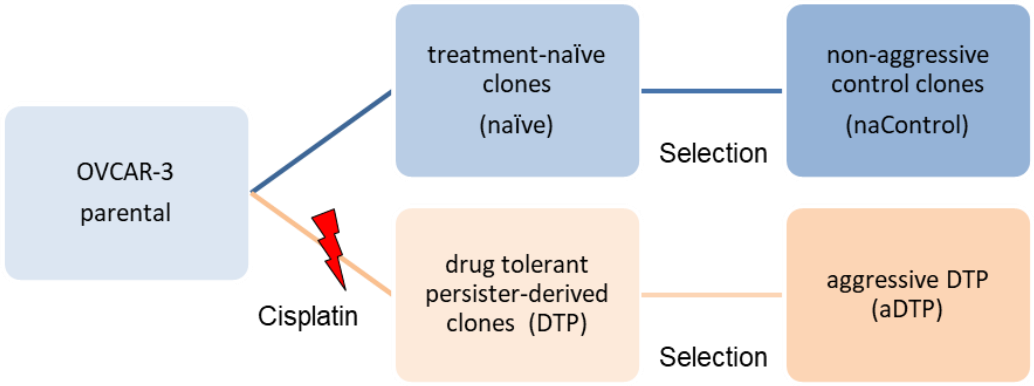

B

Clones	Attributes			Reclassification
	Short-term cisplatin survival	Long-term cisplatin survival	Migration	
Naïve	↓	↓	↓	Non-aggressive controls (naControl)
DTP	↑	↑	↑	Aggressive drug tolerant persister cells (aDTP)

Figure 17: ***Re-classification of naïve and DTP-derived clones.*** *(A) Flow chart of generation of naControl and aDTP clones. (B) Re-classification of treatment-naïve and DTP-derived clones based on functional attributes (selection criteria) according to cisplatin survival and migration correlating with aggressive tumors.*

The EC_{50} values of naControl and aDTP clones were determined, resulting in a significantly higher EC_{50} mean of aDTP (20.15 ±7.27 µM; $p<0.05$) than the mean EC_{50} of the control clones (10.37 ± 4.13 µM). This suggests a significantly higher average tolerance of aDTP to cisplatin than of the naControl clones (Figure 18).

3.1.6 Cisplatin tolerance of naControl and aDTP clones

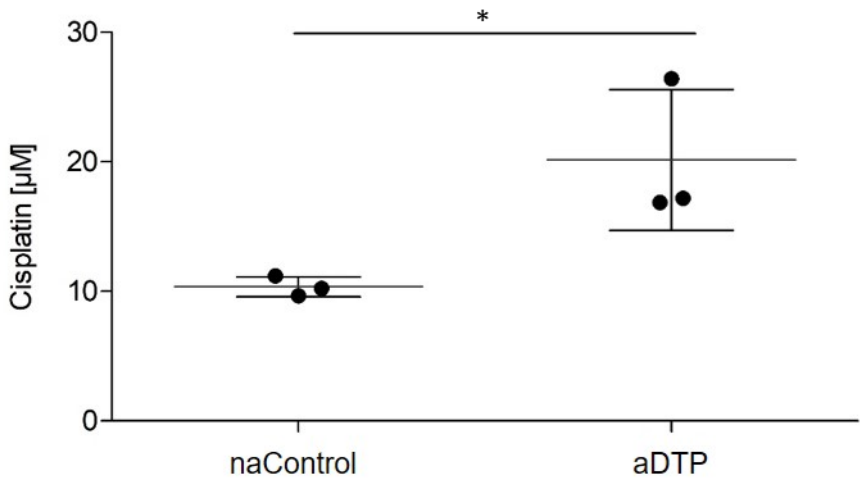

Figure 18: ***Cisplatin EC_{50} of naControl and aDTP clones.*** *Each clone is illustrated by a dot and lines represent means of triplicates ± SD. (n=3)*

Viability assays showed significant differences in naControl and aDTP clones using cisplatin concentrations between 10-20 µM (Figure 19). Nevertheless, in line with a persistent phenotype, the results showed that higher cisplatin concentrations (40 µM) still efficiently induced cell death in aDTP. Moreover, aDTP retained a drug-tolerant persister phenotype for more than 20 passages.

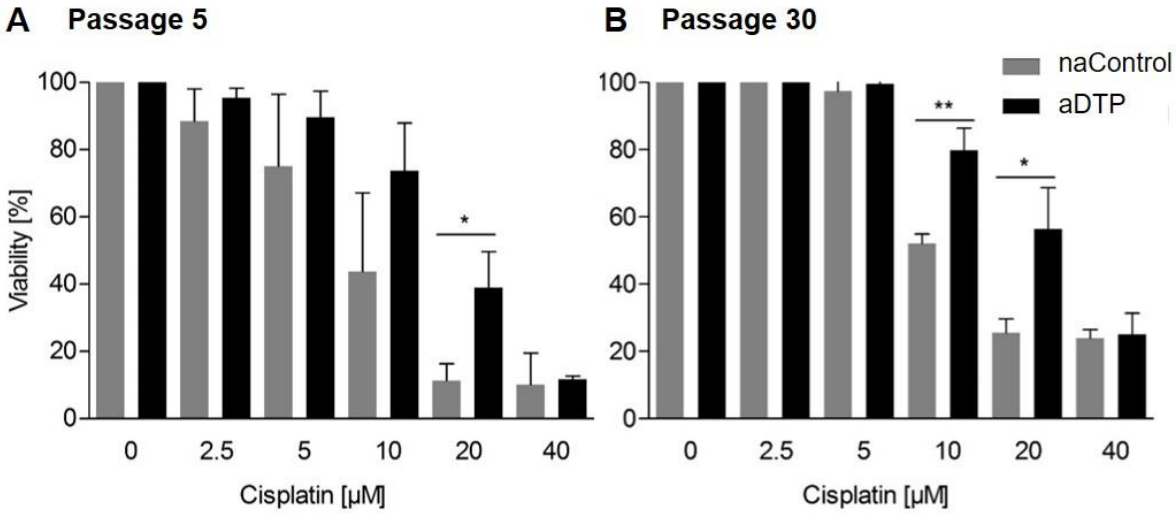

Figure 19: ***Viability assay of naControl and aDTP clones.*** *Cell viability of the six clones was analyzed using MTT and cell titer glow assays at (A) passage 5 and (B) passage 30. (n=3)*

3.1.7 Proliferation of naControl and aDTP clones

The cell proliferation of control clones and aDTPs was measured to determine the doubling time of the cells.

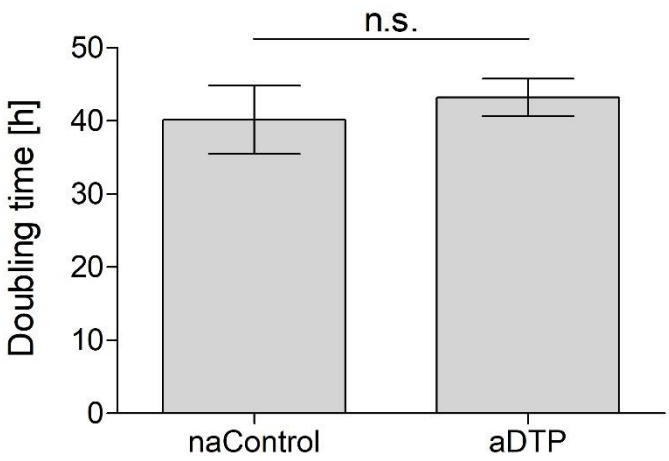

Figure 20: ***Population doubling time of naControl and aDTP clones.*** *The cells were seeded and the cell count was determined in consecutive days to calculate the doubling times. Lines indicate mean ± SD. (n=3)*

Both, naControl (40.16 ± 4.7 h) and aDTP clones (43.22 ± 2.6 h) showed similar doubling times with no significant difference (p=0.38, Figure 20), resulting in no differences in their proliferation rate.

In retrospect, the RNA-seq data were re-analyzed. This time only the selected subset of three naControl clones and three aDTPs were compared. Remarkably, this analysis revealed a much higher number of DEG (334 DEG; Appendix, A4, Figure 21) than the bulk comparison of the two groups (compare to Figure 14).

3.1.8 Gene expression analysis of naControl and aDTP clones

The list of DEG was examined with regard to upregulated genes of aDTP associated with general aggressiveness, resistance, metastasis and endoplasmic reticulum (ER) stress in cancer. In this context, several genes were identified that are significantly upregulated in aDTPs and involved in one or more of the categories. Most highly upregulated genes with a generally described oncogenic function were *COL23A1*, *TRIM29*, *ST3GAL1*, *EGR3*, *SLC2A13*, *CHST15*, *C10orf128*, *ALDOC*, *CDKN1A*, *SPTLC3*, *ABCG1*, *LGALS17A*, *CEACAM1*, *TNS4*, *SUSD2*, *HES2 and ANKRD45*.

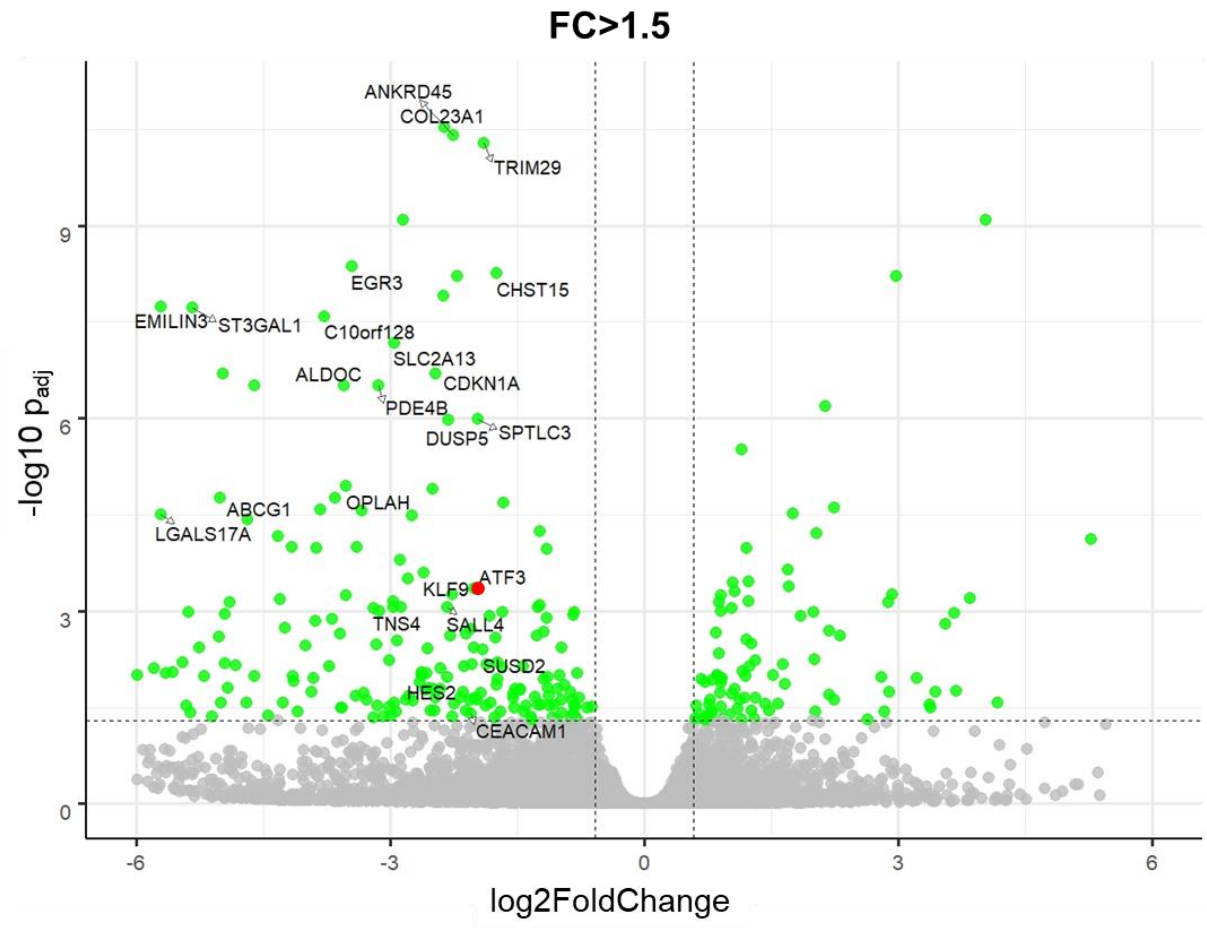

Figure 21: ***Volcano plot of all genes of the comparison naControl versus aDTP clones.*** *Green dots indicate 334 DEG (list of genes see Appendix, A4) with p_{adj}<0.05 and FC>1.5; grey dots represent genes that did not pass the threshold. Selected DEG were labeled. Red dot highlights ATF3. Negative FC's refer to upregulated genes in aDTP (naControl versus aDTP) clones.*

OPLAH and *SALL4* have been described in the context of drug resistance and *EMILIN3*, *CEACAM1* were reported to play a role in angiogenesis. *PDE4B*, *KLF9, IL-6, DUSP5* and *ATF3* were identified as genes that were involved in ER stress. Many of the already mentioned genes had no or only a small number of reads. All genes that were not expressed or only expressed in small amounts in the six clones were removed. After applying this filter step, RNA-seq additionally revealed that *ATF3*, *COL23A1*, *DUSP5*, *PTPRU* and *SLC2A9* were top hits with highest FC's. Since the effect of *ATF3* is induced by its gene expression level, the focus was set on *ATF3*. *ATF3* was significantly higher expressed in aDTP than in naControl clones (highlighted in red in Figure 21), according to high FC and low p_{adj} values. The gene expression was also validated using real time qPCR (qRT-PCR, Figure 22A). Enhanced *ATF3* expression is also an indicator of an ER stress response. Notably, differential *ATF3* expression was maintained in cultured aDTPs for more than 20 passages (p<0.01,

Figure 22B). Significantly and non-significantly regulated ER stress-related genes in three naControls and three aDTPs were illustrated in a heatmap (Figure 22C). The results indicate a tendency of an increased ER stress-related phenotype in aDTP.

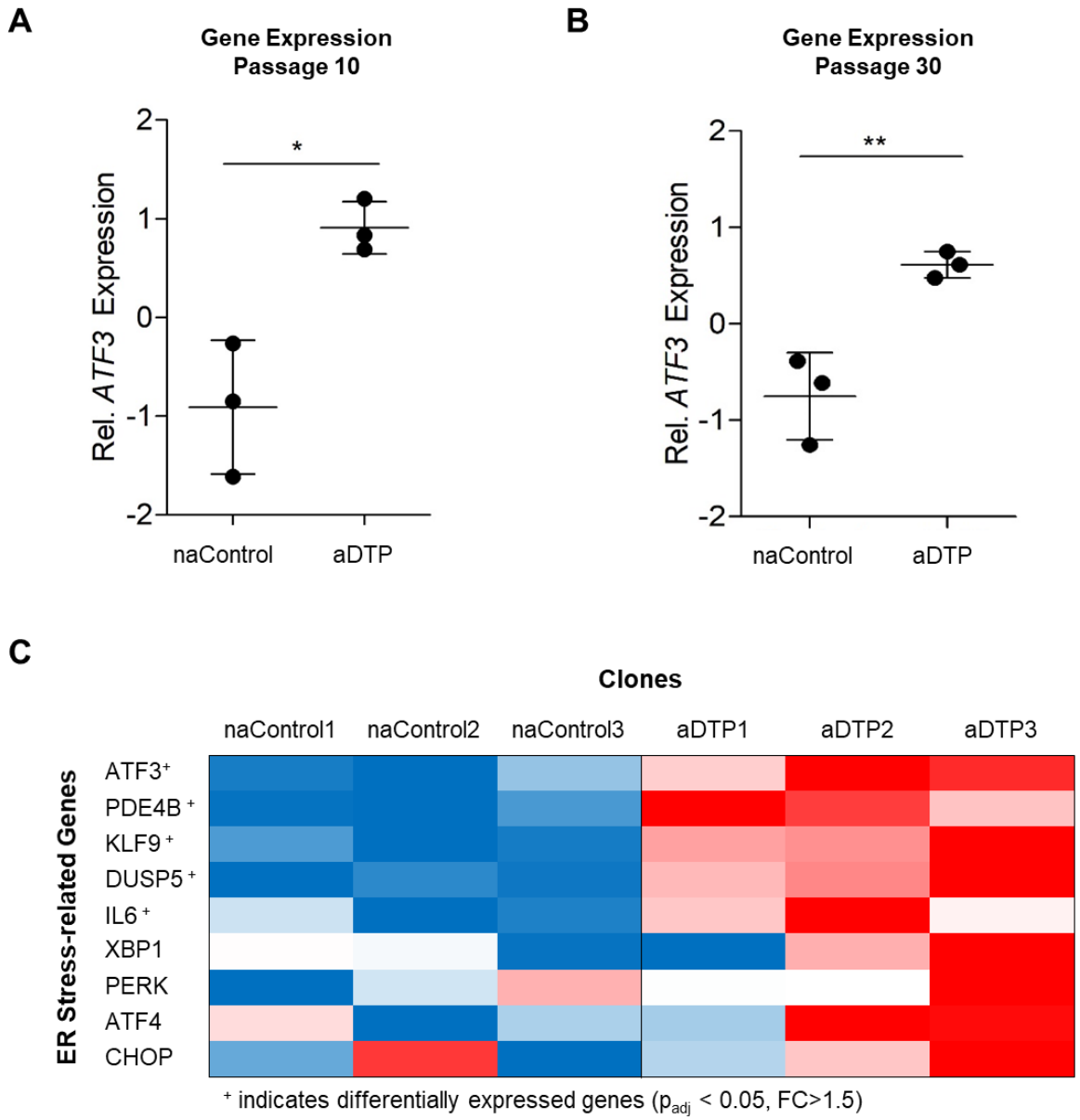

Figure 22: ***Gene expression of ER stress-related genes between naControl and aDTP clones.*** *(A) Elevated ATF3 gene expression was verified by qRT-PCR (p<0.05, n=3) and shows that (B) the upregulation is maintained over 20 passages. (n=3) (C) Heatmap of ER stress-related gene expression is illustrated for each clone. Upregulation is shown in red and downregulation in blue. + indicates DEG.*

3.1.9 *In silico* investigation of clinical data of HGSOC patients

To test the relevance of the results for HGSOC patients, clinical TCGA data from 380 patients with HGSOC was analyzed. Nearly all (>96%) HGSOC tumors are p53

mutated. Therefore, patients with mutated p53 tumor samples were selected to collect data obtained from the correct subtype and to confirm the selection criteria for HGSOC.

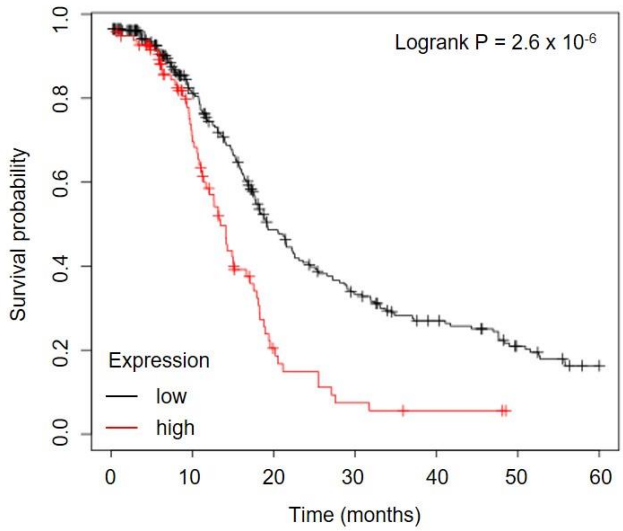

ATF3 expression	5-year survival rate
low	20%
high	0%

Figure 23: ***Kaplan-Meier-Survival plot of ATF3 gene expression in HGSOC patients.*** *TCGA survival data of a cohort with 380 p53 mutated HGSOC patients was analyzed regarding survival probability of patients with high (red line) and low (black line) ATF3 expression.*

Analysis of this data revealed that high expression of *ATF3* in the majority of cases, was associated with a significantly lower 5-year-survival rate (Figure 23, logrank $p=2.6\times10^{-6}$).

Taken together with the *in vitro* results, this suggest that ER stress markers, exemplified by *ATF3*, might correlate with cisplatin survival of aDTP that eventually give rise to tumor relapse in ovarian cancer.

3.2 Advanced 3D cancer models

In this work, advanced 3D cancer models including a 3D hydrogel-based model and a tissue slice model were optimized and cultivated under the technical aspect of methodology. Agarose and alginate were used as hydrogels to form the 3D hydrogel-based model, which had a similar shape as the tumor tissue slices. The three different cultivation methods floating (FL), Millipore Filter (MF) and the novel perfusion air culture system (PAC) were tested for their effects on the cultivation of the cell-hydrogel slices as a 3D cancer model.

3.2.1 Hydrogel embedding of cells to form 3D models with defined shapes

The cell line cells, which are commonly cultured as 2D monolayer or in suspension, were embedded in either agarose or alginate hydrogels to form the 3D hydrogel-based model with a defined shape and desired thickness.

3.2.1.1 *Agarose embedded 3D cultivation model*

In order to investigate if agarose is a suitable material to form a 3D hydrogel-based model with a defined structure, the human ovarian cancer cell line A2780 was used to be embedded in 3% agarose gel within a silicon chamber to form a slice-like 3D model using the rectangular shape of the silicon chamber. In 60 µL agarose gel, 5×10^5 cells were successfully embedded and formed the slice-like 3D model with ~0.8 mm thickness. The formed cell-agarose slices were cultured in the FL, MF or PAC system. The gelation process to form the cell-agarose slices with a silicon chamber was adapted on the temperature of the agarose. The pipetting of low volume agarose gel is hard to control and the actual volume might be not exact due to viscosity of the agarose. High temperatures are favorable for pipetting but not for cell survival. This made the time range for the experiments very short. The mixture of the cells and the agarose gel had to be done quickly. As shown in Figure 24B, the formed cell-agarose slices were not equally and consistent, different slices contained different cell densities. Figure 24A indicates that the cells were still encapsulated inside the agarose gel and started to proliferate and built cell associations in the cell-agarose slices after 3 days of culture. Immunohistochemistry (IHC) staining showed biomarkers for proliferation

(Geminin, GMNN) and apoptosis (cleaved caspase 3, CC3) (Figure 24B), indicating that IHC staining could be successfully carried out after culture in the FL system.

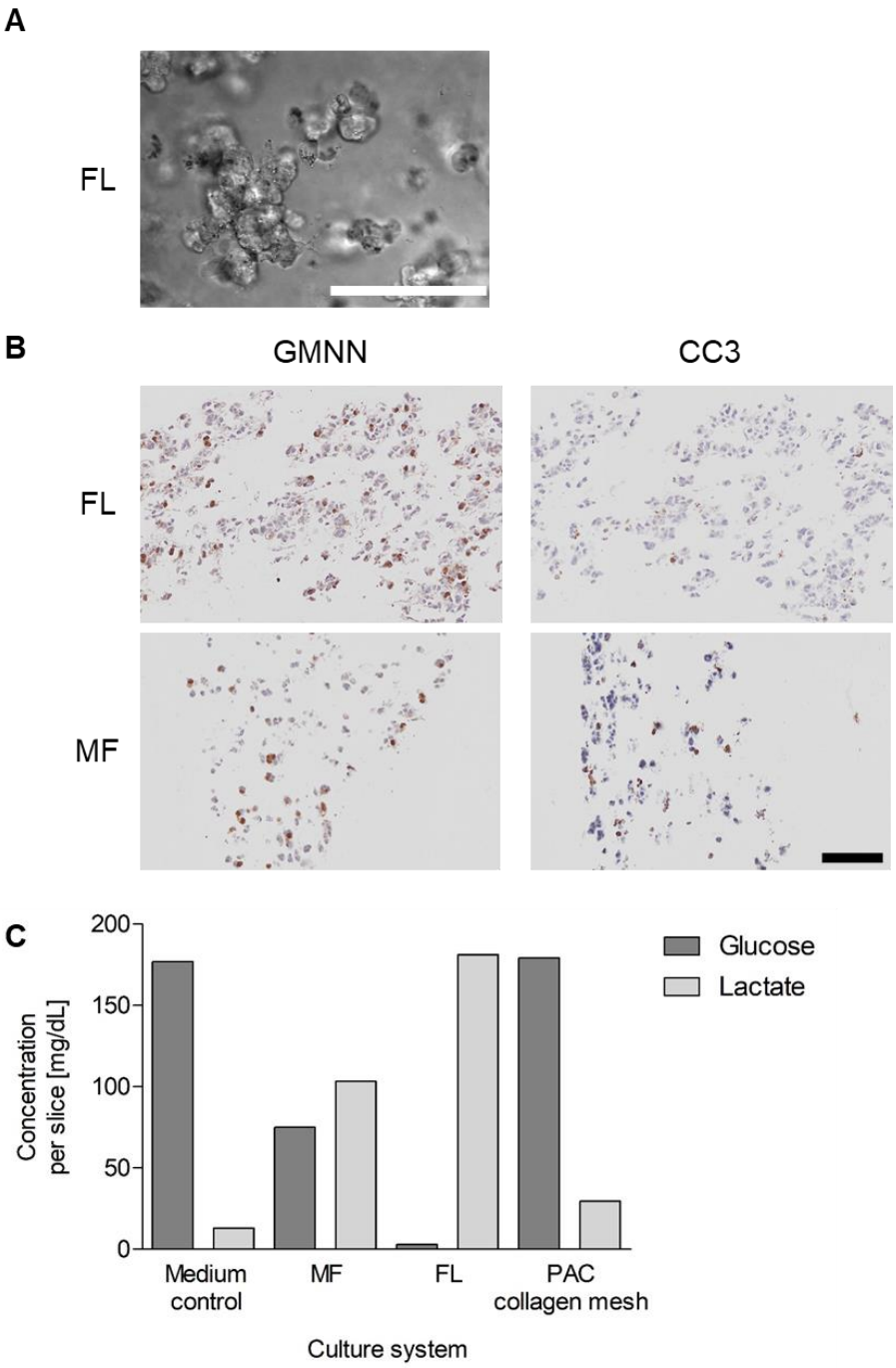

Figure 24: ***Microscopic images of agarose embedded A2780 cells and measurement of glucose and lactate in the cell culture medium****. After 3 days of culture as cell-agarose slices, the images are shown as (A) a standard transmitted-light bright-field microscope and (B) immunohistochemical (IHC) staining for proliferation (Geminin, GMNN) and apoptosis (cleaved caspase 3, CC3). All scale bars correspond to 100 µm. (C) On day 3 the cell culture medium was investigated after culture in the MF, FL, and PAC system to compare the glucose consumption and lactate production of the embedded A2780 cells. As organotypic support in the PAC system, collagen mesh is chosen with a perfusion rate of 27 µL/h. MF and FL systems do not require additional meshes. (n=1)*

The culture of the cell-agarose slice in the MF system showed similar IHC staining for GMNN+ cells and a slightly higher CC3+ cell number which suggests a similar cell proliferation, but higher apoptosis ratio compared to the FL culture system. Unfortunately, the data from the PAC system were not available since the cell-agarose slices were degraded during the process of dehydration and paraffin embedding for the IHC staining. The reason for this might be that the conditions used in the PAC system for the cell-agarose slices cultivation were not suitable for the hydrogel-based 3D models. This topic will be addressed in detail in the discussion part of the present work.

After the cultivation period, the glucose and lactate concentration in the media from the culture systems were measured to test the glucose consumption and lactate production of the embedded cells during the culture. The highest lactate and lowest glucose concentration per slice were found in the medium of the FL system (Figure 24C). This result was consistent with the high number of GMNN+ cells shown in Figure 24B. Since the MF system cultured cell slices also contained GMNN+ cells, the higher glucose and lower lactate concentration compared to FL seemed to indicate less anaerobic metabolism in the MF system. Cultivation in the PAC system indicated no detectable glucose and only a minor increased lactate concentration.

3.2.1.2 *Alginate embedded 3D cultivation model*

Alginate was also tested as a hydrogel to form the 3D hydrogel-based cultivation model with a defined structure. MCF-7 cells with a cell number of 1.3×10^6 were successfully embedded in 100 µL 1.1% (w/v) alginate to form cell-alginate slices using a silicon chamber. The ~1 mm thick cell-alginate slices were cultivated in FL, MF and PAC cultivation systems. In contrast to agarose, the gelation process to form cell-alginate slices is not depended on temperature. Alginate gels are formed with divalent cations, such as $CaCl_2$. Therefore, the gelation process was much easier to handle than that of cell-agarose slices. After 3 days culture, the cultivated cell-alginate slices could be processed to IHC and stained for cell function (estrogen receptor, ER), DNA damage (γH2AX) and hypoxia (Hif1α). Compared to the FL system, the cell-alginate slices cultured on MF system showed more ER+ cells indicating a better culture condition (Figure 25). Cells stained for γH2AX+ were found in both FL and MF systems after culture, and only very few cells were Hif1α+ after 3 days culture. The same as cell-agarose slices, the cell-alginate slices cultured in the PAC system were degraded

during the process of dehydration and paraffin embedding for the IHC staining. The reason for this is the same as the cell-agarose slices. These data were also not available and will be further addressed in the discussion.

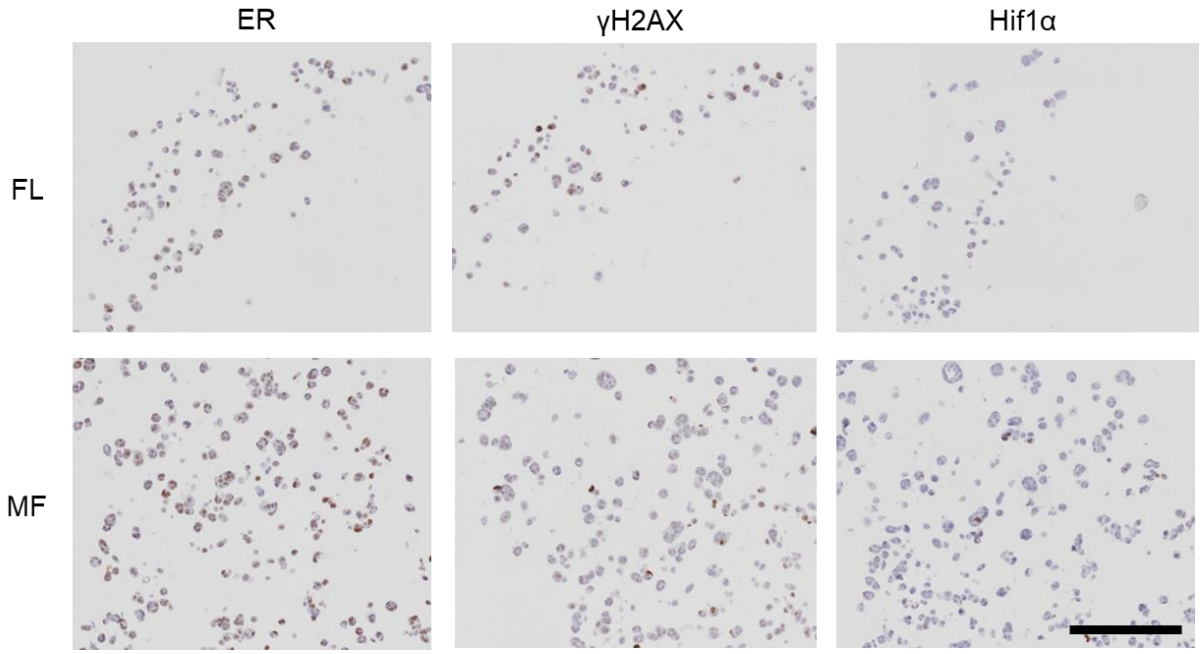

Figure 25: ***IHC staining of alginate embedded MCF-7 cells****. A number of 1.3×10^6 MCF-7 cells were embedded in 100 µL 1.1% alginate using silicone separation chambers and cell slices were cultured for three days in FL and MF. Cells were stained for function (ER), DNA damage (γH2AX) and hypoxia (Hif1α). Scale bar represents 200 µm. (n=1)*

Since IHC evaluation of the cells was difficult after PAC culture, the cell-alginate slices were also analyzed by a live-dead assay. The cells were stained with different fluorescence dyes for cell nuclei (DAPI), viable cells (TMRM) and dead (Picogreen) (Figure 26A). Cells cultured in all three systems indicated a high level of cell viability, only sporadically few dead cells could be observed, most of them were found in the PAC system. To investigate the metabolic activity of the cells, the cell culture medium was subsequently analyzed on day 3 of culture from the respective culture systems. The lowest pH value of 6.6 was measured in the cell culture medium after culture in the FL system (Figure 26B).

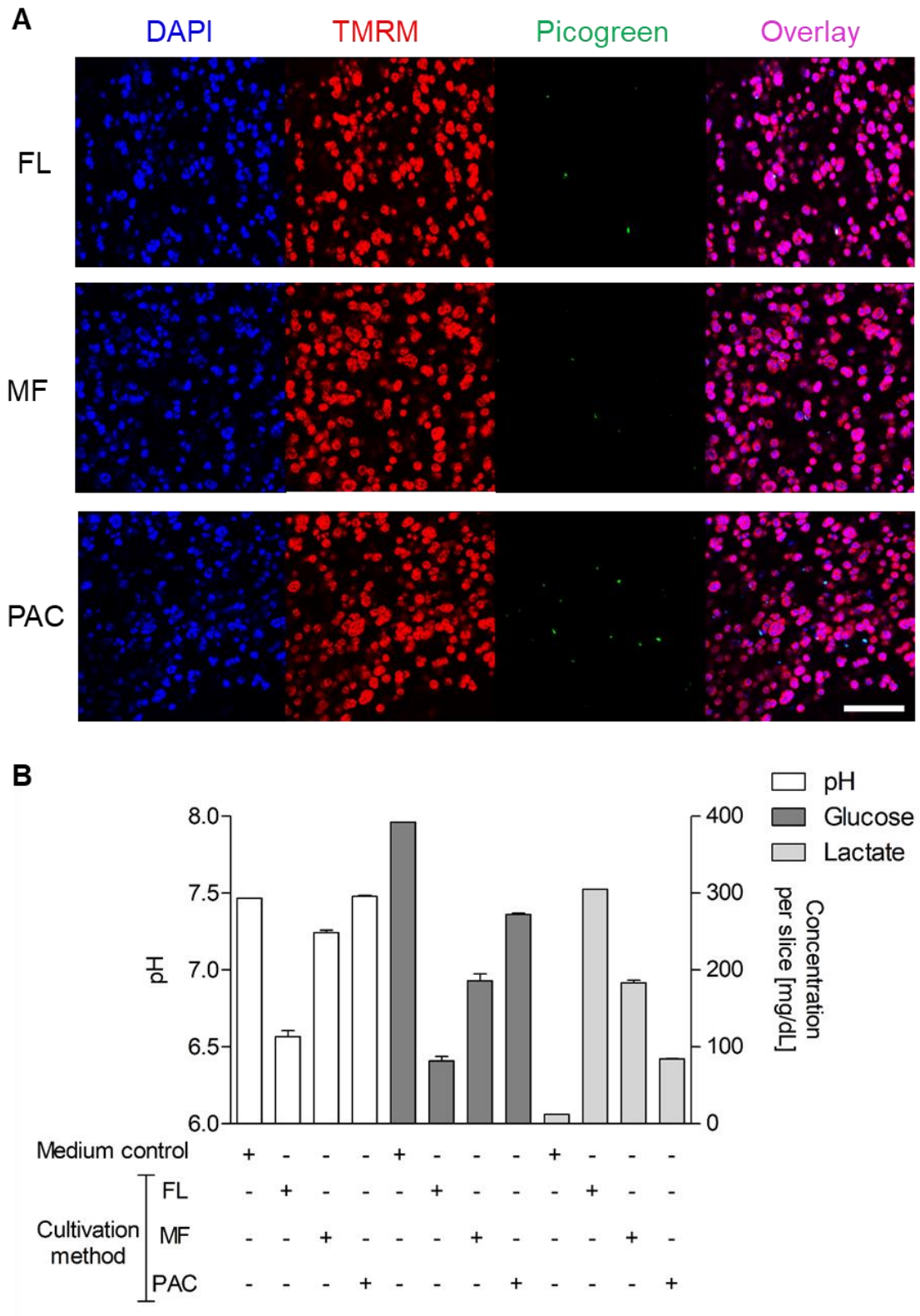

Figure 26: ***Live-dead staining of 1.1% alginate embedded MCF-7 cell slices and cell culture medium analysis after 3 days culture.*** *(A) After culture in FL, MF or PAC system, cells were stained for cell nuclei (DAPI), viability (TMRM) and dead cells (Picogreen). Images were taken from a thin part of the slices. Scale bar corresponds to 100 µm. (n=1) (B) The supernatant was collected after culture in FL, MF and the medium flow-through after culture in the PAC systems. Subsequently, pH, glucose and lactate were measured in the culture media. The organotypic support in the PAC system was cotton mesh and a perfusion rate of 27 µL/h was chosen. Bars represent means ± SD. (n=2)*

The culture in the FL system also resulted in lowest glucose (81.9 mg/dL) and highest lactate concentrations (305.1 mg/dL) compared to the other cultivation systems. Cell culture medium in the MF system showed a pH value of 7.2 with 186.2 mg/dL glucose and 183.5 mg/dL lactate concentrations. After cultivation in the PAC system, a pH value of 7.4 was measured, which was similar to the medium control and 272.5 mg/dL glucose and 84.5 mg/dL lactate were measured.

The next step was to investigate whether the cell number embedded in the gel influences the cells during the 3D cultivation. Since alginate showed better properties to form the hydrogel-based 3D models than agarose, alginate was chosen for further experiment. For this purpose, 1, 1.5 and 3×10^6 MCF-7 cells were embedded into 80 µL 1.1% alginate and cultured in the FL system for 3 days. Since alginate gel can be dissolved again, the cell-alginate slices were dissolved with 55 mM Na-Citrate in 0.15 M NaCl (pH 6.8) after culture to determine the cell viability using AnnexinV staining and flow cytometry. The cell-alginate slice containing 10^6 MCF-7 cells indicated 38.31% AnnexinV+ cells, the 1.5×10^6 containing slice showed 41.78% and the doubled cell number with 3×10^6 MCF-7 cells had 41.12% AnnexinV+ cells (Figure 27A). In conclusion, the highest number of AnnexinV+ cells in the cell-alginate slices was measured with 1.5×10^6 MCF-7 cells, but with only minor differences of 3.5% to the lowest AnnexinV measured sample. Additionally, the cell culture medium was analyzed on day 3 (Figure 27B). The highest concentrations of glucose (283.9 mg/dL) and lactate (>270.2 mg/dL, above measuring range) were measured in the cell-alginate slice with 3×10^6 MCF-7 cells. Only small differences between the 1 and 1.5×10^6 cell-alginate slices were determined: 188.1 versus 182.6 mg/dL glucose concentration and 216.1 versus 235 mg/dL lactate concentration. The cell-alginate slices with 1.5 and 3×10^6 cells were further analyzed via IHC staining (Figure 27C). Both slices showed less ER+ stained cells, many KI67+ cells and some γH2AX+ cells after 3 days of FL culture. The slice with 3×10^6 cells seemed to show slightly more γH2AX+ cells.

The chosen embedded cell numbers did not show huge differences in cell death, biomarker expression, glucose and lactate concentrations. The chosen cell density range did not seem to influence the culture condition.

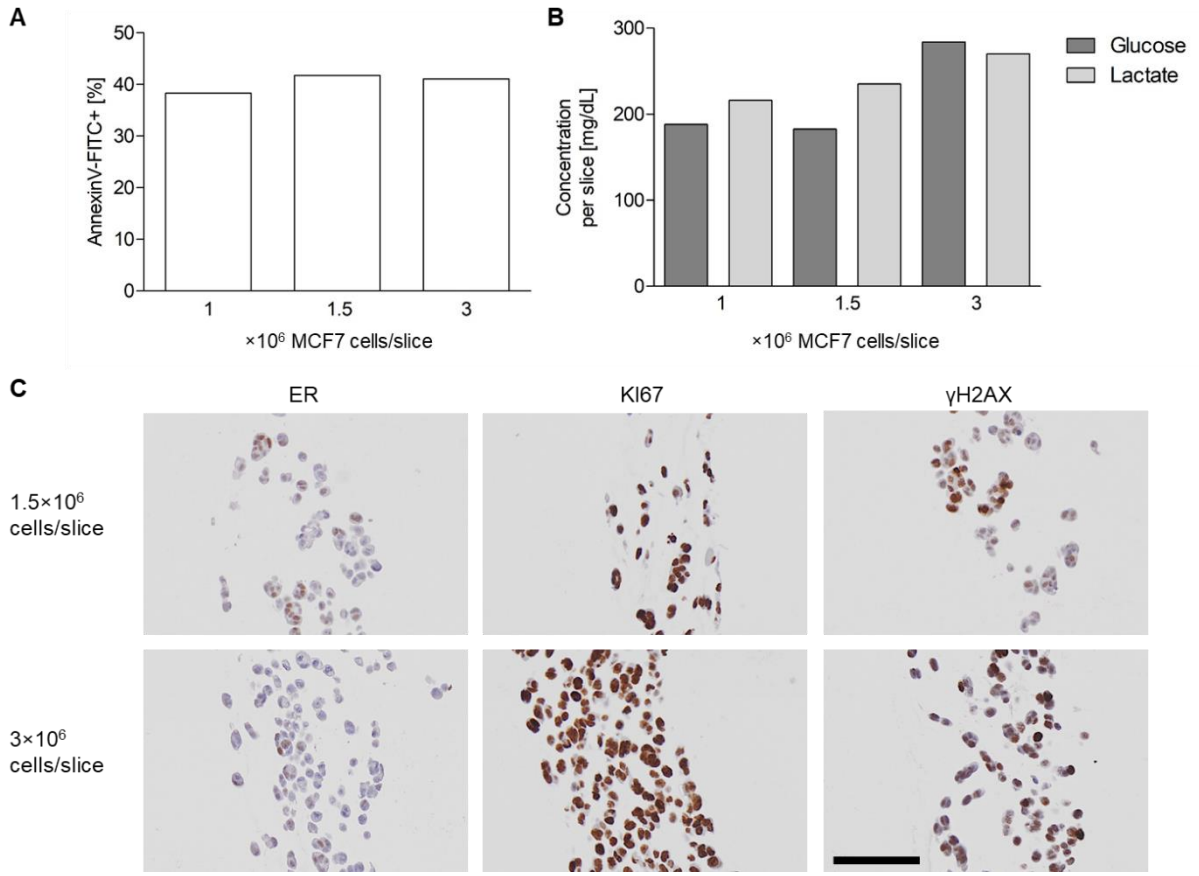

Figure 27: ***Comparison of different embedded cell numbers in alginate.*** *Alginate embedded MCF-7 cell slices containing 1, 1.5 or 3×10⁶ in 80 µL were analyzed after three days of cultivation in the FL system. (A) Flow cytometrically staining for AnnexinV to determine cell death in the cell-alginate slices with 1/1.5/3×10⁶ embedded MCF-7 cells. (B) Analysis of the cell culture supernatant after cultivation in the FL system. (C) The cells were immunohistochemically stained for their function (ER), cell proliferation (KI67) and DNA damage (γH2AX). The scale bar represents 100 µm. (n=1)*

To improve the cultivation conditions further regarding cell viability and proliferation, alginates from 3 different manufacturers were tested. In addition, the crosslinking divalent cation $BaCl_2$ was also tested as a replacement for the previously used $CaCl_2$, as $BaCl_2$ has a higher affinity to alginates. The cell viability after 3 days of cultivation on MF system was examined. The cross-linking performed with $BaCl_2$ (Figure 28A) showed the lowest number of AnnexinV+ cells in Mino using Alginate 2, most AnnexinV+ cells were found using Alginate 1 (Table 4) and Alginate 3 in the cell line. Calu-1 showed small differences between Alginate 2 and 3, and only few positive cells using Alginate 1.

In addition, the crosslinker $CaCl_2$ was used for the cell-alginate slices from Mino and Calu-1 instead of $BaCl_2$. After 3-day culture in the MF system, (apoptotic) cells were determined. It is noteworthy that no approach showed more than 25% AnnexinV+ cells, regardless of the choice of alginate or cell line (Figure 28B).

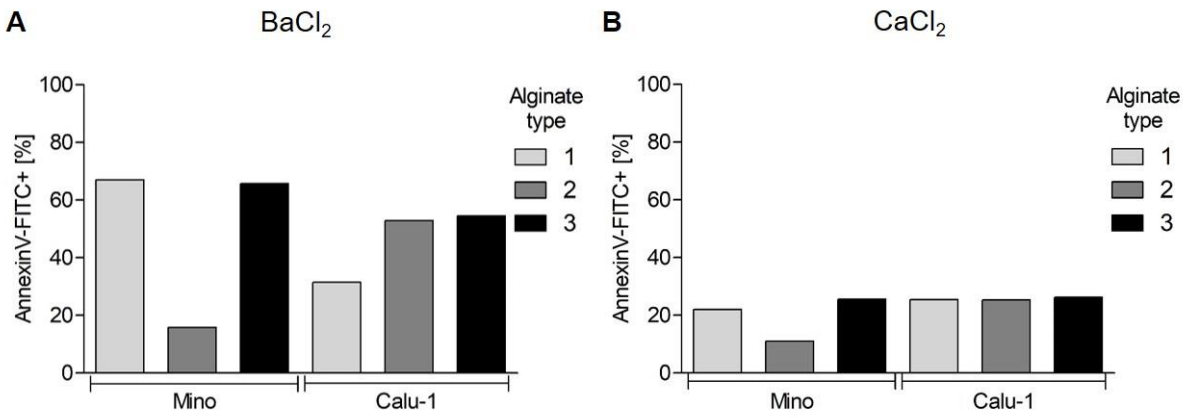

Figure 28: ***Comparison of three alginates and different crosslinking chemicals after culture in the MF system for 3 days****. The suspension MCL cell line Mino and the adherent lung cancer cell line Calu-1 were investigated. All cell types were embedded to cell-alginate slices. (A) Alginate crosslinking was conducted using $BaCl_2$ and the cells were flow cytometrically analyzed with AnnexinV staining. (B) Alginate crosslinker $CaCl_2$ was used and AnnexinV+ cells of the dissolved cell-alginate slices were determined. (n=1)*

Overall, using the crosslinker $CaCl_2$ resulted in fewer AnnexinV+ cells in all Alginate types used compared to $BaCl_2$. Therefore, $CaCl_2$ seemed to be the better choice of crosslinker regarding the cell viability after cell-alginate slice cultivation.

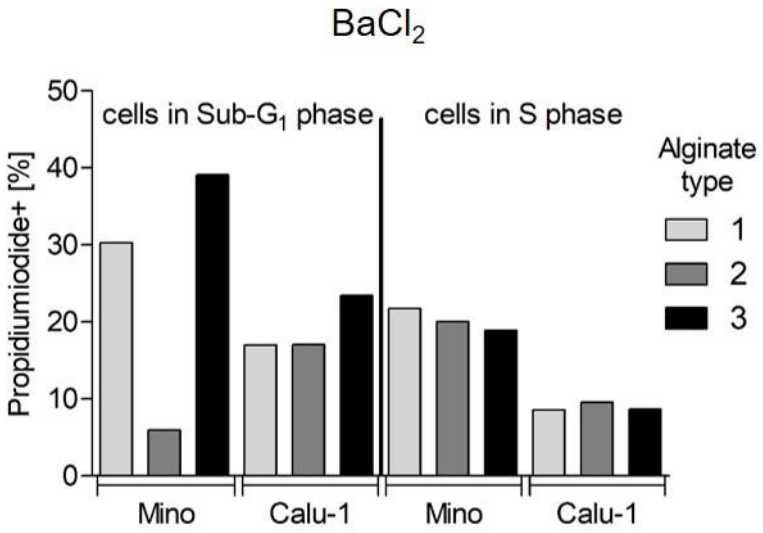

Figure 29: **Cell cycle analysis of cell-alginate slices after 3-day cultivation on a MF.** Cell cycle analysis of cells after cell-alginate slice cultivation using $BaCl_2$ as crosslinker. PI staining was conducted to determine cells in the S or Sub-G_1 phase.

Staining the cells with PI allowed differentiation between the cell cycle phases in which the cells are in. The Sub-G_1 phase indicated fragmented and apoptotic cells. This revealed that the most apoptotic cells ranged between 23.42 - 43.94% after culture in Alginate 3 for all cell lines (Figure 29). Less apoptotic cells (5.97%) were seen using

Alginate 2 in the MCL cell line and Alginate 1 culture led to 22.93% apoptosis. Calu-1 showed 17% apoptotic cells using Alginates 1 or 2. Interestingly, all approaches of the MCL cell lines ranged around 20% cells in S phase. In Calu-1 all used Alginates showed 8.6-9.6% cells in the S phase after 3 days culture. These experiments were further conducted with the MCL cell line Jeko-1 with similar results as seen in Mino cells (data not shown). Taking the proliferation and apoptosis into account, for Mino cells Alginate 2 was the alginate of choice and Calu-1 cells were best cultured in Alginate 1 or Alginate 2.

3.2.2 Tumor tissue slice culture

3.2.2.1 *Culture of cell-line derived xenograft (CDX) tissue slices in the MF and PAC system*

Tissue slices from different types of cell line-derived xenografts (CDX) were cultured in the perfused air culture (PAC) system. For comparison, tissue slices were also cultivated in the commonly used procedure on a Millipore filter (MF) at the same time. For H1437 lung cancer CDX tissue slices, hypoxia (Hif1α), DNA damage (γH2AX), proliferation (KI67) and apoptosis (cleaved caspase 3, CC3) were used as biomarker read-out in IHC staining to evaluate culture stress in MF and PAC culture systems. Tissue slices were compared to non-cultivated control tissue from day 0 (d0).

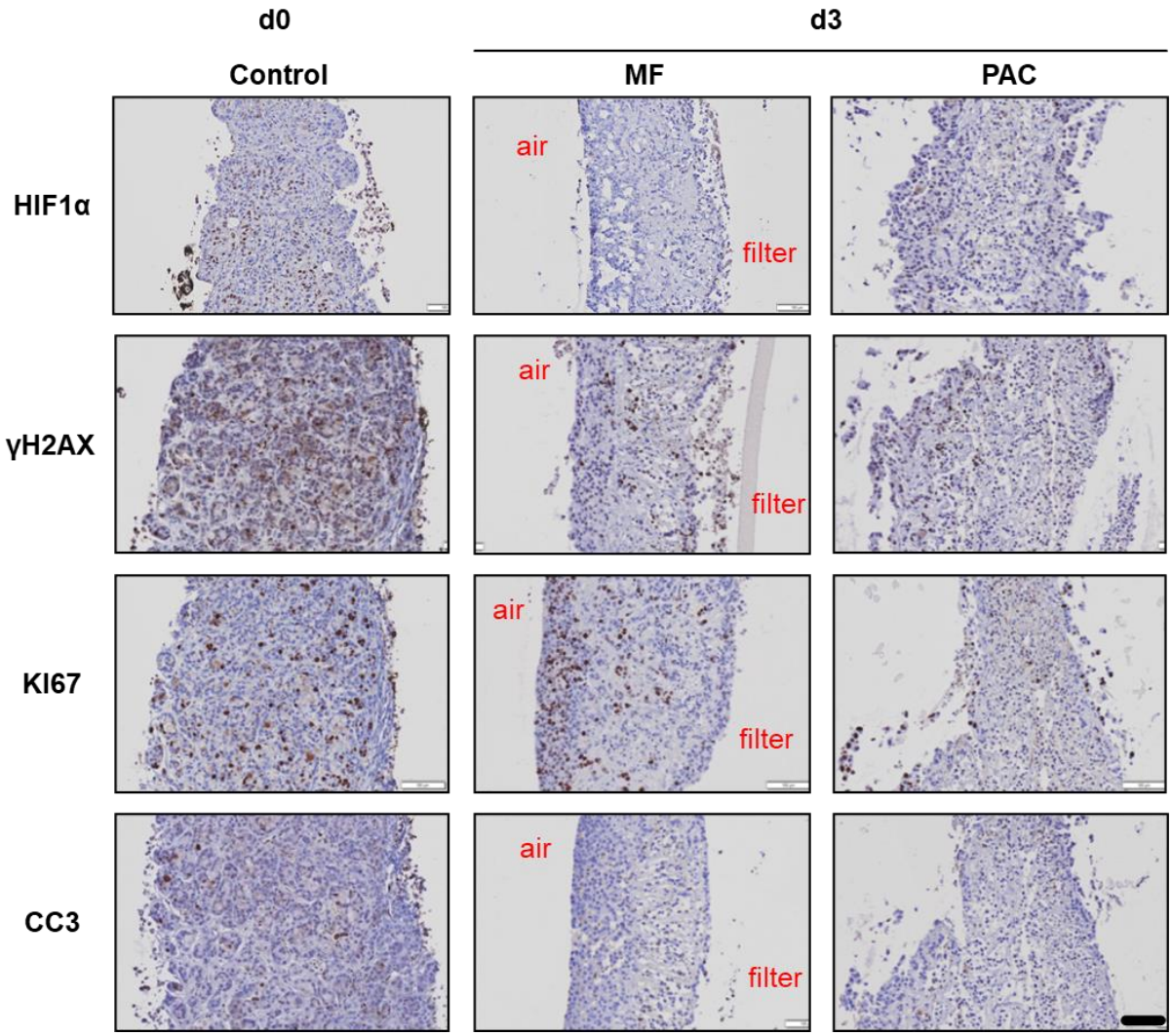

Figure 30: ***IHC staining of H1437 CDX tissue slices after 3 days culture in the MF and PAC systems****. Tumor tissue slices were IHC stained for hypoxia (Hif1α), DNA damage (γH2AX), proliferation (KI67) and apoptosis (cleaved caspase 3, CC3) to examine culture stress in the different culture systems. All stains were compared after 3 days (d3) to d0 control tissue slices. The orientation in the MF culture is indicated with air and filter side. As organotypic support for the PAC culture cotton mesh is chosen and the perfusion rate amounts to 83.3 µL/h. Scale bar corresponds to 100 µm. (n=3)*

After 3 days of culture, the tumor tissue slices showed a similar morphology and structure as the slices as the d0 control tissue (Figure 30). The MF culture slightly induced Hif1α expression and γH2AX expression strongly on the filter side. Interestingly, KI67 expression was predominantly found in cells on the air side of the tissue slice. Cultivation in the PAC system did not lead to an increased biomarker expression and no gradient was formed.

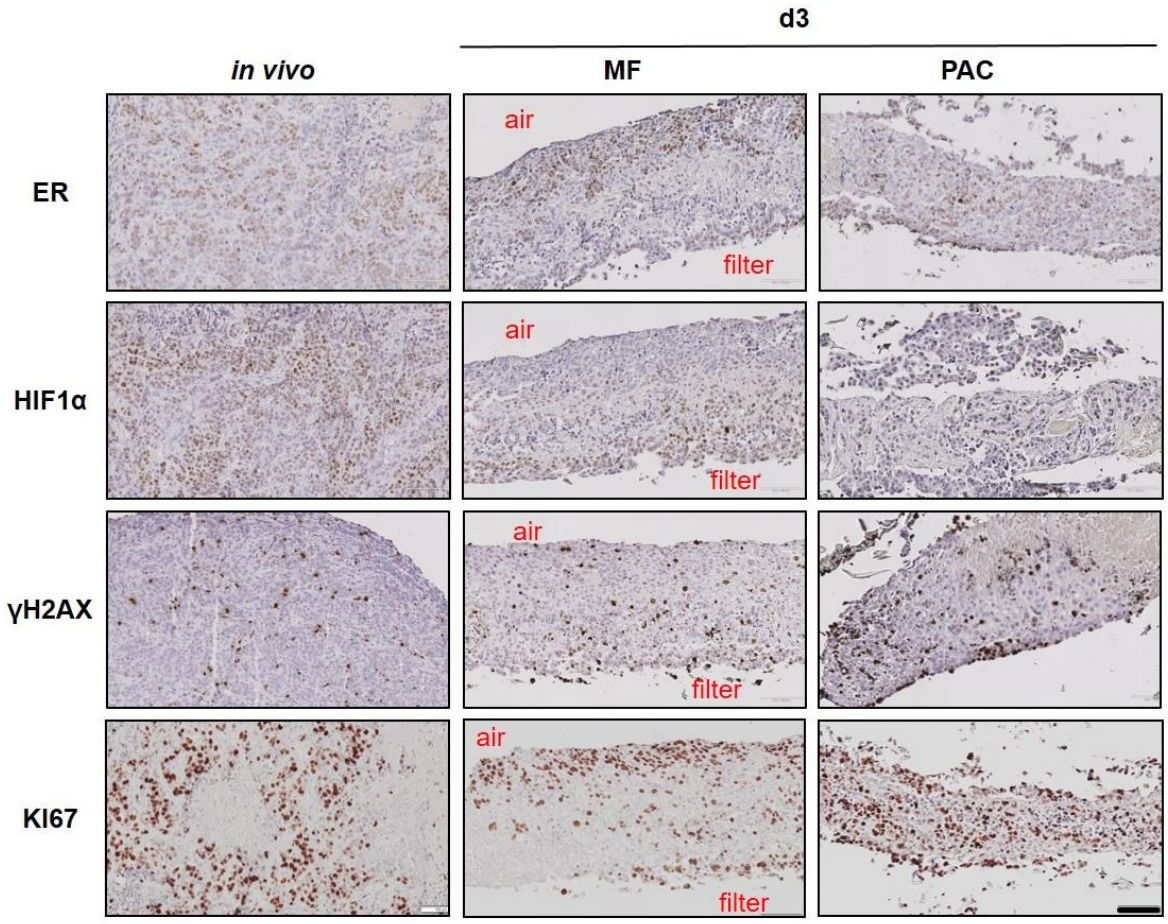

Figure 31: ***Cultivation of MCF-7 CDX tissue slices for 3 days in the MF and PAC system****. CDX tissue slices were IHC stained for estrogen receptor (ER), the hypoxia marker Hif1α, DNA damage marker γH2AX and proliferation marker KI67 expression to examine culture stress of the culture systems. All stains were compared to in vivo control tissue. Air and filter side in the MF culture is indicated. Cotton mesh was chosen as organotypic support for the PAC culture and the perfusion rate was 83.3 µL/h. Scale bar represents 100 µm. (n=6)*

Three days of culture in the MF system caused loco-regional changes in the tumor tissue slice of MCF-7 CDX (Figure 31): ER and KI67 expression were induced on the air side of the tumor tissue slices and Hif1α+ cells were predominantly found on the filter side. The expression of γH2AX was homogeneously distributed through the slice. The slices cultured in the PAC system did not show an artificial gradient formation after culture in the MF system. All biomarkers were homogenously expressed throughout the tissue slice. The tissue structure and morphology of both culture systems was similar as in the *in vivo* control tissue.

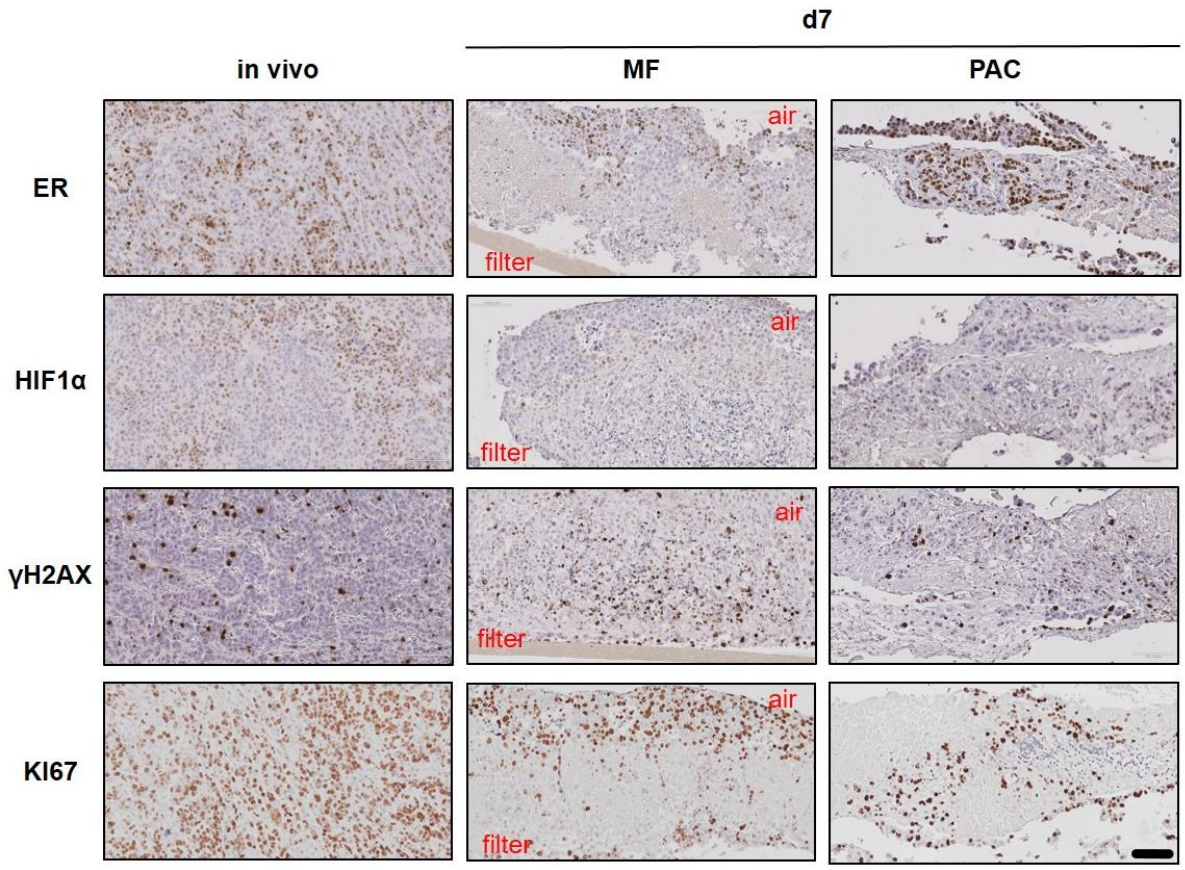

Figure 32: ***Cultivation of MCF-7 CDX tissue slices for 7 days in the MF and PAC system****. IHC staining of cultivated CDX tissue slices and in vivo control tumor tissue in the MF and PAC system. Cotton was chosen as organotypic support and the perfusion rate was 83.3 µL/h. Scale bar corresponds to 100 µm. (n=4)*

Staining of MCF-7 CDX for ER, γH2AX and KI67 indicated a gradient from the air to the filter side after long-term culture (7 days) in the MF system which was not observed after cultivation in the PAC system (Figure 32). Hif1α was expressed at low levels. The tissue morphology and structure after 7 days cultivation in PAC were comparable to the *in vivo* control tissue as well as the biomarkers expression.

3.2.2.2 *Primary ovarian tumor tissue slice culture in the PAC system*

The next experiment was conducted with primary human ovarian cancer tissue. The tissue morphology and structure could be maintained for 3 days in MF and PAC system (Figure 33). Cultivation in the MF system led to an increased biomarker expression of Hif1α and γH2AX on the filter side. Interestingly, KI67+ cells were found on the air side of the slice. After 3 days of culture in the PAC system, the tumor tissue slices showed a similar morphology and biomarker expression as the d0 control tissue. Even after 8

days of PAC culture with cell-free porcine intestine scaffold as organotypic support, the tissue was highly similar to the control.

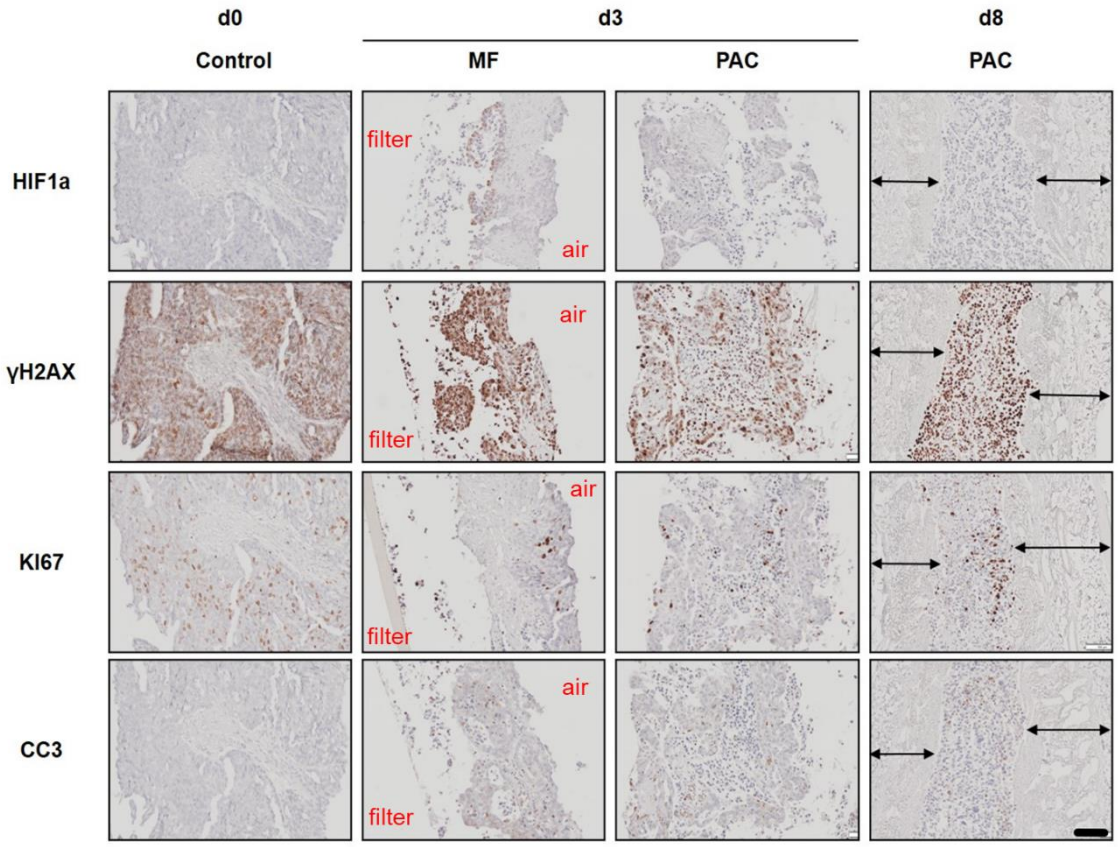

Figure 33: ***Cultivation of primary human ovarian cancer tissue slices in the MF and PAC system****. The tissue was IHC stained for Hif1α, γH2AX, KI67 and CC3. The cultivation period ranged from 3-8 days depending on the cultivation system. In the PAC system two different organotypic supports were chosen: d3 culture with cotton mesh and d8 culture using cell-free porcine intestine (indicated with black arrows). The scale bar represents 100 µm. (n=12)*

Based on these results, together with a previous publication of our group (Davies et al., 2015), it can be concluded that the artificial gradient generated in MF culture system can be prevented with the PAC system.

3.2.3 Cisplatin treatment of CDX and human ovarian cancer tissue slices

After validation of the suitability of the PAC system for cultivation of tumor tissue slices, the PAC system was employed to analyze the cellular response of tumor tissue to cisplatin. Tumor tissue slices were set up in the MF or PAC system and incubated with control medium or medium supplemented with 13 µM cisplatin. The cultivation in the MF system induced a gradient formation of γH2AX on the filter side and KI67 biomarker

expression on the air side (Figure 34). In the presence of cisplatin, both biomarkers indicated an increased expression and γH2AX was also highly expressed on the filter side. There was no CC3 expression observed during the MF cultivation. In the absence of cisplatin, only minor biomarker expression was seen in the PAC system. After cisplatin exposure, γH2AX, KI67 and CC3 expression was observed in the tissue slices. The effects of cisplatin incubation appeared to be stronger in the PAC system than in the MF system.

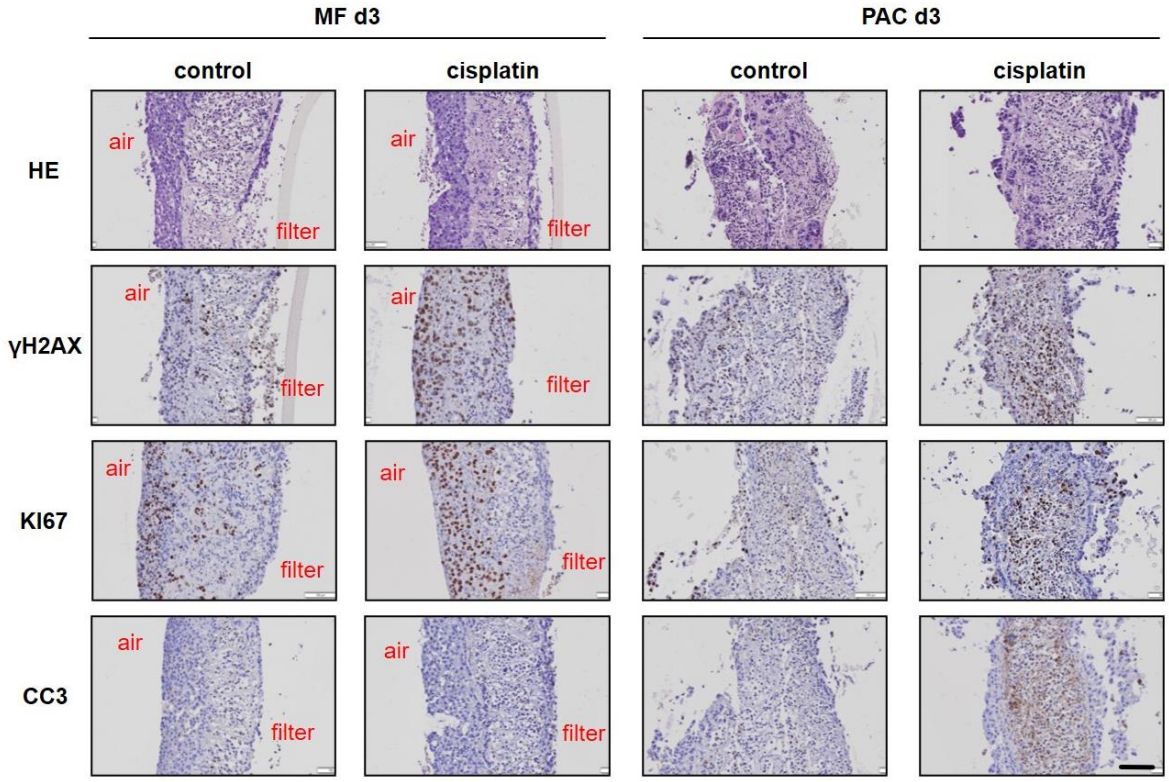

Figure 34: ***Cisplatin treatment of H1437 CDX tissue slices in the MF and PAC system****. CDX tissue slices were incubated in the presence or absence of 13 µM cisplatin for three days. Tissue was IHC stained for HE, γH2AX, KI67 and CC3. Scale bar represents 100 µm. (n=2)*

Next, primary human ovarian cancer tissue slices were treated with 13 µM cisplatin. The presence of cisplatin led to changes in the biomarker expression of KI67 (Figure 35). In both cultivation systems, MF and PAC, the KI67 expression was decreased in the presence of cisplatin. Only a slight increase in the expression of γH2AX was observed in the presence of cisplatin in both culture systems. Remarkably, different patients (patient 1 and 2) showed different CC3 expression after cisplatin treatment while only in the PAC system strongly enhanced CC3 was observed. The platin-based effects in the PAC system seemed to be stronger and patient-specific.

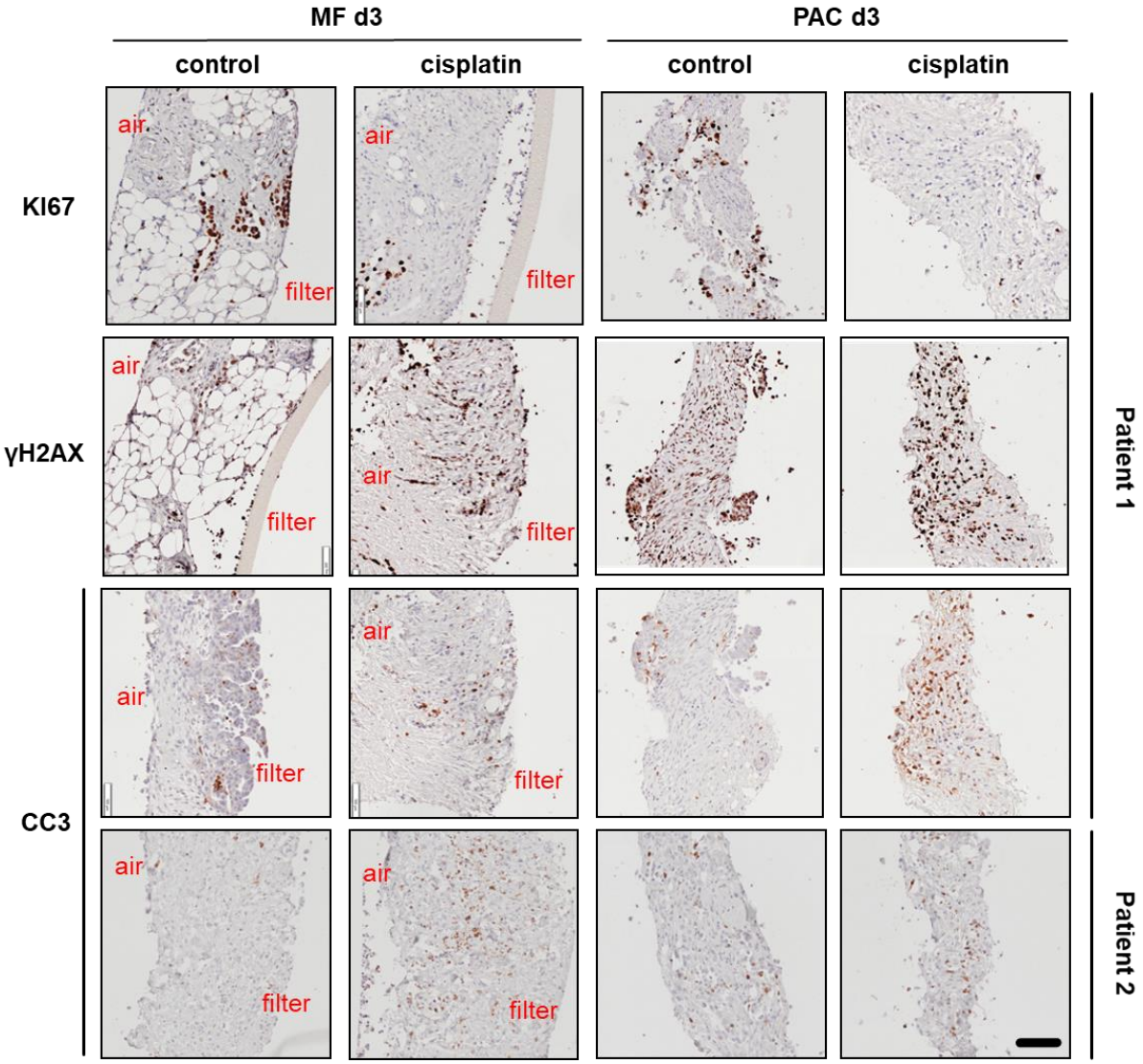

Figure 35: ***Cisplatin treatment of primary human ovarian cancer tissue slices in the MF and PAC system****. Tissue slices were incubated for 3 days in the presence or absence of 13 µM cisplatin. IHC stains were performed for KI67 and γH2AX. CC3 stains are shown from two patients. The scale bar corresponds to 100 µm. (n=8)*

3.2.4 Investigation of culture-related stress after MF and PAC culture using high-throughput gene expression methods

Besides imaging analysis after tumor tissue slice cultivation by HE and IHC staining, the gene expression of the tissue slices was examined. For this purpose, a panel of 134 stress and p53-associated genes (Davies et al., 2015) was evaluated with a high-throughput technique (Appendix, A1). For gene expression analyses, tumor tissue slices from H1437 CDX, MCF-7 CDX and primary human ovarian cancer tissue were incubated in the respective culture system and in the presence or absence of cisplatin. RNA was isolated from the tissue, cDNA was synthesized, and a pre-amplification of

the target genes was performed. The measurements were executed using the BioMark HD system. Finally, the log2 ΔΔCt values of the samples were calculated and displayed by means of principal component analysis (PCA) and heatmaps.

Cultivation of H1437 CDX tissue slices for 3 days led to clustering of the conditions in 3 of 4 tumor samples (Figure 36). The samples that cluster in the upper left corner belonged to one same tumor sample. The remaining samples showed that the gene expression of the d0 control samples was more similar to that after PAC culture than the gene expression after MF culture.

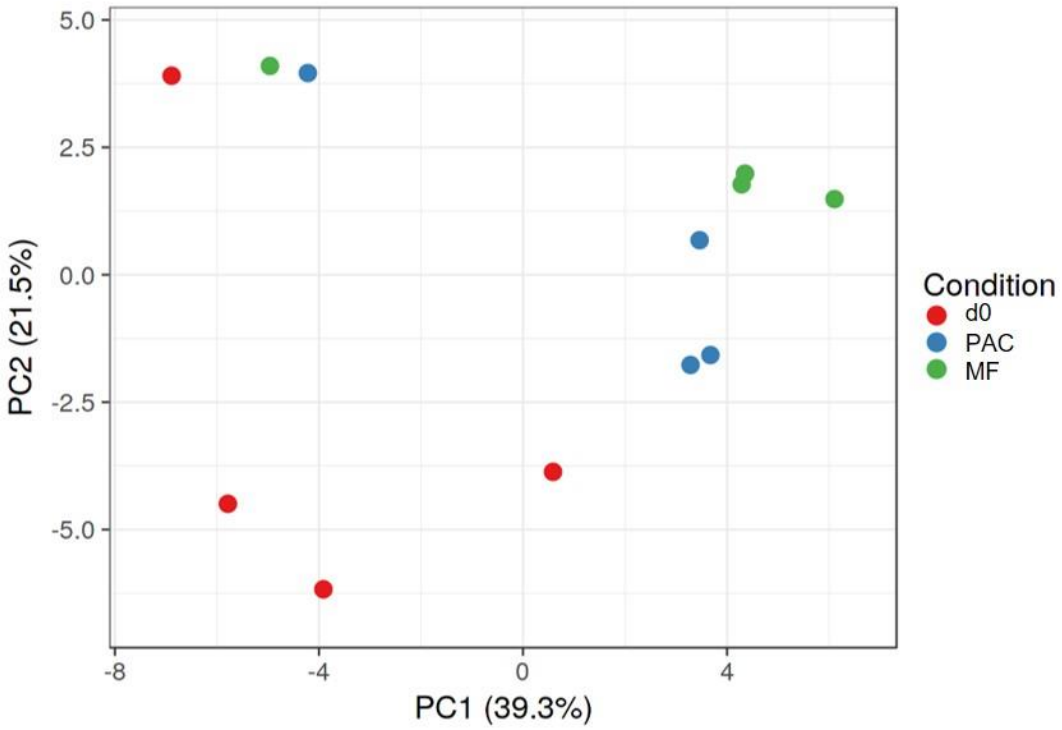

Figure 36: ***Principal component analysis (PCA) of gene expression of H1437 CDX tissue slices after cultivation in MF or PAC for 3 days.*** *The axes indicate principal component 1 (PC1, 39.3% variance displayed) and PC2 (21.5% variance). Non-cultivated control samples are shown in red, PAC culture in blue and MF cultivation in green. (n=4)*

The cultivation of MCF-7 CDX tumor tissue slices in the MF and PAC system is displayed in Figure 37. The *in vivo* control represented fresh tumor samples one day after shipping and before cutting the tumor tissue slices. The d0 control samples were uncultured tissue control samples after shipment and the cutting process. The samples from both control situations were grouped closest to each other and compared to the samples after cultivation in the respective system, with one exception in the lower left corner. All samples after MF cultivation were tightly clustered and showed a higher

similarity to the control samples in terms of gene expression than the PAC-cultured samples.

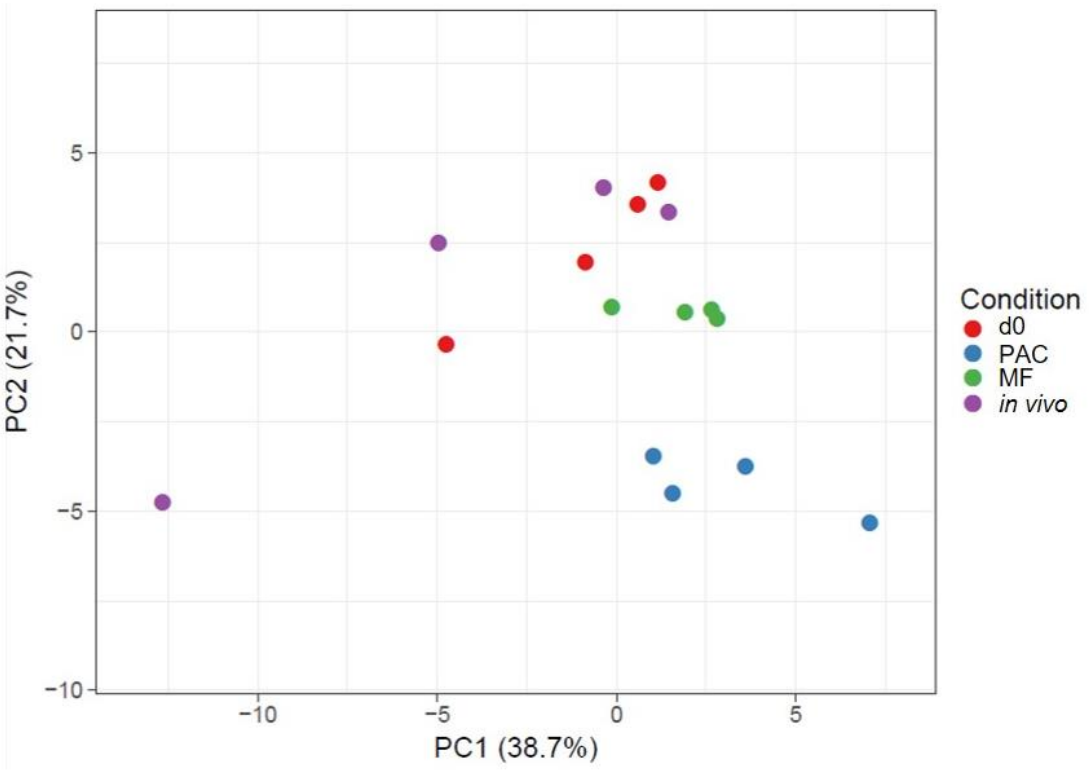

Figure 37: ***PCA of MCF-7 CDX tissue slice's gene expression after MF or PAC cultivation.*** *Principal components (PC) are shown on the axis of the graph and relative variances are shown in brackets. Purple dots indicate fresh-frozen control samples directly after surgery, red displays d0 controls. The PAC system samples are shown in blue and MF in green. (n=4)*

Furthermore, the MCF-7 CDX samples were also examined for the oxygen influence in gene expression changes by cultivation in different atmospheric oxygen conditions. The tissue slices were cultivated in the above-mentioned systems either under hypoxia (1.5% O_2) or normoxia (20% O_2) and compared to *in vivo* control samples of the same tumor tissue. All samples after cultivation either on MF or in PAC clustered tightly and showed an overlap (Figure 38). Apparently, the normoxic and hypoxic cultured samples showed only slight differences in gene expression. In conclusion, hypoxia with 1.5% O_2 did have a minor impact on gene expression in the tissue slice culture. The cultivated hypoxic samples tended to have a slightly greater distance to the *in vivo* control samples.

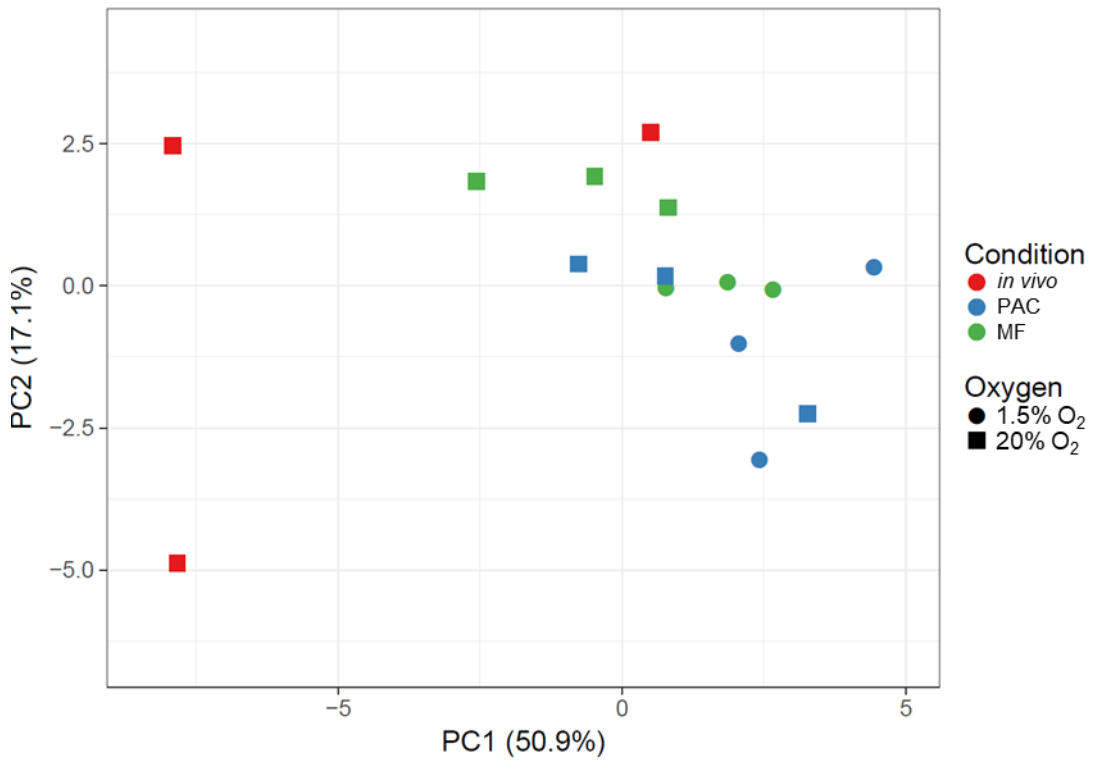

Figure 38: ***PCA of gene expression of MCF-7 CDX tissue slices after 3 days cultivation in MF or PAC system under hypoxic or normoxic conditions.*** *The axes show PC and variances. Controls are displayed in red, MF cultivation in green and PAC in blue. Squares indicate normoxia cultivation and dots refer to the hypoxia condition. (n=3)*

Analyses of tissue slices from primary human ovarian cancer showed that all d0 control samples were grouped at the bottom of the graph (Figure 39). Samples after MF and PAC culture did not show cultivation-related clusters and appear mixed. However, the green marked samples (after MF culture) indicated a tendency to approach the red controls, while the blue samples (after PAC culture) seemed to have a larger distance from the controls. Because of the huge heterogeneity of the primary ovarian tumor tissue, it is hard to draw a conclusion that which culture system is closer to the *in vivo* situation; more samples need to be tested.

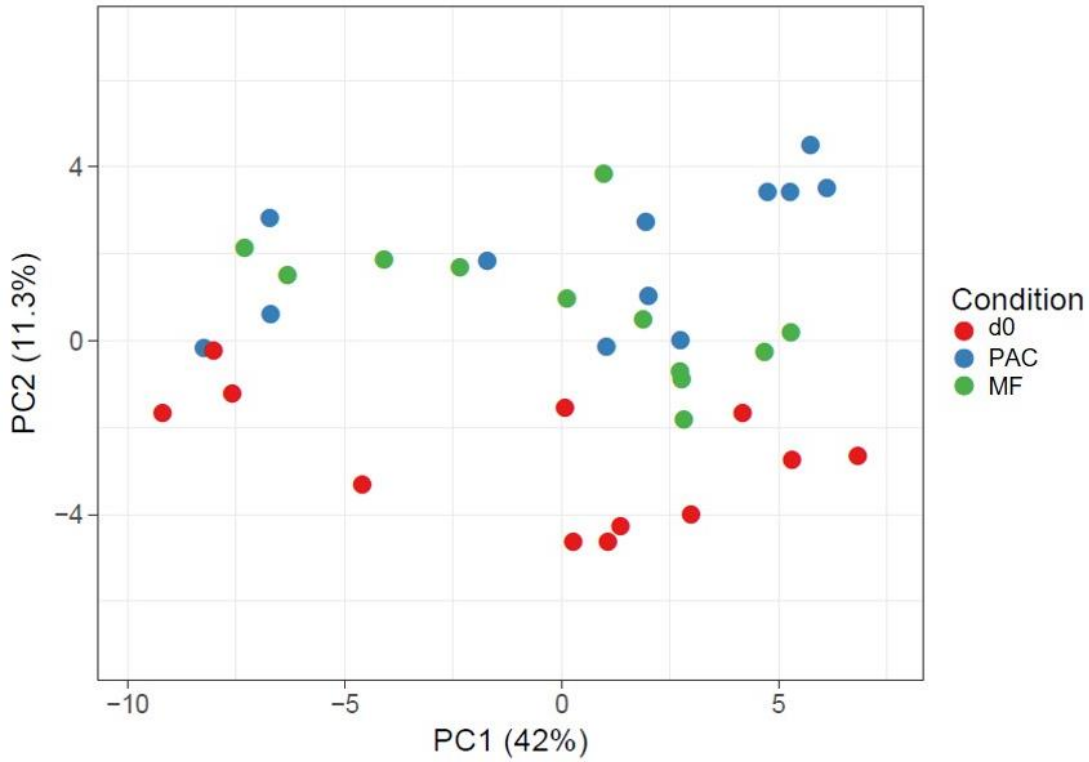

Figure 39: ***PCA of primary human ovarian cancer tissue slice's gene expression after cultivation in MF or PAC for 3 days.*** *The axes indicate PC and the displayed variances. Non-cultivated control samples are shown in red, PAC culture in blue and MF culture in green. (n=12)*

The ovarian cancer tissue slice gene expression of the same samples was also visualized as a heat map. Dendrograms in Figure 40 show hierarchical clustering by sample similarity (X-axis) and by gene similarity (Y-axis), respectively. The gene expression of all samples that were previously shown in Figure 39 are visualized as a heatmap in Figure 40A. Noticeably, two clusters were built of d0 samples from different tumors grouping together. By comparing the tumor samples on the bottom, the remaining tumor samples clustered by sample.

To prevent the batch (tumor) effect, in Figure 40B the respective d0 control sample was eliminated from the samples after cultivation. After elimination of the batch effect, clusters by tumors were still formed rather than by cultivation conditions. From this, it can be concluded that cultivation did not lead to serious changes in gene expression.

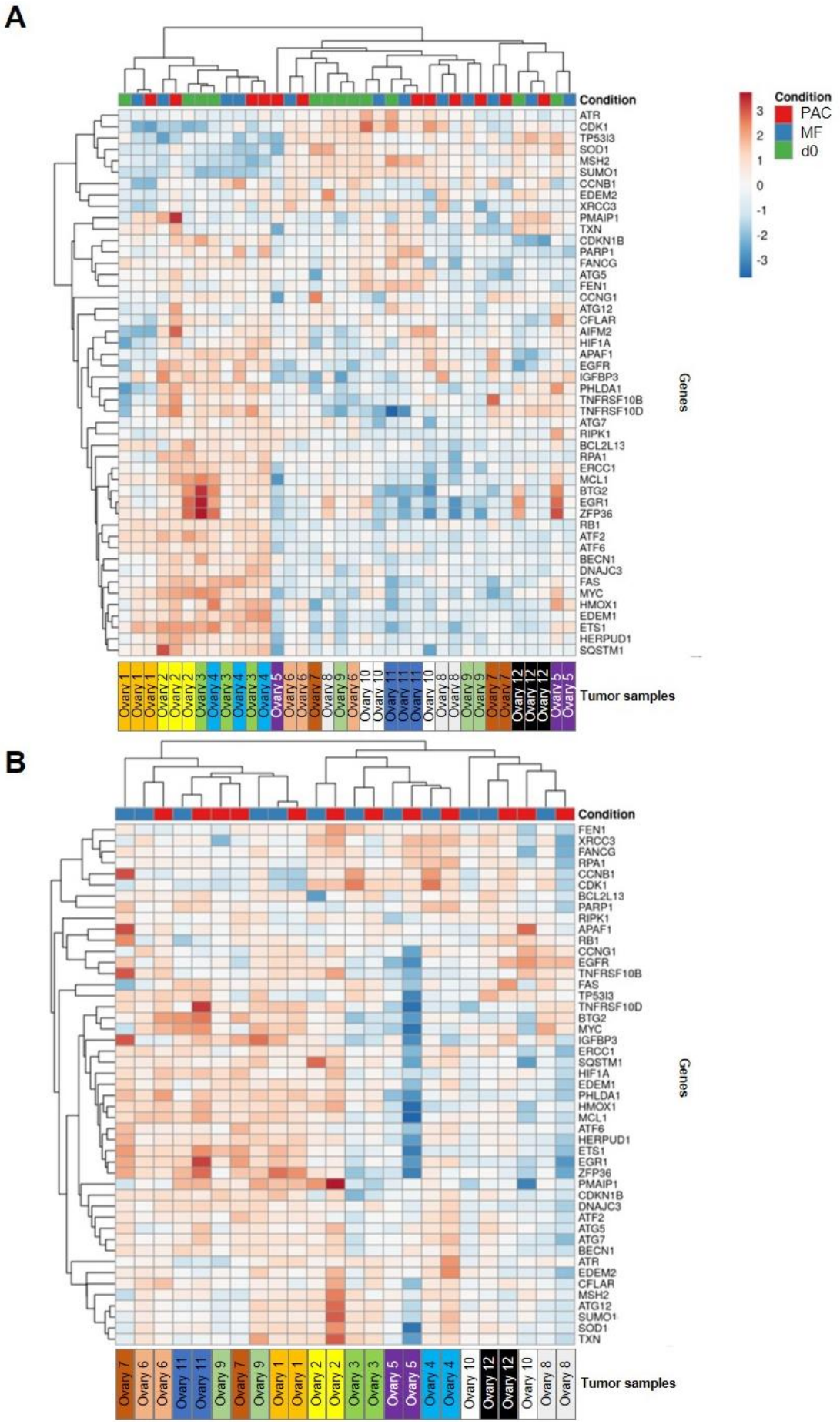
A
Condition
PAC
MF
d0
3
2
1
0
-1
-2
-3
ATR
CDK1
TP53I3
SOD1
MSH2
SUMO1
CCNB1
EDEM2
XRCC3
PMAIP1
TXN
CDKN1B
PARP1
FANCG
ATG5
FEN1
CCNG1
ATG12
CFLAR
AIFM2
HIF1A
APAF1
EGFR
IGFBP3
PHLDA1
TNFRSF10B
TNFRSF10D
ATG7
RIPK1
BCL2L13
RPA1
ERCC1
MCL1
BTG2
EGR1
ZFP36
RB1
ATF2
ATF6
BECN1
DNAJC3
FAS
MYC
HMOX1
EDEM1
ETS1
HERPUD1
SQSTM1
Genes
Ovary 1
Ovary 1
Ovary 1
Ovary 2
Ovary 2
Ovary 2
Ovary 3
Ovary 4
Ovary 3
Ovary 4
Ovary 3
Ovary 4
Ovary 5
Ovary 6
Ovary 6
Ovary 6
Ovary 7
Ovary 8
Ovary 9
Ovary 6
Ovary 10
Ovary 10
Ovary 10
Ovary 11
Ovary 11
Ovary 11
Ovary 10
Ovary 8
Ovary 8
Ovary 9
Ovary 9
Ovary 9
Ovary 7
Ovary 7
Ovary 12
Ovary 12
Ovary 12
Ovary 5
Ovary 5
Tumor samples
B
Condition
FEN1
XRCC3
FANCG
RPA1
CCNB1
CDK1
BCL2L13
PARP1
RIPK1
APAF1
RB1
CCNG1
EGFR
TNFRSF10B
FAS
TP53I3
TNFRSF10D
BTG2
MYC
IGFBP3
ERCC1
SQSTM1
HIF1A
EDEM1
PHLDA1
HMOX1
MCL1
ATF6
HERPUD1
ETS1
EGR1
ZFP36
PMAIP1
CDKN1B
DNAJC3
ATF2
ATG5
ATG7
BECN1
ATR
EDEM2
CFLAR
MSH2
ATG12
SUMO1
SOD1
TXN
Genes
Ovary 7
Ovary 6
Ovary 6
Ovary 11
Ovary 11
Ovary 9
Ovary 7
Ovary 9
Ovary 1
Ovary 1
Ovary 2
Ovary 2
Ovary 3
Ovary 3
Ovary 5
Ovary 5
Ovary 4
Ovary 4
Ovary 10
Ovary 12
Ovary 12
Ovary 10
Ovary 8
Ovary 8
Tumor samples

Figure 40: ***Visualization of gene expression data of primary human ovarian cancer tissue as heatmap after 3-day culture in MF or PAC.*** *The X-axis shows the tumor samples and the Y-axis depicts the genes studied from the gene panel. Dendrograms reveal gene expression similarities by means of genes and samples. The condition PAC culture is indicated in red and MF in blue. Samples of the same tumors are color-coded at the bottom of the heat map independent from other colors of the image. The colors of the tumor samples are applied uniformly in Figure A and B to highlight samples from the same tumors. (A) All cultivation conditions and control samples are shown. (B) The tumor (batch) effect in the samples is removed, and the cultivation conditions PAC and MF are depicted. (n=12)*

The final analysis of high-throughput data from primary human ovarian cancer tissue compared the cultivation systems plus-minus cisplatin. Ovarian cancer tissue slices were cultivated in MF or PAC in the presence or absence of 13 µM cisplatin. The first result (Figure 41) was that the gene expression of the d0 control was comparable to the non-treated (control) samples than to the samples treated with cisplatin. Otherwise, no grouping based on cultivation was observed. However, it could be observed that the two samples based on the presence or absence of cisplatin always had similar gene expression, regardless of the cultivation system.

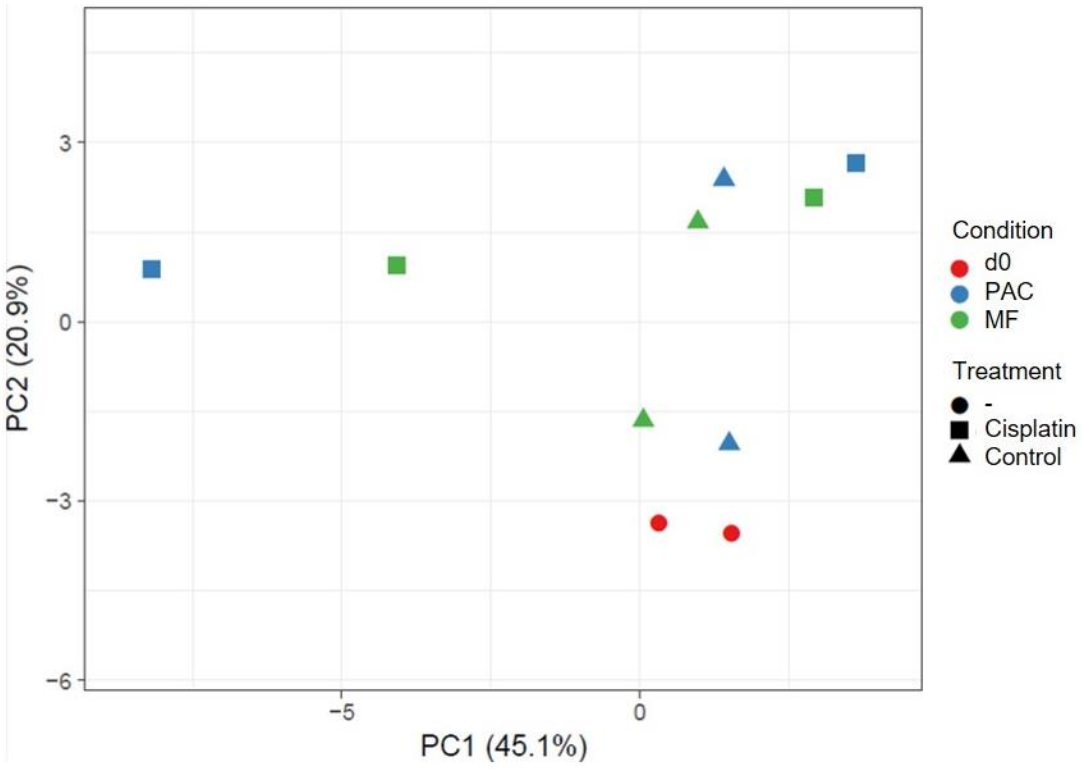

Figure 41: ***PCA of gene expression of primary human ovarian cancer tissue slices with or without cisplatin treatment.*** *Principal components (PC) are shown on the axes of the graph and relative variances in brackets. Conditions are displayed in colors and 13 µM cisplatin presence (square) and absence (triangle) is visualized in different shapes. (n=2)*

3.2.5 Examination of alternative organotypic supports in the PAC system

In order to optimize the organotypic support for the PAC system, many materials were tested and evaluated. Several criteria were required to minimize culture-related stress of the tumor tissue slices. On the one hand, it must be gas permeable to ensure sufficient supply of oxygen; on the other hand, it should be liquid conducting to ensure equal nutrient transport to the cultured slices. Therefore, several membranes from different manufacturers and collaboration partners were tested in the PAC system.
H1437 CDX and primary human ovarian cancer tissue slices were used to evaluate the membranes. After 3 days culture, the tissue slices were stained for HE to analyze the tissue structure and morphology. The cultured tissue slices were compared to d0 control tissue slices of the tumor.

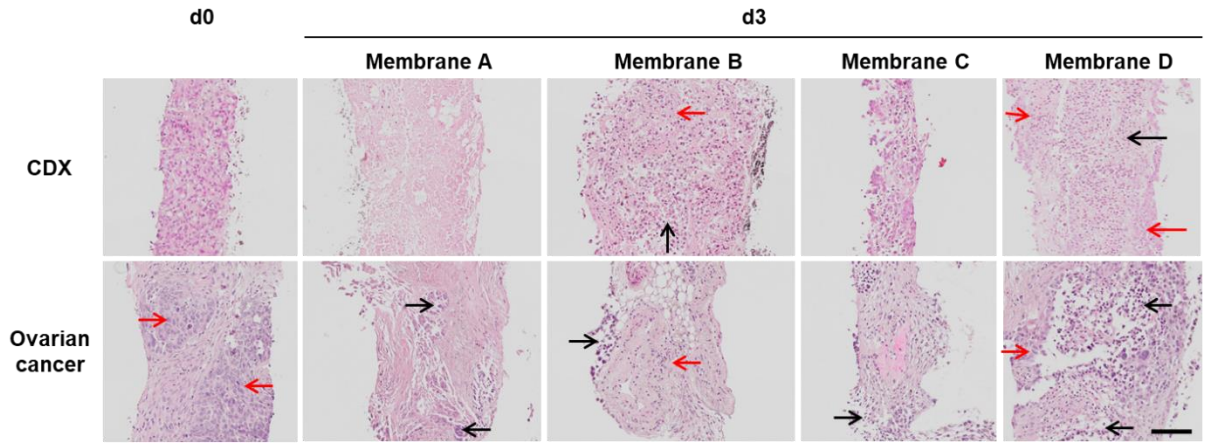

Figure 42: ***Comparison of four different organotypic supports in the PAC system using H1437 CDX and primary ovarian cancer tissue slices****. Tissue slices were cultured for 3 days and stained for HE. Tissue structure and morphology after culture was compared to d0 control tissue slices. Red arrows indicate good structure and morphology, whereas black arrows show destroyed morphology of the tissue. Scale bar represents 100 µm. (n=1)*

In Figure 42, red arrows indicated good structure and morphology, while black arrows corresponded to condensed nuclei (apoptosis) and vasculated regions with destroyed morphology. CDX and ovarian cancer tissue slices cultured in-between membrane B and membrane D showed an intact structure and similar morphology compared to d0 control. The other membranes (A and C) showed disrupted tissue structure and an altered morphology compared to the control.
In summary, the membranes B and D were promising candidates to improve cultivation conditions for the PAC system.

In addition, a 3D printer was used to print hydrogel meshes using alginate and collagen (Figure 43) (Hinton et al., 2015). The hydrogels were printed in 3D in a gelatin support bath and then applied in the PAC culture as organotypic supports.

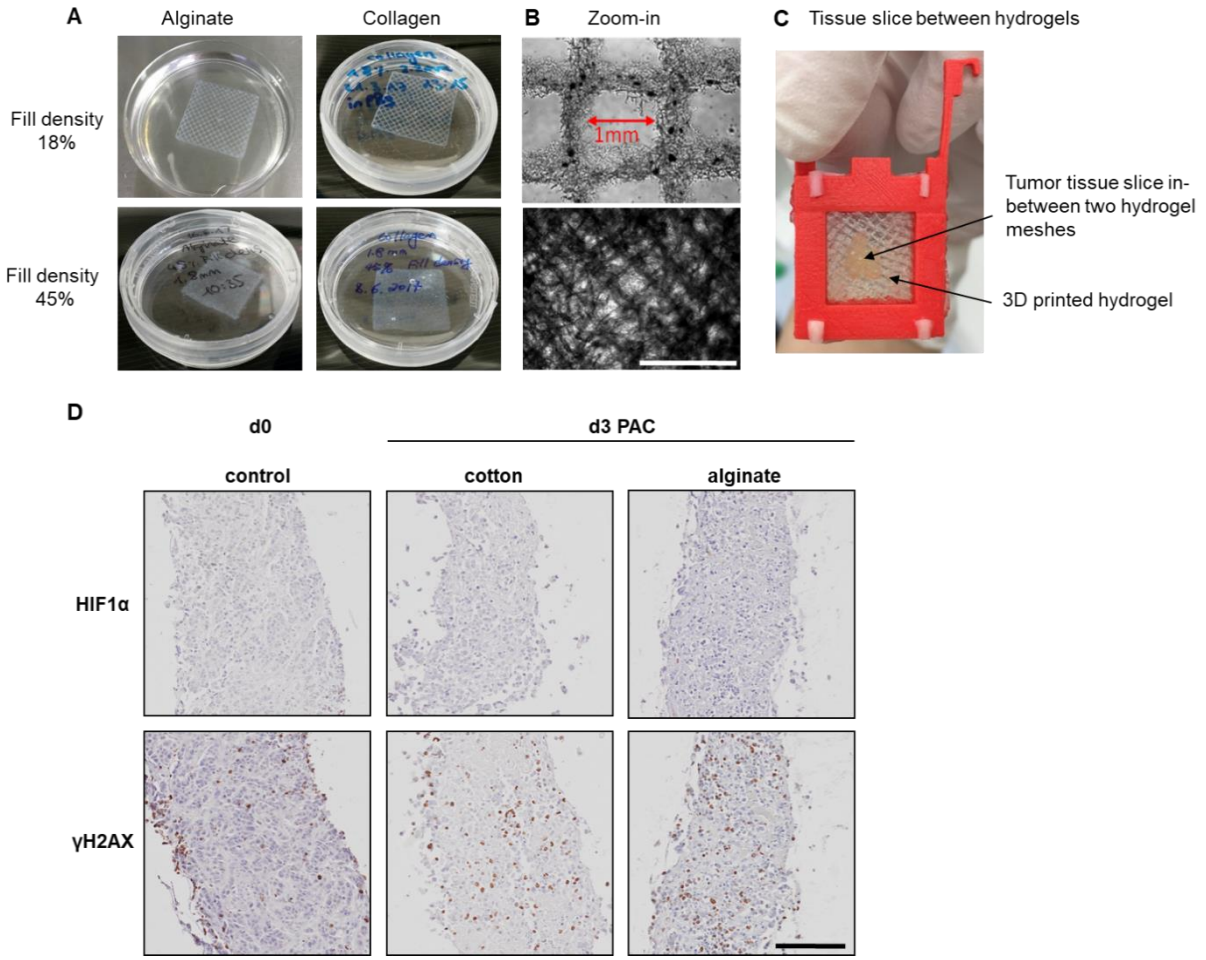

Figure 43: ***3D printed hydrogel organotypic supports used in the PAC system for tissue slice cultivation.*** *(A) Hydrogel meshes of alginate and collagen with 18% and 45% fill density. (B) Zoom-in microscope images of different fill density to illustrate a pore size of 1 mm. White scale bar of zoomed-in images represents 2 mm. (C) Set-up of tissue slice between hydrogels in the frame holder for PAC cultivation. (D) IHC staining of MCF-7 CDX tissue slices after three days of culture in the PAC system using different organotypic support. IHC staining was conducted for hypoxia (Hif1α) and DNA damage (γH2AX). As organotypic supports in the PAC culture cotton mesh and 3D printed alginate hydrogel were used. Black scale bar corresponds to 200 µm. (n=1)*

Both 18% and 45% were tested as fill density for the printing (Figure 43A). The lower fill density had a visible pore size, appeared well-ordered and a better structure (Figure 43B). For experiments 18% fill density was used for the meshes and it can be installed together with the tissue slices in the PAC system (Figure 43C).

After three-day culture in the PAC system with different organotypic supports, the results show that the process of IHC was feasible and the samples cultured with 3D printed hydrogel could be evaluated by IHC. Expression of hypoxic marker Hif1α and

DSB marker γH2AX was not induced during PAC culture using different organotypic supports. The 3D printed hydrogel can be used as organotypic supports in PAC system for tissue slices culture.

3.2.6 3D-organoid cultivation of patient-derived ovarian tumors in Matrigel

Another established method to cultivate primary tissue is the patient-derived organoid culture using Matrigel as embedding matrix. The method was originally published with colon tissue (Sato et al., 2009), then it was further developed to other tissues. The method offers the possibility to test different drugs on organoids of a single patient in a small-scale but high-throughput procedure.

Ovarian cancer organoids were successfully generated from fresh ovarian tumor tissue and they could be cultured for more than 2 months (Figure 44A). IHC stains from the organoids in Figure 44B showed GMNN+ cells indicating proliferation. In addition, the organoids were also stained with EpCAM to ensure that the cells were epithelial cells.

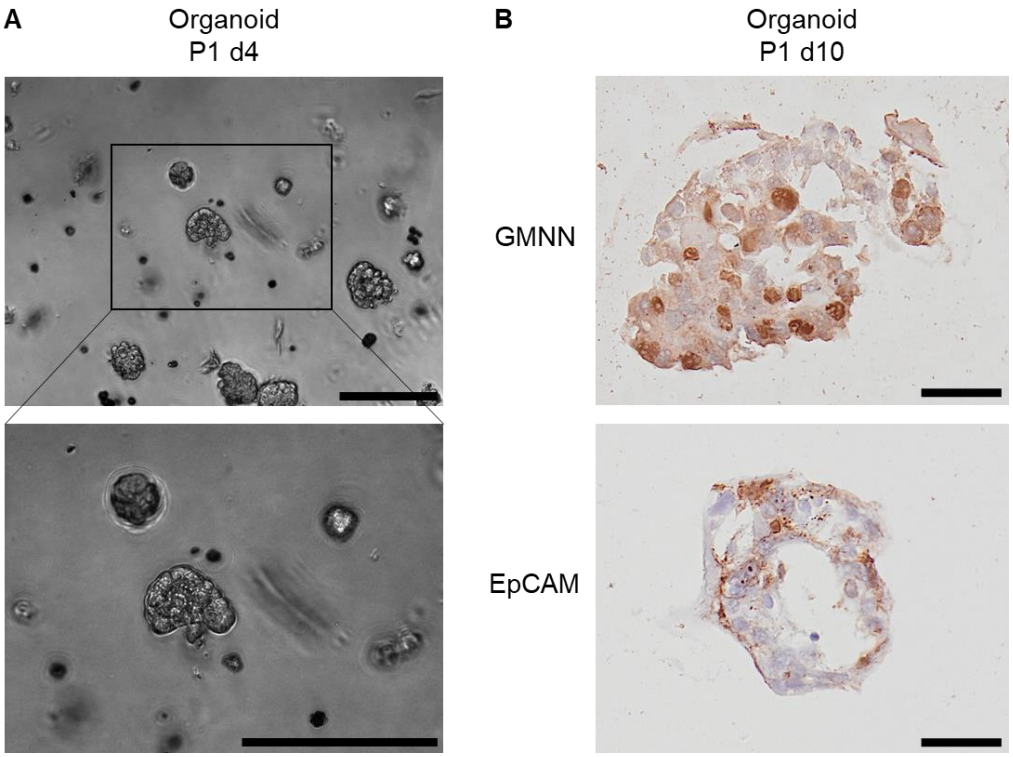

Figure 44: ***Bright-field microscope images of ovarian cancer-derived organoids.*** *(A) Organoids grew in Matrigel on day 4 (passage 1). Images were taken by a standard transmitted-light bright-field microscope. Scale bars represent 200 µm. (B) IHC staining for proliferation (geminin, GMNN) and epithelial tissue (epithelial cell adhesion molecule, EpCAM). The scale bar corresponds to 50 µm. (n=3)*

Furthermore, the organoids were examined for cell viability using a live-dead assay: The TMRM staining visualized the mitochondrial membrane potential in living cells. Picogreen stained the DNA strand in dead cells and DAPI dyed cell nuclei. Very few green (dead) cells were seen (Figure 45A).

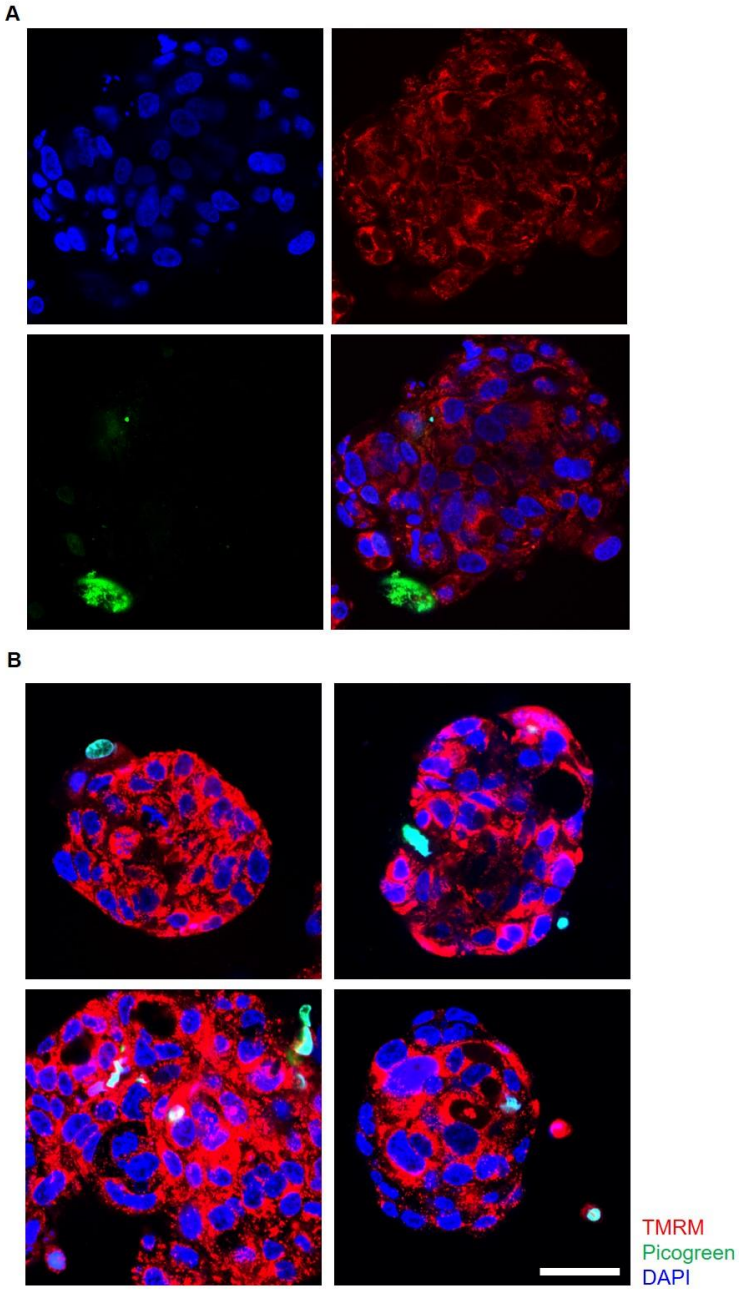

Figure 45: ***Images of live-dead stained organoids on day 7 in passage 1.*** *Images were taken by a confocal laser scanning microscope. (A) Organoids were stained for cell viability (TMRM), cell death (Picogreen) and cell nuclei (DAPI). (B) Further organoids of different sizes were stained from the same patient. The scale bar represents 50 µm. (n=1)*

Most of the cells were red, indicating viable cells. Figure 45B shows further organoids obtained from the same patient tissue, confirming that most tumor cells appeared viable (red) and only a few cells were dead (green).
In summary, it could be shown that primary ovarian cancer tissue could be cultivated and expanded as organoids.

3.2.7 Organoid cultivation from cisplatin-treated human ovarian tumor tissue slices

Once the organoid culture and the tumor tissue slice cultivation systems have been established for ovarian cancer, a combination and unification of the advantages of both systems was tested. After the tumor tissue slice cultivation in the cultivation systems, organoids would offer the possibility to use them as a read-out after cisplatin incubation. Tumor tissue slices from ovarian cancer tissue were cultured either in the MF or PAC system and cultivation was conducted in the presence or absence of cisplatin. After the cultivation period, the slices were dissociated and embedded in Matrigel to generate organoids.
Remarkably, the organoids derived from two tumors led to different results. In contrast to the untreated sample, almost no organoids isolated from tumor 1 tissue slices were seen after cisplatin-incubation (Figure 46). Interestingly and contrary to tumor 1, organoids generated from tumor 2 tissue slices were surrounded by a high number of fibroblasts that infiltrated the Matrigel to a high extend. This was a rather surprising outcome. To draw a conclusion, the experiments will have to be repeated with more tumor samples. Nevertheless, it could be shown that organoid culture from cultured tissue slices was feasible.

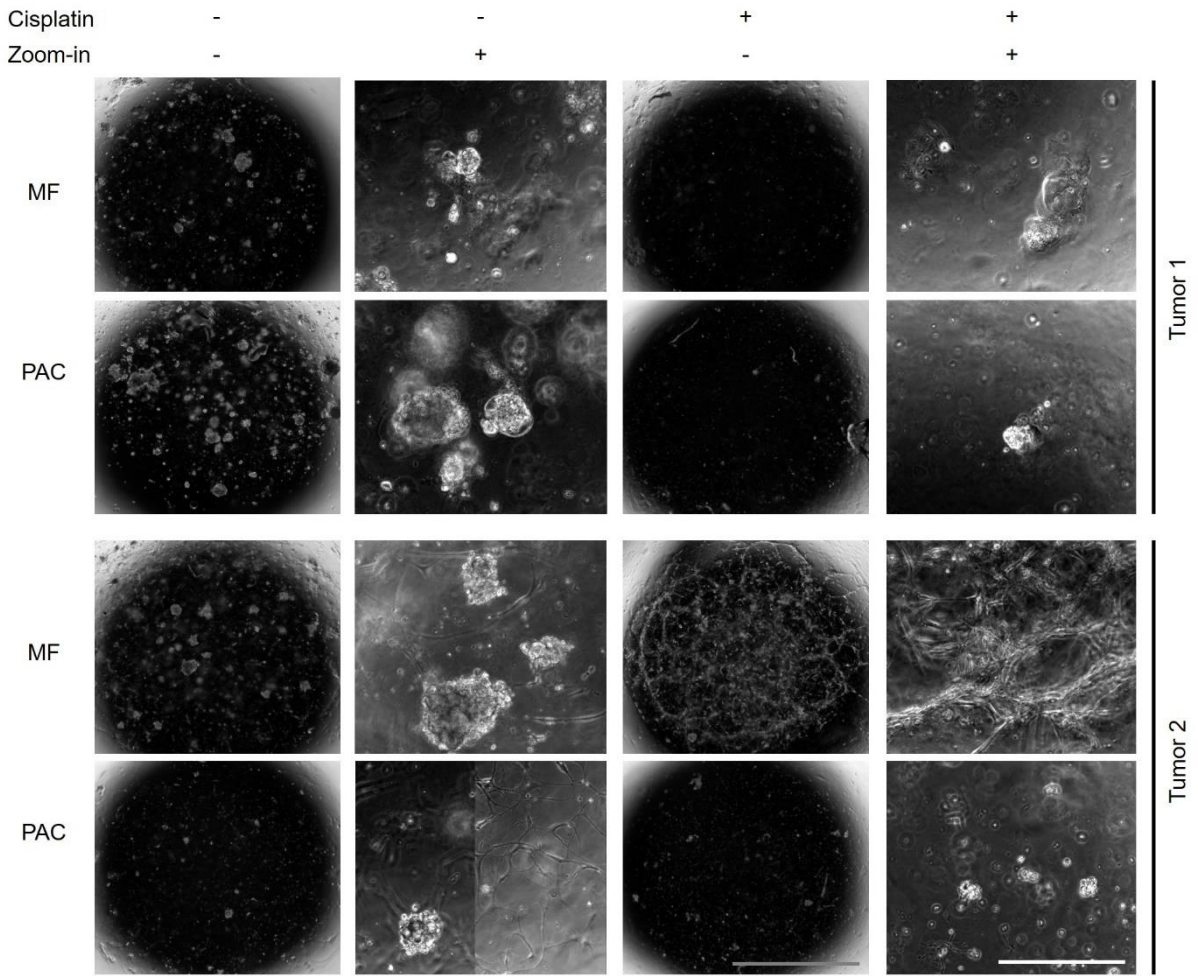

Figure 46: ***Bright-field microscope images of organoids isolated from ovarian cancer tissue slices.*** *Tumor tissue slices were either cultured in the MF or PAC system in the presence or absence of 13 µM cisplatin. Tumor samples of two patients were analyzed. Tumor tissue slices were dissociated after culture and embedded between Matrigel for further cultivation as organoids. Only cells tolerating and surviving the cisplatin incubation during slice culture were able to grow in Matrigel. The grey scale bar for overview images corresponds to 2 mm whereas the white scale bar in zoomed-in images represents 200 µm. (n=2)*

3.2.8 Cytokine quantification in the culture medium of human ovarian tumor tissue slices after culture in the MF or PAC system using flow cytometry

Another interesting question that can be addressed to the cultivation systems for tumor tissue slices is whether the different cell types communicate with each other. Tumor tissue slices from primary human tumor tissue contain the patient's tumor microenvironment. MF and PAC cultivation enabled the investigation of which messenger substances or metabolites were detectable in the cell culture medium supernatant and medium flow-through during or after culture. The following results

were focused on cytokines from two patient samples that were cultivated in the MF or PAC system, respectively.

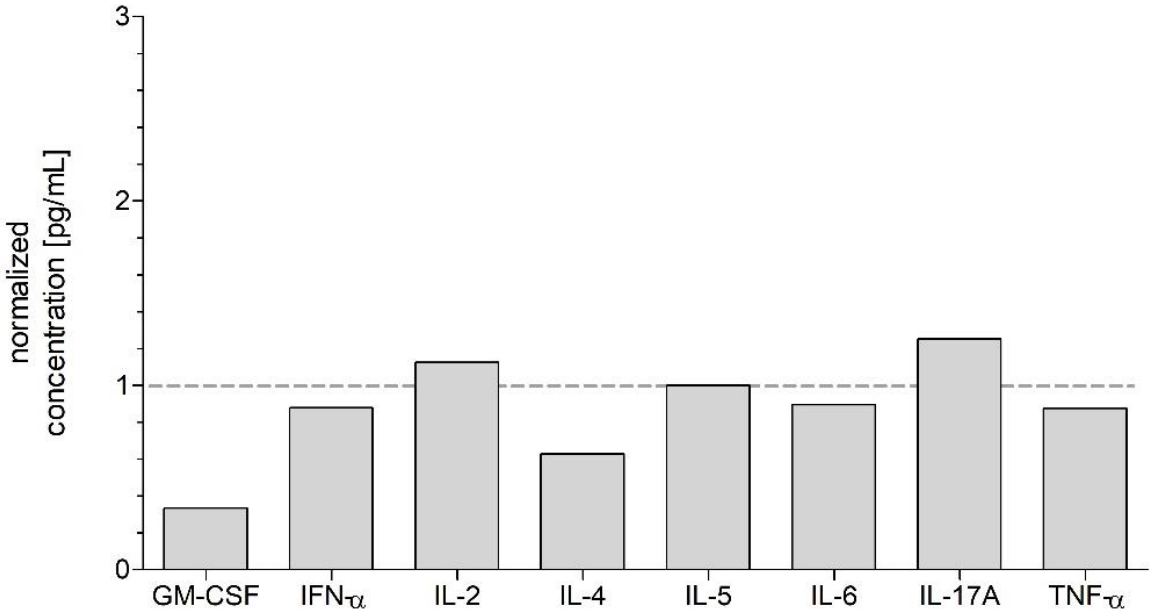

Figure 47: ***Examination of the cell culture medium supernatant of patient 1 after tissue slice culture in the MF system****. Cytokine concentrations were determined after 24 h (dashed line) and 48 h culture (bars were normalized to 24 hours).*

From a panel of 12 possible cytokines, 8 cytokines could be determined in the cell culture medium supernatant of tissue slice samples of patient 1 (Figure 47). The 4 missing cytokines of the panel (IFN-γ, IL-9, IL-10, IL-12) were not detected. The cytokine concentration was measured after 24 and 48 hours and normalized to the concentration at 24 hours for the respective cytokines (dashed line). After 24 hours IL-2 and IL-17A were slightly elevated and no change was observed in IL-5 concentration. All remaining cytokine concentrations were reduced after 48 hours.

Next, the supernatant of tumor tissues slices from patient 2 was investigated. To exclude the possibility that few cells secreted too low concentrations of cytokines in the cultivation system, two tumor tissue slices were cultivated from patient 2 per approach. Analyses from the supernatant after MF culture showed that 10 cytokines were detected after 3 days culture in the presence or absence of 13 µM cisplatin (Figure 48). In the presence of cisplatin, the highest IL-9 (3-fold) concentration and a slightly increased IL-5 concentration were determined compared to cell culture medium without cisplatin. The GM-CSF concentration decreased in the presence of cisplatin, and the same tendency, but less pronounced, was observed for IL-12, IL-2, TNF-α,

IL-10 and IL-4. Minor differences in the cytokine concentrations of IFN-α and IL-6 seemed to indicate that cisplatin did not affect their secretion.

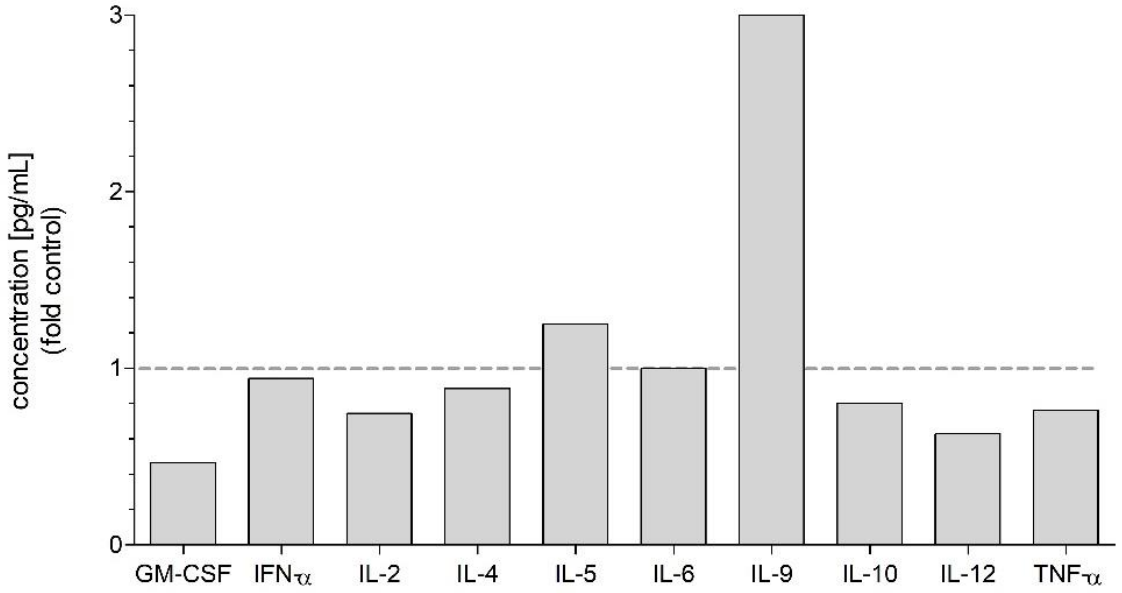

Figure 48: ***Examination of supernatant after MF culture in the presence and absence of cisplatin of patient 2.*** *Cytokine concentrations in the cell culture medium were measured after 3 days with or without 13 µM cisplatin. The cytokine concentration in the supernatant incubated with cisplatin (bars) was normalized to the cytokine concentration of cell culture control medium without cisplatin (dashed line).*

In the next approach, the medium flow-through after 3 days of PAC culture either using cotton mesh or using cell-free porcine intestine (scaffold) as organotypic supports in tissue slices from patient 2 was compared. From 12 cytokines, 11 were detected regardless of the organotypic support selection (Figure 49). Interestingly, some cytokine concentrations differed strongly between the two organotypic supports. GM-CSF, IL-6 and IL-10 showed the greatest differences, and each cytokine concentration of the three cultivated with cotton fabric was noticeably higher. All other cytokine concentrations differed only slightly from each other. Only IFN-γ could not be detected in this approach. IL-5, IL-10 and IL-17A showed one of the two measured values that were outside the detection range.

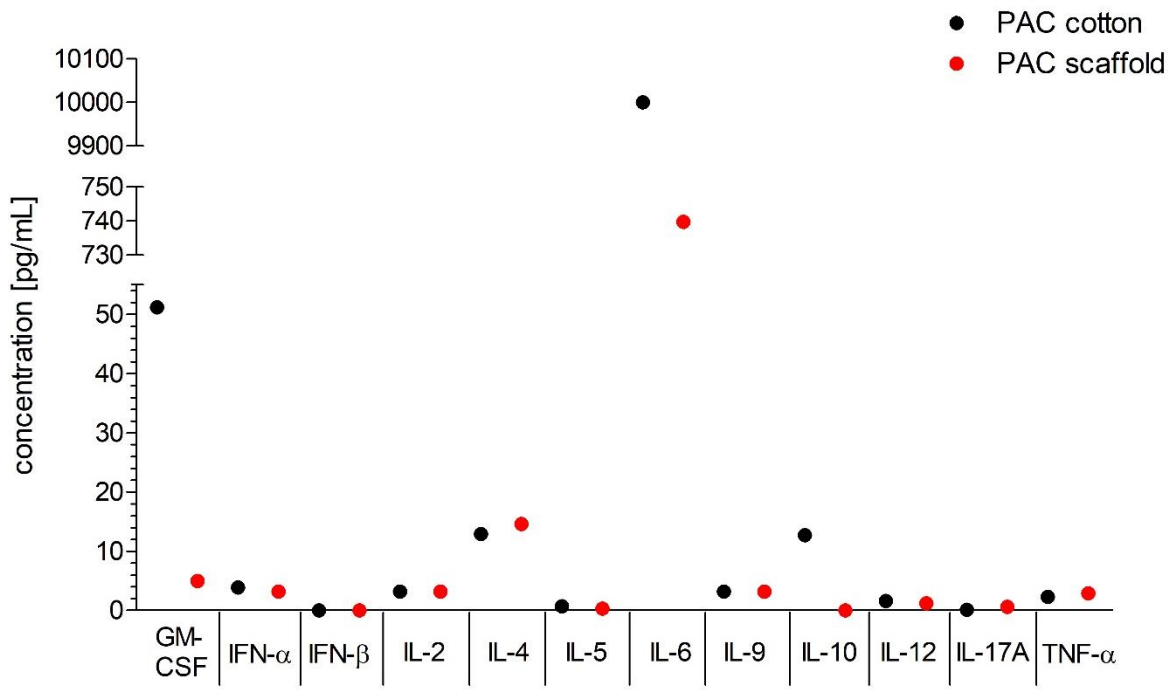

Figure 49: ***Examination of PAC culture medium flow-through of patient 2 after 3 days culture.*** *The organotypic supports cotton mesh and cell-free porcine intestine (scaffold) were compared. The PAC cultivation was conducted with two tumor tissue slices each. The perfusion rate was 83.3 µL/h.*

In the next step, the influence of cisplatin on tumor tissue slice cytokine production of patient 2 in the flow-through after PAC culture was investigated. The medium flow-through after 3 days of culture in the presence or absence of 13 µM cisplatin was examined with cotton mesh as the organotypic support (Figure 50). From a total of 12 cytokines, 9 cytokines were detected. The cytokine concentrations of GM-CSF and IL-10 were increased in the presence of cisplatin. IL-5, IL-4, INF-α and TNF-α showed decreased concentrations when cisplatin was present and no changes in cytokine concentrations were observed for IL-2, IL-6, and IL-9.

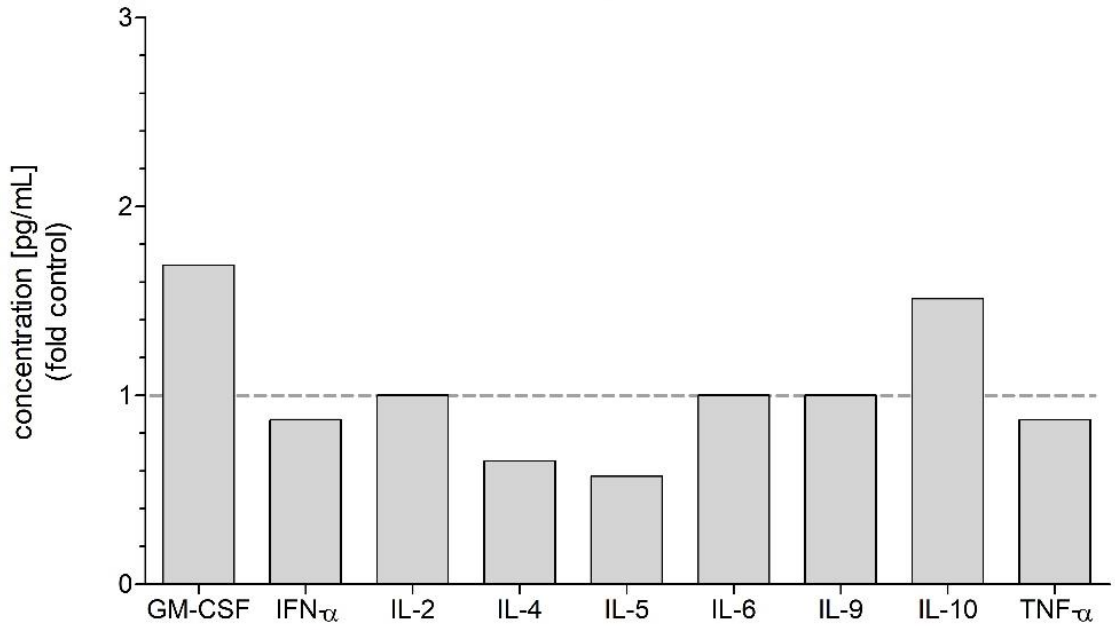

Figure 50: ***Examination of medium flow-through with or without 13 µM cisplatin after culture of tumor tissue slices from patient 2 after cultivation in the PAC system.*** *The chosen organotypic support was cotton mesh and the tissue slices were cultured for 3 days. The concentration of cytokines was determined in the presence of 13 µM cisplatin (bars) and normalized to the concentration of the cell culture control medium (dashed line).*

Overall, these results suggest that most cytokines were detectable at different time points, after cultivation in different tumor tissue slice systems and after additional cisplatin-treatment. In addition, no cisplatin-induced instability of the cytokines was observed since the cytokines could be measured in the presence of the drug. However, cisplatin incubation of the tumor tissue slices seemed to have an impact on the cytokine's secretion.

3.2.9 Analysis of the cell viability in tumor tissue slices after culture

After successful cytokines detection in the supernatant and medium flow-through post culture in the MF and PAC system, the tissue slices were further examined regarding their single cell viability. Tumor tissue slices after culture in the MF and PAC system were dissociated and tumor cells were isolated. Analyses showed that a majority of 89.75% to 98.17% of isolated tumor cells from ovarian cancer tissue slices cultivated in either the MF or PAC system were viable (Figure 51A). This was not the case in Figure 51B where the remaining cells showed only 11.53-38.13% cell viability. In both cultivation systems, the samples incubated with cisplatin contained less viable tumor cells: Tissue slices with cisplatin incubation on MF system led to 3.62% tumor cell

death, while in the PAC system the cell death in tumor cells after cisplatin treatment was 7.68%. Analyses of the remaining cells showed a 25.7% increased cell death with cisplatin incubation cultivated in the MF system. In the PAC system the situation was vice versa: 15.05% decreased cell death was observed in the presence of cisplatin.

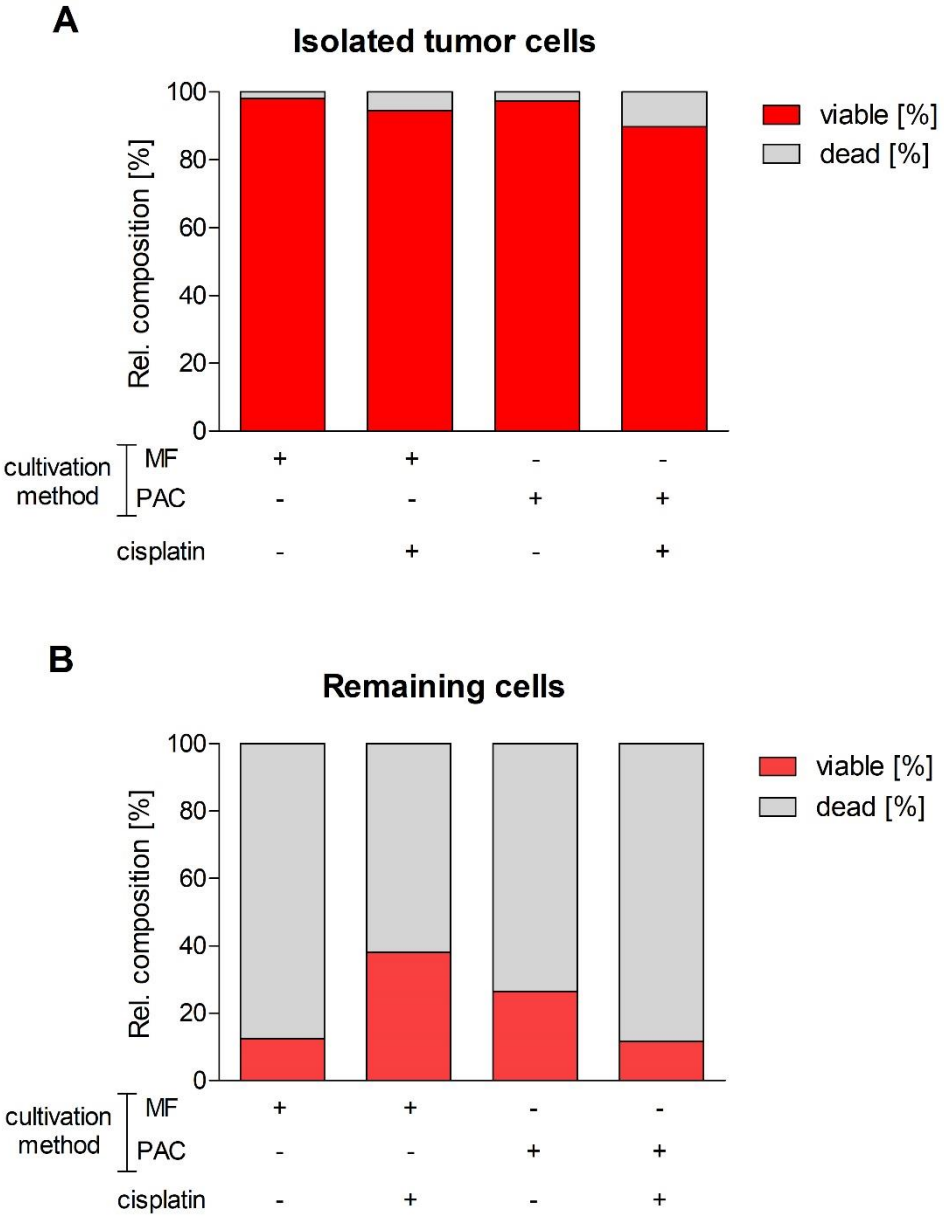

Figure 51: ***Investigation of cell viability in primary tissue slices of human ovarian cancer tumors.*** *Two slices each were cultivated in the PAC and MF system with and without 13 µM cisplatin and analyzed after 3 days of culture. Tumor cells were isolated from the remaining cells via magnetic beads and the relative (rel.) composition of cell viability of (A) tumor and (B) remainig cells was analyzed using flow cytometry. (n=2)*

Taken together, these preliminary results indicated that the cell viability analysis of tissue slices was possible. However, in the future, the studies should be repeated with more tumor tissue slices.

3.2.10 Analysis of tumor cell migration of tumor tissue slices

Using cell-free porcine intestine as organotypic support, migrating cells were observed during cultivation in the PAC system. To analyze the tumors, the samples were stained for HE. If more than 10 cells per tissue slice were found that have migrated into the scaffold, the tumor was considered invasive. To test the migration assay, already known invasive and non-invasive CDX tissue slices from lung cancer were used (Figure 52). Non-invasive H1437 and invasive Calu-1 CDX tissue slices were cultivated in the PAC system in-between the organotypic support cell-free porcine intestine. HE stains were performed on d3 and d5 and indicated that H1437 cells did not migrate from the tissue in contrast to Calu-1 cells. No differences between the two time points were observed.

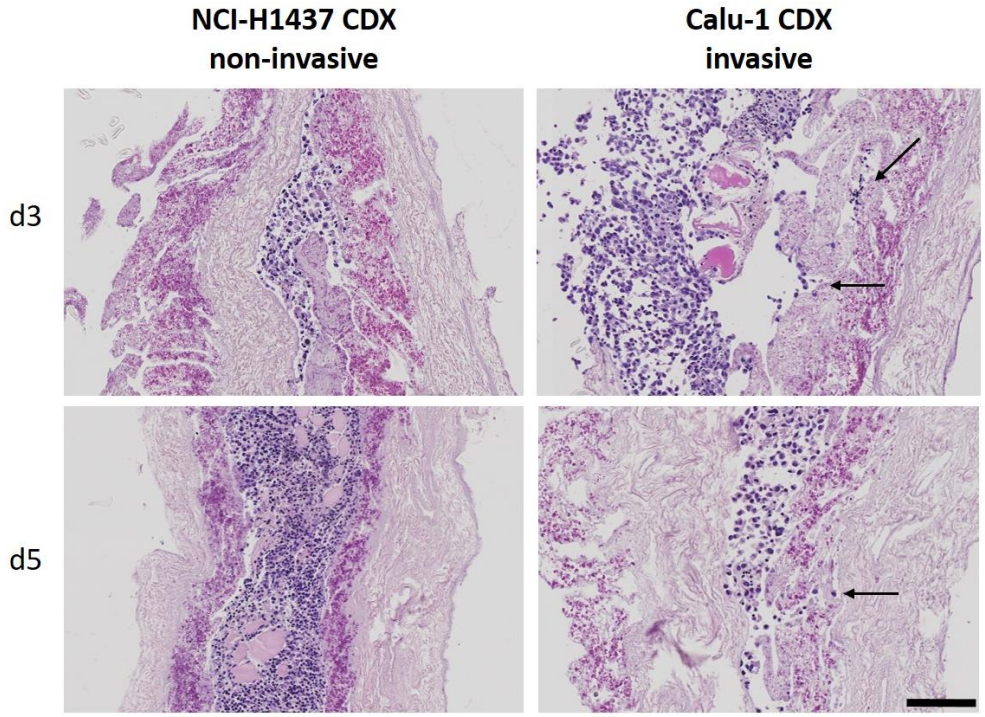

Figure 52: ***Investigation of tumor cell migration of lung cancer CDX tissue slices.*** *Tissue slices were cultured for 3 or 5 days in the PAC system using cell-free porcine intestine as organotypic support. HE stains were performed to analyze the tumor cell migration of non-invasive and invasive tumors. Black arrows indicate migrating tumor cells. Scale bar represents 100 µm. (n=3)*

Additionally, primary human ovarian cancer tissue was analyzed for cell migration. The tumor tissue slices were stained for HE after 3 and 5-8 days of culture in the PAC system. Tumor samples from 10 different patients were examined (Table 12).

Table 12: Summary of the migration assay results from 10 different ovarian cancer patient samples and study of invasiveness.

Cultivation days	**Invasion**	
	+	**-**
3	3	2
≥5	2	3
∑	5	5

In summary, 50% of the tumors showed cell migration into the scaffold. Representative images of invasive tumors are displayed in Figure 53. Invasive tumors were IHC stained for p53 and showed that the invasiveness of the cells is p53-independent.

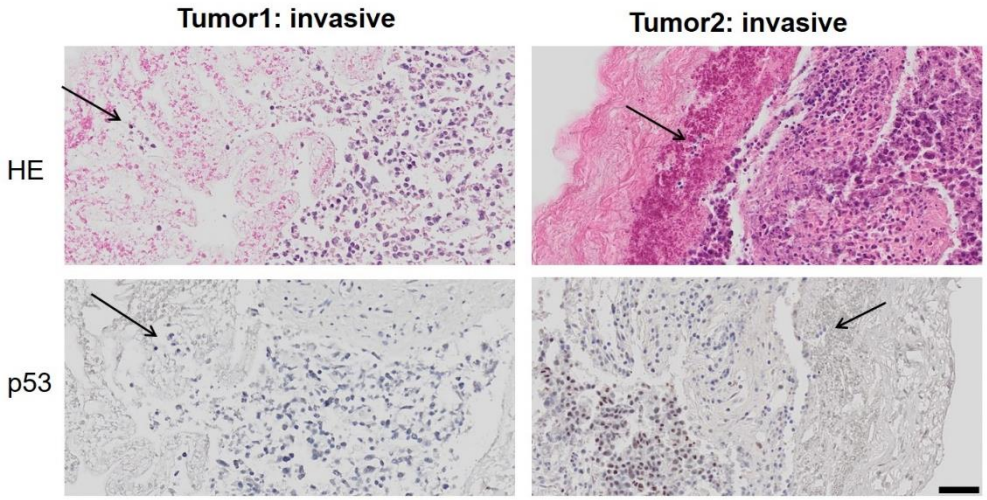

Figure 53: ***Representative images of invasive primary ovarian cancer tumor tisssue slices between cell-free porcine intestine.*** *HE stains visualize morphology and structure of the tissue. IHC stains for p53 show p53+ and p53- cells were migrating into the scaffold. Black arrows highlight migrating cells. The scale bar corresponds to 50 µm. (n=10)*

4 Discussion

In this work, ovarian cancer persister cells and different 3D cancer models were characterized especially using hydrogels and the novel tumor tissue slice cultivation system named perfusion air culture (PAC) was examined. In the first part, high-grade serous ovarian cancer persister cells (DTP) were generated, indicating filopodia-like structures on the cell surface, and compared to control cells without such structures. Individual clones of both approaches were compared, and a significantly increased ER stress expression pattern, including *ATF3*, of the three most aggressive DTP clones compared to the three least aggressive control clones was shown. *In vivo* patient survival data corroborated the finding that high *ATF3* expression was not beneficial for survival.

The second part of this work focused on 3D cultivation of tumor cells, patient-derived organoids, and tumor tissue slices. Cancer models that enabled 3D cell culture using various hydrogels were established and led to optimized culture conditions. Furthermore, common cultivation systems of tumor tissue slices were compared to the novel PAC system by using tissue slices of CDX and primary human ovarian cancer tumors. The PAC system was then further investigated regarding the cytokine secretion into the medium flow-through and the single cell viability of dissociated tumor tissue slices. Proof of principle analyses revealed that two tissue slices were sufficient to detect messenger substances and to analyze cells from tissue slices. In summary, these results showed that the PAC system was a useful platform for tumor tissue slice cultivation and further investigation of tumor tissue slices.

4.1 Ovarian cancer persister cells

This study aimed the identification of gene programs associated with aggressive DTP. In addition, the overall goal was to predict the response to therapy and identify biomarkers to overcome treatment tolerance, eventually eradicate DTPs and prevent tumor recurrence.

By using a clinical relevant drug concentration of cisplatin therapy in a cisplatin-sensitive (Kleih et al., 2019) ovarian cancer cell line, drug-tolerant clonal populations were generated. These clones showed an enhanced motility as a phenotypic marker of DTP-derived cells. This migratory phenotype of persister-derived cells is consistent with data from Gonzalez et al, who found that poor prognosis of HGSOC patients

correlates with a fast migrating cellular phenotype and that incidence of the migratory phenotype correlates with a transitional EMT phenotype and metastasis formation (Gonzalez et al., 2018). To identify underlying molecular processes, a RNA-seq analysis was performed, reflecting downstream effects including non-mutational changes not detectable by genome analysis. RNA-seq data from 8 treatment-naïve and 12 DTP-derived clones identified 55 DEG (p_{adj}<0.05, FC>1.5). However, the number of differential genes across the entire panel of clones was rather low, presumably as a result of the large phenotypic heterogeneity within each of the two groups, which is often seen in p53 mutated cells (Kanjilal et al., 1993, Mirchandani et al., 1995). Therefore, the further analysis of the RNA-seq data was limited to three clones with an aggressive persister-specific phenotype (aDTP) characterized by reduced drug-induced cell death, increased clonogenic survival and increased motility. Comparison of these three clones to three least aggressive treatment-naïve-derived control clones (naControl) revealed 334 DEG (p_{adj}<0.05, FC>1.5) including that the ER stress response, whose deregulation is recognized as a hallmark of cancer (Urra et al. 2016), is enhanced in the aDTPs. In addition to *ATF3*, *DUSP5*, *PDE4B* and *KLF9* are involved in the ER stress response and are significantly upregulated in aDTP. These genes represent targets of the ER stress pathway or are directly correlated with poor patient survival (Aurtenetxe et al., 2018, Fink et al., 2018, Jo et al., 2019, Mihailidou et al., 2010). In breast cancer, *ATF3* was reported to contribute to pro-metastic alterations aggravated by chemotherapy (Chang et al., 2017), and in addition, in squamous cell carcinoma of the tongue, downregulation of *ATF3* expression has been shown to inhibit cell invasion and EMT (Shi et al., 2018), linking aggressive cancer attributes to stress. ER stress is induced by misfolded proteins and amino acid deprivation and induces unfolded protein response (UPR) via activation of IRE1α, ATF6 or PERK. Active IRE1α splices XBP1 mRNA and the resulting changed ORF is translated into XBP1s (Lu et al., 2014), augmenting the expression of downstream target genes involved in folding, glycosylation and ER-associated degradation (ERAD) (Walter, Ron, 2011). The kinase PERK phosphorylates and inactivates the eukaryotic translation initiation factor 2 (eIF2), resulting in global inhibition of protein translation (Walter, Ron, 2011) and preferential expression of mRNAs that contain a short open reading frame, such as ATF4 (Harding et al., 2003, Lange et al., 2008). ATF4 mediates expression of ATF3 (Jiang et al., 2004), resulting in upregulation of UPR target genes such as “growth arrest and DNA damage-inducible protein 34” (GADD34) and “C/EBP homologous

protein" (CHOP/GADD153) (Ma, Hendershot, 2004). However, upregulation of ATF3 has also been reported downstream of cATF6 or IRE1α (Jiang et al., 2004). Only a limited number of ER stress modulators are expected to be detected by RNAseq, since a large part of the upstream gene products involved in ER stress response is not subject to transcriptional control.

In line with previous results from the GSEA of naïve versus DTP-derived clones, upregulated genes (*EMILIN3*, *CEACAM1*) were found that are involved in the hallmark of cancer angiogenesis (Christian et al., 2001, Dango et al., 2008) as well as suggested biomarkers for pancreatic cancer (Simeone et al., 2007), underlining the increased aggressiveness of aDTP.

In the context of increasing motility, aDTP indicated an elevated expression of migration, invasion or EMT promoting genes, such as, *ST3GAL1* (Chong et al., 2016, Wu et al., 2018), *EGR3* (Inoue et al., 2004), *CDKN1A* (Kreis et al., 2019), *ABCG1* (Tian et al., 2017), *LGALS17A* (Balan et al., 2010, Ebrahim et al., 2014), *SALL4* (Zhang et al., 2015) and *SUSD2* (Xu et al., 2018). These upregulated genes could contribute to an increased motility and pseudopodia-like structures in aDTP. Since *SALL4* and *CDKN1A* were also significantly regulated in the first comparison of treatment-naive versus DTP-derived clones, this suggests that the two genes play a pivotal role in enhanced motility of *in vitro* aDTPs.

Furthermore, a stress-related transcriptional profile including *ATF3* has been described, which was enriched during platinum-based chemotherapy in HGSOC and was significantly associated with poor progression-free survival (Zhang et al., 2020). In conclusion, the increased expression of ER stress response genes might be a feature of aDTPs in HGSOC.

Finally, survival data of HGSOC patients revealed that high expression of *ATF3* is associated with a reduced 5-year survival rate. This is consistent with the proposed role of *ATF3* in drug tolerance and tumor recurrence. In line with this, in prostate cancer, high expression of ATF3 was described to be correlated with poor prognosis (Pelzer et al., 2006). ATF3 represses expression of CHOP/GADD153 (Wolfgang et al., 1997); because CHOP/GADD153 induces cell cycle arrest and apoptosis in response to cellular stress (Maytin et al., 2001, Zinszner et al., 1998), its suppression by ATF3 supports proliferation and viability, consistent with pro-oncogenic activity. However, ATF3 is also attributed to tumor-suppressive activities, because overexpression of ATF3 increases apoptosis of human prostate cancer cells (Huang et al., 2008).

Additionally, low expression of ATF3 has been found in ovarian cancer cells but the opposite was found in non-cancerous ovarian epithelial cells (Syed et al., 2005). A possible explanation for these seemingly contradictory results, thus enhanced ATF3 expression and reduced drug-sensitivity of aDTP, might be defective signal transduction by ATF3. This might explain why ATF3 downstream target genes are not among the DEG prominently upregulated in aDTP.

The ER stress response has been implicated in tolerance and resistance to cisplatin and targeted therapies (Katano et al., 2002, Mishima et al., 2002). Recently, drug tolerance has received much attention and various mechanisms have been identified that promote cell survival in the presence of cytotoxic drugs. In this work, the ER stress response as a drug tolerance mediating mechanism was identified, along with further significantly upregulated genes in aDTP (*OPLAH, SALL4*) that are correlated with drug resistances (Oikawa et al., 2013, Shi et al., 2019). In the context of platinum-based therapy, cisplatin induces mitochondrial DNA damage and oxidative stress (Kleih et al., 2019, Marullo et al., 2013), which in turn elicits an ER stress response. While the assumption that constitutively elevated ER stress favors survival seems reasonable at first, it seems a paradox when considering the pro-apoptotic effect of the ER stress response. However, this question can be addressed by the assumption that DTP inherit defects in signaling pathways that are downstream of ATF3. The reason for aDTP tolerating an increased pro-apoptotic threshold might be mutations or epigenetic aberrations in central effector proteins, such as BAX (Sakuragi et al., 2002), which are selected for in tumor cells. Irrespective of whether increased ER stress itself or activation of anti-apoptotic mechanisms facilitate drug tolerance, the findings of this work may offer new clues for therapeutic intervention.

4.2 Hydrogel embedded 3D cell cultivation systems

Pre-test experiments using cell lines revealed that embedding with alginate was beneficial to the cell cultivation in contrast to agarose as cell embedding gel since the polymerization of alginate was reversible under physiological conditions and did not depend on the gel temperature. This was advantageous for cell analysis after experiments. The process to mix the cells and the agarose gel together were hard to be performed because it was not easy to control the temperature of the agarose gel. It is also reported that alginate allows vascularization, degradation, and provokes only

minimal inflammation in *ex vivo* cell culture (Vanacker et al., 2012). This makes alginate a more favorable hydrogel for further experiments.

Both, $CaCl_2$ and $BaCl_2$, have been described as useful alginate crosslinker for cultivation of different cell types (Mandal, Kundu, 2009, Schrezenmeir et al., 1993). Results from cell line experiments showed less AnnexinV+ cells when alginate-embedding was crosslinked with $CaCl_2$. Therefore, $CaCl_2$ was chosen for further experiments. There was no improvement of cultivation conditions when choosing higher cell numbers to be embedded in the alginate gel. Probably because the cell number range that was used in this study (1, 1.5 or 3×10^6 cells) was still too low that the effects of different cell numbers could not be observed. Furthermore, when $CaCl_2$ was used, only slight differences in AnnexinV+ cells (~10%) were found between the three tested alginates. Cell cycle experiments of cell lines in Sub-G_1 phase showed comparable results with the AnnexinV experiment. Nevertheless, for MCL cell line Mino Alginate 2 indicated low cell death rates and for the lung cancer cell line Calu-1 Alginate 1 was slightly better compared to the other alginates.

All three culture methods floating (FL), Millipore filter (MF) and perfusion air culture (PAC) systems were used for the hydrogel-based 3D models. Since alginate showed better properties than agarose, for the hydrogel-based 3D models, the further experiments focused on the cell-alginate slices. Compared to the FL system, the MCF-7 cell-alginate slices cultured on MF system showed more ER+ cells which indicated a better culture condition. There might be two reasons to explain this. One reason is the air-liquid interface of the MF system might supply enough oxygen to the slices. Another reason might be the filter support of the MF system; it can keep the cell-alginate slices out from the culture medium and support the slices structure to be stable during the culture process. Alginate is a biodegradable hydrogel which can be slowly degraded during the culture because of the culture medium and the proliferation of the embedded cells inside of the gel. Agarose can also be degraded but enzymatically (Shoichet et al., 1996). When Figure 26A of the live-dead assay showed a similar cell distribution and density after 3 days culture with all the three culture methods (FL, MF and PAC), which means after 3 days culture the cells were still encapsulated inside the gel no matter which cultivation method was used. But both the cell-agarose and the cell-alginate slices cultured in the PAC system were degraded during the process of dehydration and paraffin embedding for the IHC staining although they still showed similar morphology as other hydrogel slices cultured in FL and MF

systems after 3 days culture. The fact that hydrogel slices cannot go through the dehydration process for the paraffin block embedding process is a sign of degradation of the hydrogel during culture in PAC system. This may not be induced by the PAC system itself, but the parameters used in the system. The extremely low perfusion rate of 27 µL/h was used in the PAC system for these hydrogel experiments. The low perfusion rate was not sufficient to keep the physiological conditions of the hydrogel slices, they lost water and started degradation during the culture process. Most likely, the hydrogels collapse and the structure is somehow destroyed. Further experiments should be carried out to optimize the experiment parameters of the PAC system for hydrogel slice cultivation. The results of the hydrogel slices indicated that the optimal perfusion rate in the PAC system is very important and the perfusion rate was raised to 83.3 µL/h for further experiments with the tumor tissue slices culture.

As observed in tumor tissue slice culture, the O_2 availability is depending on the chosen culture system. In line with tumor tissue slice experiments, matrix-embedded cell cultivation in the PAC system reproducibly showed a lower lactate production compared to the MF and FL systems.

As Matrigel is not a defined matrix, a certain variability must be assumed, however, it is known that Matrigel contains many growth factors that influence cell behavior and supports cell proliferation (Vukicevic et al., 1992). The isolated patient-derived organoids from primary ovarian cancer cells were embedded exclusively in Matrigel according to the established protocol optimized for colon cancer. The EpCAM staining showed that the organoids were epithelial cells. Since ovarian cancer is also epithelial cells, this confirms that the correct cell type was cultured. Further IHC and live/dead staining revealed that the cells continued to proliferate and showed high cell viability. After 3 days in the PAC system, tumor tissue slices with or without cisplatin treatment were dissociated and further cultivated as organoids in Matrigel. After incubation with cisplatin, fewer and smaller organoids were observed in tumor 1 and in tumor 2 the Matrigel was strongly infiltrated by fibroblasts. After MF culture of tumor 2 tissue slices, no organoids were seen in the Matrigel after organoid embedding. The samples after PAC culture showed very few organoids from the cisplatin-treated tissue slices. Maybe the cisplatin exposure in the PAC system was more efficient, in contrast to the static MF culture. Another reason for these observations might be explained by the inter- and intra-tumoral heterogeneity and the number of fibroblasts in the selected tumor area.

4.3 Tissue slice culture as 3D cancer model system

Considering the heterogeneity and tissue architecture of tumors, the tumor tissue slices reflect the original tissue. For this reason, tumor tissue slice culture is a suitable method for the closer examination of tumors regarding the different cell types and interaction of the tumor microenvironment (TME). The tumor tissue slice culture also enables preclinical testing of drugs and the resulting response of tumor cells. The method also has limitations that still pose a challenge at the present time. An important point is the availability of oxygen and nutrients in the tumor tissue slice. Since the existing vascular system in the tumor was partially destroyed by the cutting process (Kallendrusch et al., 2017), the distribution of these parameters in the cell culture medium can only take place by diffusion (Davies et al., 2015, Minchinton, Tannock, 2006). In mammals, oxygen transport in the blood is executed by the hemoglobin of erythrocytes. Henry's law states that under standard conditions (RT, 1 bar air pressure) 0.2768 mmol/L oxygen is measured in an air-saturated liquid like water (Somerville, Proctor, 2013). Since the cell culture medium also contains salts, the oxygen concentration is even lower. The atmospheric oxygen content under the same conditions is 8.6 mmol/L (oxygen partial pressure 159 mmHg). In comparison, up to 1.4 mL of O_2/g are bound in the blood by hemoglobin at an oxygen partial pressure in the arterial blood of 100 mmHg (Strehl et al., 2004). A blood oxygen content in arteries of 8.47 mmol/L is calculated (1.5% dissolved oxygen, 98.5% hemoglobin-bound oxygen), which is very similar to that in the atmosphere with 8.6 mmol/L. Although the partial pressure of oxygen in the blood is much lower, approximately the same amount of O_2 can be transported in the blood as the atmosphere provides. This is about a factor of 10 more oxygen content (delta arterial and venous O_2 content in blood) than is present in the air-saturated cell culture medium. The oxygen concentration in the medium, in the absence of cells, is only about 2% of the oxygen in the surrounding atmosphere (Chen et al., 2013). This explains why only limited amounts of oxygen can be transferred to the tumor tissue slices through the cell culture medium during the experiments. Therefore, there is an intra-slice gradient formed in the tissue slices cultured on the MF system. The MF system has two different sides: one is the air interface (air side) and the other one is the filter-liquid interface (filter side). While the oxygen diffuses from the air side into the tumor tissue slice, the nutrient and agent deliveries take place from the filter side and after passing the filter to the slice. Since

the cultivation system is static, a low and not comparable efficiency of nutrient exchange to the *in vivo* situation is to be expected. The formation of a loco-regional gradient after culture in the MF system with CDX and primary material has been published (Davies et al., 2015). Oxygen gradients are of course also formed in solid tumors *in vivo* (Hammond et al., 2014), but it must be noted that in the MF system the oxygen and the nutrients and active ingredients diffuse into the tumor tissue slice from two opposite directions. Therefore, attention regarding the gradient formation is required when interpreting the results.

With the PAC system, the problem of gradient formation is eliminated because the supply of O_2, nutrients and medication is provided by both sides of the slice. This is similar to the *in vivo* situation. The cotton organotypic support, which supports the tumor tissue slices from both sides, also has conductivity for the cell culture medium. This results in the possibility that the thickness of the slices is not limited to 300 µm and that thicker slices can be cultivated if necessary. If the oxygen supply is changed, hypoxia may be induced in the middle of the slice during culture in the PAC system. This can be regulated by the choice of organotypic support, which is a key parameter of the system. Two important functions have to be fulfilled: The vascular system of the *in vivo* system must be imitated in order to always supply the tumor tissue slice with sufficient oxygen and nutrients, and it must keep the slice stable and support it, like an artificial extracellular matrix. Thus, the matrix should protect the slice from additional stress (e.g. shear stress) and maintain the required stiffness. Tumor tissue tends to be stiffer than normal tissue, which also influences cell function (Egeblad et al., 2010). Matrix stiffness can influence tissue growth and morphogenesis by modulating cell contractility, and tensional homeostasis (Paszek et al., 2005).

Many different materials have already been tested as organotypic support with regard to their use in the PAC system. In this work, four different membranes were tested. Tumor tissues cultivated in-between membrane B or membrane D indicated only a low amount of destroyed tissue and condensed nuclei. These two membranes were promising candidates to improve the PAC culture. Cotton mesh with a pore size of 500 µm features a very good distribution of O_2, nutrients and active ingredients. The next step would be to compare the two membrane candidates with cotton mesh. A known disadvantage using cotton is that cell loss occurs from the tissue slice surface due to the large pores. By perfusion of the slice in the PAC system, cells were taken by the medium. Therefore, a short-term cultivation limited to 3 days was chosen in the

experiments. The loss of the cells can be prevented by using the cell-free porcine intestine as an organotypic support. It minimizes shear stress caused by the medium and therefore allows a long-term cultivation of tumor tissue slices. Slices from primary ovarian cancer tissue could be cultivated between the intestines for up to 8 days in the PAC system. Despite its good fluid conductivity, the cotton mesh has another disadvantage. When the formalin-fixed and paraffin-embedded (FFPE) blocks were later sectioned for IHC, the cotton makes the cutting process considerably difficult and after only a few cutting operations the blade is blunt. The blade must be changed very often to avoid tearing the fabric during cutting with a dull blade. This requires a high degree of experience in the entire procedure, which is not necessary with cell-free porcine intestines. Although cotton mesh is still necessary as a support and medium distribution around the porcine intestine, it can be easily removed after the culture. In the culture without intestine, the cotton mesh cannot be removed, as otherwise the uppermost cell layers would be removed as well.

Using 3D bioprinting technique, hydrogel meshes were also formed and tested in the PAC system. Both alginate and collagen can be printed out as hydrogel mesh and further applied in the PAC system for slices cultivation. Due to the soft structure, these hydrogel meshes were difficult to be handled during the assembling process of the PAC system. The meshes still need to be developed as an organotypic support for the PAC system. Further optimization of the PAC system would be useful to select an even more suitable organotypic support material. Overall, the PAC system needs to be further optimized, especially with regard to the search for perfect organotypic carriers and a suitable oxygen concentration surrounding the tissue slices during culture.

By culture in the MF or PAC system, similar changes in the major stress signaling pathways were observed in the tumor tissue slices dependent on the tumor entity. This result was confirmed by the expression analysis of the biomarkers. The samples from H1437 CDX mainly indicated clustering by condition with one tumor exception. The lung cell tissue slices cultivated in the PAC system showed most similar gene expression as the d0 control samples. In contrast to the MCF-7 CDX, where the MF cultured samples showed a higher similarity to the control. One explanation could be that the lung tumor cells generally require more oxygen, which is made possible by the PAC system in combination with cotton mesh. Perhaps the MCF-7 breast cancer cells are habituated to a more hypoxic situation due to their tissue origin. What argues against this is that the slices after hypoxia are not more similar to controls. Therefore,

there must be another unknown advantage in the MF that could possibly be due to the static culture without shear stress for the cells. Since the primary *in vivo* ovarian cancer samples in the PCA plot showed a strong heterogeneity, it is difficult to make a conclusion. The heatmap shows that the tumor sample clusters are still formed rather than of cultivation conditions. In summary, the cultivation did not lead to serious changes in gene expression of primary ovarian cancer samples. The cisplatin treatment of the tissue slices induced a higher gene expression alteration in the samples. Expectedly, control samples' gene expression showed a higher similarity to untreated tissue slices' gene expression. Either more experiments should be performed to better cover the heterogeneity or a more suitable method of analysis of the RNA from the tumor tissue slices should be chosen.

The migration experiments using cell-free porcine intestine as organotypic support, show that 50% of the tested tumors indicate migration. Migration is defined as more than 10 cells per tissue slice migrate into the surrounding intestine. It is known that mutant p53 has a major influence on the progression of metastases and regulates the migration and invasion of cells (reviewed in (Muller et al., 2011)). Other groups have shown that genetic modifications of p53 alone are sufficient to promote metastasis formation in cancer (Gadea et al., 2007). In this work, IHC stains for p53 indicate that cells can migrate p53-indepently. A different or further mechanism must therefore take place and allow the cells to migrate out of the tumor tissue.

Cisplatin incubation of tumor tissue slices led to a small increase in γH2AX expression in both systems, MF and PAC, and only in the PAC system an increased CC3 expression was observed. This could be due to a higher aerobic metabolism in the PAC system (Kleih et al., 2019). It is possible that the PAC system is more sensitive to drug treatment and thus the functional reaction of the cells to the drug is sensitized. Further investigations of the varying cisplatin response of the primary tumor tissue slices and in particular the correlation of CC3 expression with clinical patient data could provide more information about the treatment response of the patients. In the ideal case, therapeutic success would be predicted.

Since the medium is perfused in the PAC system, it is possible to observe the secreted messenger substances in temporal resolution without disturbing the culture of the tumor tissue slice. First preliminary experiments showed that at least 8 of 12 cytokines secreted into the medium can be detected. However, only comparisons between time and treatment were made. Since no baseline measurement of the background

cytokines from the medium with supplemented FBS was performed, no conclusion could be drawn on the absolute quantification. This preliminary experiment successfully showed that cytokines were measurable and that they differentiated at different points in time or in combination with drugs. More advanced methods for analysis are available, which e.g. exclusively quantify newly synthesized proteins (Eichelbaum et al., 2012). Only slight differences were seen comparing cotton mesh and cell-free porcine intestine during PAC culture: GM-CSF, IL-6 and IL-10 tended to be increased using cotton as organotypic support. In this work, it was observed that after MF culture with cisplatin, IL-9 increased, and GM-CSF decreased. In contrast to the PAC culture in combination with cisplatin, where GM-CSF and IL-10 concentrations strongly increased, and IL-4 and IL-5 decreased. This was observed in tumor tissue slices of the same patient. Interestingly, in the presence of cisplatin, GM-CSF seemed to decrease in the MF system but increased during PAC cultivation. This could again reflect the more efficient cisplatin treatment in the PAC system, since GM-CSF belongs to the group of pro-inflammatory cytokines (Hamilton, 2002) and therefore acts analogously in the physiologically expected way. Cisplatin-induced cytokine release has already been reported. In the context of inflammation and the secretion of pro-inflammatory molecules, it can even result in hearing loss of the patient (Gentilin et al., 2019). Besides GM-CSF, IL-6 also belongs to the group of pro-inflammatory and IL-10 to anti-inflammatory cytokines. IL-6 is also reported in the context of cisplatin resistance induction in ovarian cancer cells (Wang et al., 2010). The further observed cytokines, e.g. IL-4 and IL-10, are associated with macrophage regulation. IL-5 regulates eosinophil activation (Milburn et al., 1993) and IL-9 is a key regulator of hematopoietic cells (Perumal, Kaplan, 2011). There is no known direct effect of cisplatin on these cytokines, but the cytotoxic agent obviously acts on all proliferating cells of the organism and can thus influence many different signaling pathways. An indirect effect can therefore not be excluded.

In this work, the single cell viability of tumor tissue slices was investigated as well. First, tumor cells were isolated and enriched from the remaining cells of the slice. Both approaches were analyzed separately. The tumor cell approaches showed a very high viability and only ~10-40% of remaining cells were measured viable. Unfortunately, it is not known which antibody exactly was used for tumor cell isolation because a commercial antibody kit was used. No strong correlation between viability and the presence of cisplatin could be observed. Nevertheless, what could be learned from this

preliminary experiment was that the cells from the tumor tissue slices survived the post-culture segregation process and the flow cytometric analyses could be added to the slice culture. Still, this experiment must be repeated with more samples to draw conclusions.

4.4 Avenues to precision and personalized medicine

The basis of precision and personalized medicine in the context of cancer is knowledge of the tumor profile. Meaning, the more information about the *in vivo* situation in the patient is given, the more precisely physicians can adapt cancer therapy. Many mutation targeted drugs are available but due to cancer evolution and inter- or intra-tumoral heterogeneity, drug resistance is acquired and accumulated (Fisher et al., 2013). Therefore, tumor tissue slice culture or any possible primary cell culture including the patient's complex TME should be followed to investigate tumors in patients. An important factor is of course the cost of sequencing and its qualified analysis. These costs of the new analytical methods must be subject to legal regulations and therefore made available to the general public in cancer therapy. At the same time, the newly acquired data must be handled with care and data protection must be regulated. Only then can it be imagined that the current research methods will also be used in all fields. To date, the human genome has been deciphered, in the base sequence yes, but not yet functionally. Further basic research is therefore necessary to gain a better understanding of the entire TME interplay. Simpler models allow conclusions to be drawn about mechanisms and interactions. However, the human organism is not a simple model and is very complex. The tumor tissue slice model provides a useful platform having the possibility to test drugs or drug combinations directly on patient tumors. It further allows, under precisely controlled standard protocols, a prediction to the tumor response. This could improve cancer therapy and enable a major step in the direction of precision and personalized medicine for cancer patients.

5 Conclusion and outlook

In conclusion, in the first part of the work, the ovarian cancer DTP-derived cells were created and characterized. Morphological alterations and an increased expression of an ER stress phenotype in aggressive DTP (aDTP) compared to non-aggressive control ovarian cancer cells were observed. Corroborating the *in vitro* findings, ovarian cancer *in vivo* patient survival data showed high *ATF3* expression is linked with poor survival. Nevertheless, further studies should be conducted to uncover *ATF3* protein expression and thus to find a possible drug target.

In the second part of the work, the optimization and cultivation of advanced 3D cancer models including the 3D hydrogel-based model and the tissue slice model were carried out. Pre-tests of 3D hydrogel embedded with cells allowed finding optimal cultivation conditions, such as choice of hydrogel, embedded cell numbers and suitable cultivation methods. The culture method also played an important role for the 3D cancer models. Under optimized conditions, it represents a promising platform for further analyses and drug tests. Furthermore, the advanced tumor tissue slice culture system named PAC system was tested and the culture conditions for this system were optimized. In comparison to MF culture, the PAC system induced no loco-regional changes in the tumor tissue slices during culture process. Regarding tissue morphology, biomarker expression and stress induction, PAC system showed similar results as MF system for CDX tissue slices culture. Cultivation of ovarian cancer tissue slices, both, PAC and MF cultivation, led to comparable tissue structure alteration and stress induction, whereas cultivation in the PAC system between cell-free porcine intestines allowed an extended cultivation up to 8 days. Cisplatin incubation of the tissue slices showed an increase of CC3 and γH2AX expression. Compared to the corresponded control, the CC3 expression was considerably stronger in the PAC system than in the MF system after 3 days cisplatin treatment. For the tumor tissue slice culture, the PAC system facilitates homogenous and precisely controlled supply of oxygen, nutrients and drugs. It allows long-term culture of tumor tissue and analysis of therapy response. A strategy to further improve the PAC system would be an automated and standardized machine covering all cultivation condition requirements for the tissue slices. This would allow a higher throughput of experiments to analyze statistically evaluable samples more rapidly, thus enabling an approach to personalized cancer medicine.

Furthermore, organoids from ovarian cancer tissue have been successfully established and might be integrated as a selection method of cisplatin-surviving cells subsequent to tumor tissue slice culture. This would allow to quantify drug-tolerant and resistant tumor cells from the tissue slices and to specifically target these cells in a further step. Analyses of the cell culture medium flow-through in the PAC system enabled to compare cytokine concentrations between culture methods and cisplatin incubation. If further investigations can precisely correlate cytokine concentrations to immune cell invasion of the tumor, this could allow differentiation between hot and cold tumors in a quick and straightforward way. It can lead to an easy and fast therapy adaption for the patient. The present study revealed that dissociation of ovarian cancer tumor tissue slices enabled for single cell viability analyses. Therefore, future quantification and comparison of cell viability of different cell types from tumor tissue sections incubated with different drugs or drug combinations might also be possible. This could provide information on the interaction and communication of the tumors and their TME with respect to stroma and immune cells. Thus, the tissue slice culture in PAC system represents a very promising preclinical model for the treatment of cancer on the basis of patient material and can support the fine tuning of cancer therapy. The 3D hydrogel-based model and tumor tissue slice model represent powerful platforms with a variety of options for further development. The advanced 3D cancer models showed great potential for patient specific *in vitro* and *ex vivo* tests and thus allows personalized therapy adaption.

6 List of figures

7 List of tables

8 References

Abdullah, L. N.; Chow, E. K.-H. Mechanisms of chemoresistance in cancer stem cells. *Clinical and translational medicine* **2013,** *2* (1), 3. DOI: 10.1186/2001-1326-2-3.

Agudelo, C. A.; Teramura, Y.; Iwata, H. Cryopreserved agarose-encapsulated islets as bioartificial pancreas: a feasibility study. *Transplantation* **2009,** *87* (1), 29–34. DOI: 10.1097/TP.0b013e318191b24b.

Andersen, T.; Auk-Emblem, P.; Dornish, M. 3D Cell Culture in Alginate Hydrogels. *Microarrays (Basel, Switzerland)* **2015,** *4* (2), 133–161. DOI: 10.3390/microarrays4020133.

Andreassen, P. R.; Ho, G. P. H.; D'Andrea, A. D. DNA damage responses and their many interactions with the replication fork. *Carcinogenesis* **2006,** *27* (5), 883–892. DOI: 10.1093/carcin/bgi319.

Antoniou, A.; Pharoah, P. D. P.; Narod, S.; Risch, H. A.; Eyfjord, J. E.; Hopper, J. L.; Loman, N.; Olsson, H.; Johannsson, O.; Borg, A.; Pasini, B.; Radice, P.; Manoukian, S.; Eccles, D. M.; Tang, N.; Olah, E.; Anton-Culver, H.; Warner, E.; Lubinski, J.; Gronwald, J.; Gorski, B.; Tulinius, H.; Thorlacius, S.; Eerola, H.; Nevanlinna, H.; Syrjäkoski, K.; Kallioniemi, O.-P.; Thompson, D.; Evans, C.; Peto, J.; Lalloo, F.; Evans, D. G.; Easton, D. F. Average risks of breast and ovarian cancer associated with BRCA1 or BRCA2 mutations detected in case Series unselected for family history: a combined analysis of 22 studies. *American journal of human genetics* **2003,** *72* (5), 1117–1130. DOI: 10.1086/375033.

Aurtenetxe, O.; Zaldumbide, L.; Erramuzpe, A.; López, R.; López, J. I.; Cortés, J. M.; Pulido, R.; Nunes-Xavier, C. E. DUSP5 expression associates with poor prognosis in human neuroblastoma. *Experimental and molecular pathology* **2018,** *105* (3), 272–278. DOI: 10.1016/j.yexmp.2018.08.008.

Aylon, Y.; Oren, M. Living with p53, dying of p53. *Cell* **2007,** *130* (4), 597–600. DOI: 10.1016/j.cell.2007.08.005.

Aymard, F.; Bugler, B.; Schmidt, C. K.; Guillou, E.; Caron, P.; Briois, S.; Iacovoni, J. S.; Daburon, V.; Miller, K. M.; Jackson, S. P.; Legube, G. Transcriptionally active chromatin recruits homologous recombination at DNA double-strand breaks. *Nature structural & molecular biology* **2014,** *21* (4), 366–374. DOI: 10.1038/nsmb.2796.

Balan, V.; Nangia-Makker, P.; Raz, A. Galectins as cancer biomarkers. *Cancers* **2010,** *2* (2), 592–610. DOI: 10.3390/cancers2020592.

Ballman, K. V. Biomarker: Predictive or Prognostic? *Journal of clinical oncology : official journal of the American Society of Clinical Oncology* **2015,** *33* (33), 3968–3971. DOI: 10.1200/JCO.2015.63.3651.

Barker, N.; Huch, M.; Kujala, P.; van de Wetering, M.; Snippert, H. J.; van Es, J. H.; Sato, T.; Stange, D. E.; Begthel, H.; van den Born, M.; Danenberg, E.; van den Brink, S.; Korving, J.; Abo, A.; Peters, P. J.; Wright, N.; Poulsom, R.; Clevers, H. Lgr5(+ve) stem cells drive self-renewal in the stomach and build long-lived gastric units in vitro. *Cell stem cell* **2010,** *6* (1), 25–36. DOI: 10.1016/j.stem.2009.11.013.

Bell, D. A. Origins and molecular pathology of ovarian cancer. *Modern pathology : an official journal of the United States and Canadian Academy of Pathology, Inc* **2005,** *18 Suppl 2*, S19-32. DOI: 10.1038/modpathol.3800306.

Bell, D. e. a. Integrated genomic analyses of ovarian carcinoma. *Nature* **2011,** *474* (7353), 609–615. DOI: 10.1038/nature10166.

Benton, G.; Kleinman, H. K.; George, J.; Arnaoutova, I. Multiple uses of basement membrane-like matrix (BME/Matrigel) in vitro and in vivo with cancer cells. *International journal of cancer* **2011,** *128* (8), 1751–1757. DOI: 10.1002/ijc.25781.

Benzoni, E.; Torre, M. L.; Faustini, M.; Stacchezzini, S.; Cremonesi, F.; Conte, U.; Villani, S.; Russo, V.; Ricevuti, G.; Vigo, D. Transient transfection of porcine granulosa cells after 3D culture in barium alginate capsules. *International journal of immunopathology and pharmacology* **2005,** *18* (4), 677–682. DOI: 10.1177/039463200501800409.

Bernstein, C. DNA repair/pro-apoptotic dual-role proteins in five major DNA repair pathways: fail-safe protection against carcinogenesis. *Mutation Research/Reviews in Mutation Research* **2002,** *511* (2), 145–178. DOI: 10.1016/S1383-5742(02)00009-1.

Bian, X.; Xiao, Y.-T.; Wu, T.; Yao, M.; Du, L.; Ren, S.; Wang, J. Microvesicles and chemokines in tumor microenvironment: mediators of intercellular communications in tumor progression. *Molecular cancer* **2019,** *18* (1), 50. DOI: 10.1186/s12943-019-0973-7.

Bigger, J. Treatment of Staphyloeoeeal Infections with Penicillin by Intermittent Sterilisation. *Lancet* [Online] **1944**, 497–500.

Blighe, K. *EnhancedVolcano;* Bioconductor, 2018.

Bos, J. L. ras oncogenes in human cancer: a review. *Cancer Res* **1989,** *49* (17), 4682–4689.

Bouaoun, L.; Sonkin, D.; Ardin, M.; Hollstein, M.; Byrnes, G.; Zavadil, J.; Olivier, M. TP53 Variations in Human Cancers: New Lessons from the IARC TP53 Database and Genomics Data. *Human Mutation* **2016,** *37* (9), 865–876. DOI: 10.1002/humu.23035.

Bouwman, P.; Aly, A.; Escandell, J. M.; Pieterse, M.; Bartkova, J.; van der Gulden, H.; Hiddingh, S.; Thanasoula, M.; Kulkarni, A.; Yang, Q.; Haffty, B. G.; Tommiska, J.; Blomqvist, C.; Drapkin, R.; Adams, D. J.; Nevanlinna, H.; Bartek, J.; Tarsounas, M.; Ganesan, S.; Jonkers, J. 53BP1 loss rescues BRCA1 deficiency and is associated with triple-negative and BRCA-mutated breast cancers. *Nature structural & molecular biology* **2010,** *17* (6), 688–695. DOI: 10.1038/nsmb.1831.

Bowman, K. J.; White, A.; Golding, B. T.; Griffin, R. J.; Curtin, N. J. Potentiation of anti-cancer agent cytotoxicity by the potent poly(ADP-ribose) polymerase inhibitors NU1025 and NU1064. *British journal of cancer* **1998,** *78* (10), 1269–1277. DOI: 10.1038/bjc.1998.670.

Bryant, H. E.; Schultz, N.; Thomas, H. D.; Parker, K. M.; Flower, D.; Lopez, E.; Kyle, S.; Meuth, M.; Curtin, N. J.; Helleday, T. Specific killing of BRCA2-deficient tumours with inhibitors of poly(ADP-ribose) polymerase. *Nature* **2005,** *434* (7035), 913–917. DOI: 10.1038/nature03443.

Cai, Z. H.; Shi, Z. Q.; O'Shea, G. M.; Sun, A. M. Microencapsulated hepatocytes for bioartificial liver support. *Artificial organs* **1988,** *12* (5), 388–393. DOI: 10.1111/j.1525-1594.1988.tb02793.x.

Chang, Y. S.; Jalgaonkar, S. P.; Middleton, J. D.; Hai, T. Stress-inducible gene Atf3 in the noncancer host cells contributes to chemotherapy-exacerbated breast cancer metastasis. *Proceedings of the National Academy of Sciences of the United States of America* **2017,** *114* (34), E7159-E7168. DOI: 10.1073/pnas.1700455114.

Chatterjee, N.; Walker, G. C. Mechanisms of DNA damage, repair, and mutagenesis. *Environmental and molecular mutagenesis* **2017,** *58* (5), 235–263. DOI: 10.1002/em.22087.

Chen, B.; Longtine, M. S.; Nelson, D. M. Pericellular oxygen concentration of cultured primary human trophoblasts. *Placenta* **2013,** *34* (2), 106–109. DOI: 10.1016/j.placenta.2012.11.011.

Chen, S.; Parmigiani, G. Meta-analysis of BRCA1 and BRCA2 penetrance. *Journal of clinical oncology : official journal of the American Society of Clinical Oncology* **2007,** *25* (11), 1329–1333. DOI: 10.1200/JCO.2006.09.1066.

Chipuk, J. E.; Maurer, U.; Green, D. R.; Schuler, M. Pharmacologic activation of p53 elicits Bax-dependent apoptosis in the absence of transcription. *Cancer cell* **2003,** *4* (5), 371–381. DOI: 10.1016/s1535-6108(03)00272-1.

Chong, Y. K.; Sandanaraj, E.; Koh, L. W. H.; Thangaveloo, M.; Tan, M. S. Y.; Koh, G. R. H.; Toh, T. B.; Lim, G. G. Y.; Holbrook, J. D.; Kon, O. L.; Nadarajah, M.; Ng, I.; Ng, W. H.; Tan, N. S.; Lim, K. L.; Tang, C.; Ang, B. T. ST3GAL1-Associated Transcriptomic Program in Glioblastoma Tumor Growth, Invasion, and Prognosis. *Journal of the National Cancer Institute* **2016,** *108* (2). DOI: 10.1093/jnci/djv326.

Christian, S.; Ahorn, H.; Novatchkova, M.; Garin-Chesa, P.; Park, J. E.; Weber, G.; Eisenhaber, F.; Rettig, W. J.; Lenter, M. C. Molecular cloning and characterization of EndoGlyx-1, an EMILIN-like multisubunit glycoprotein of vascular endothelium. *The Journal of biological chemistry* **2001,** *276* (51), 48588–48595. DOI: 10.1074/jbc.M106152200.

Clayton, H. A.; London, N. J.; Colloby, P. S.; Bell, P. R.; James, R. F. The effect of capsule composition on the biocompatibility of alginate-poly-l-lysine capsules. *Journal of microencapsulation* **1991,** *8* (2), 221–233. DOI: 10.3109/02652049109071490.

Correia, A. L.; Bissell, M. J. The tumor microenvironment is a dominant force in multidrug resistance. *Drug resistance updates : reviews and commentaries in antimicrobial and anticancer chemotherapy* **2012,** *15* (1-2), 39–49. DOI: 10.1016/j.drup.2012.01.006.

Crowley, L. C.; Christensen, M. E.; Waterhouse, N. J. Measuring Survival of Adherent Cells with the Colony-Forming Assay. *Cold Spring Harbor protocols* **2016,** *2016* (8). DOI: 10.1101/pdb.prot087171.

Crum, C. P.; Drapkin, R.; Miron, A.; Ince, T. A.; Muto, M.; Kindelberger, D. W.; Lee, Y. The distal fallopian tube: a new model for pelvic serous carcinogenesis. *Current opinion in obstetrics & gynecology* **2007,** *19* (1), 3–9. DOI: 10.1097/GCO.0b013e328011a21f.

Czerniecki, S. M.; Cruz, N. M.; Harder, J. L.; Menon, R.; Annis, J.; Otto, E. A.; Gulieva, R. E.; Islas, L. V.; Kim, Y. K.; Tran, L. M.; Martins, T. J.; Pippin, J. W.; Fu, H.; Kretzler, M.; Shankland, S. J.; Himmelfarb, J.; Moon, R. T.; Paragas, N.; Freedman, B. S.

High-Throughput Screening Enhances Kidney Organoid Differentiation from Human Pluripotent Stem Cells and Enables Automated Multidimensional Phenotyping. *Cell stem cell* **2018,** *22* (6), 929-940.e4. DOI: 10.1016/j.stem.2018.04.022.

Dango, S.; Sienel, W.; Schreiber, M.; Stremmel, C.; Kirschbaum, A.; Pantel, K.; Passlick, B. Elevated expression of carcinoembryonic antigen-related cell adhesion molecule 1 (CEACAM-1) is associated with increased angiogenic potential in non-small-cell lung cancer. *Lung cancer (Amsterdam, Netherlands)* **2008,** *60* (3), 426–433. DOI: 10.1016/j.lungcan.2007.11.015.

Davies, E. J.; Dong, M.; Gutekunst, M.; Närhi, K.; van Zoggel, H. J. A. A.; Blom, S.; Nagaraj, A.; Metsalu, T.; Oswald, E.; Erkens-Schulze, S.; Delgado San Martin, J. A.; Turkki, R.; Wedge, S. R.; af Hällström, T. M.; Schueler, J.; van Weerden, W. M.; Verschuren, E. W.; Barry, S. T.; van der Kuip, H.; Hickman, J. A. Capturing complex tumour biology in vitro: histological and molecular characterisation of precision cut slices. *Scientific reports* **2015,** *5*, 17187. DOI: 10.1038/srep17187.

Dimicco, M. A.; Kisiday, J. D.; Gong, H.; Grodzinsky, A. J. Structure of pericellular matrix around agarose-embedded chondrocytes. *Osteoarthritis and cartilage* **2007,** *15* (10), 1207–1216. DOI: 10.1016/j.joca.2007.03.023.

Dong, M.; Philippi, C.; Loretz, B.; Nafee, N.; Schaefer, U. F.; Friedel, G.; Ammon-Treiber, S.; Griese, E.-U.; Lehr, C.-M.; Klotz, U.; Mürdter, T. E. Tissue slice model of human lung cancer to investigate telomerase inhibition by nanoparticle delivery of antisense 2'-O-methyl-RNA. *International journal of pharmaceutics* **2011,** *419* (1-2), 33–42. DOI: 10.1016/j.ijpharm.2011.07.009.

Dong, M.; Schwab, M.; van der Kuip, H. Device for cultivating tissue sections (patented).

Dupuy, B.; Gin, H.; Baquey, C.; Ducassou, D. In situ polymerization of a microencapsulating medium round living cells. *Journal of biomedical materials research* **1988,** *22* (11), 1061–1070. DOI: 10.1002/jbm.820221109.

Eagle, H.; Foley, G. E. Cytotoxicity in Human Cell Cultures as a Primary Screen for the Detection of Anti-Tumor Agents. *Cancer Res* [Online] **1958,** *18* (9), 1017–1025. https://cancerres.aacrjournals.org/content/18/9/1017.short.

Ebrahim, A. H.; Alalawi, Z.; Mirandola, L.; Rakhshanda, R.; Dahlbeck, S.; Nguyen, D.; Jenkins, M.; Grizzi, F.; Cobos, E.; Figueroa, J. A.; Chiriva-Internati, M. Galectins in cancer: carcinogenesis, diagnosis and therapy. *Annals of translational medicine* **2014,** *2* (9), 88. DOI: 10.3978/j.issn.2305-5839.2014.09.12.

Egeblad, M.; Nakasone, E. S.; Werb, Z. Tumors as organs: complex tissues that interface with the entire organism. *Developmental cell* **2010,** *18* (6), 884–901. DOI: 10.1016/j.devcel.2010.05.012.

Eichelbaum, K.; Winter, M.; Berriel Diaz, M.; Herzig, S.; Krijgsveld, J. Selective enrichment of newly synthesized proteins for quantitative secretome analysis. *Nature biotechnology* **2012,** *30* (10), 984–990. DOI: 10.1038/nbt.2356.

Estes, J. M.; Oliver, P. G.; Straughn, J. M.; Zhou, T.; Wang, W.; Grizzle, W. E.; Alvarez, R. D.; Stockard, C. R.; LoBuglio, A. F.; Buchsbaum, D. J. Efficacy of anti-death receptor 5 (DR5) antibody (TRA-8) against primary human ovarian carcinoma using a novel ex vivo tissue slice model. *Gynecologic oncology* **2007,** *105* (2), 291–298. DOI: 10.1016/j.ygyno.2006.12.033.

Evan, G. I.; Lewis, G. K.; Ramsay, G.; Bishop, J. M. Isolation of monoclonal antibodies specific for human c-myc proto-oncogene product. *Molecular and cellular biology* **1985,** *5* (12), 3610–3616. DOI: 10.1128/MCB.5.12.3610.

Even-Ram, S.; Yamada, K. M. Cell migration in 3D matrix. *Current opinion in cell biology* **2005,** *17* (5), 524–532. DOI: 10.1016/j.ceb.2005.08.015.

Farmer, H.; McCabe, N.; Lord, C. J.; Tutt, A. N. J.; Johnson, D. A.; Richardson, T. B.; Santarosa, M.; Dillon, K. J.; Hickson, I.; Knights, C.; Martin, N. M. B.; Jackson, S. P.; Smith, G. C. M.; Ashworth, A. Targeting the DNA repair defect in BRCA mutant cells as a therapeutic strategy. *Nature* **2005,** *434* (7035), 917–921. DOI: 10.1038/nature03445.

Feeley, K. M.; Wells, M. Precursor lesions of ovarian epithelial malignancy. *Histopathology* **2001,** *38* (2), 87–95. DOI: 10.1046/j.1365-2559.2001.01042.x.

Fink, E. E.; Moparthy, S.; Bagati, A.; Bianchi-Smiraglia, A.; Lipchick, B. C.; Wolff, D. W.; Roll, M. V.; Wang, J.; Liu, S.; Bakin, A. V.; Kandel, E. S.; Lee, A.-H.; Nikiforov, M. A. XBP1-KLF9 Axis Acts as a Molecular Rheostat to Control the Transition from Adaptive to Cytotoxic Unfolded Protein Response. *Cell reports* **2018,** *25* (1), 212-223.e4. DOI: 10.1016/j.celrep.2018.09.013.

Fisher, R.; Pusztai, L.; Swanton, C. Cancer heterogeneity: implications for targeted therapeutics. *British journal of cancer* **2013,** *108* (3), 479–485. DOI: 10.1038/bjc.2012.581.

Frederick, P. J.; Kendrick, J. E.; Straughn, J. M.; Della Manna, D. L.; Oliver, P. G.; Lin, H.-Y.; Grizzle, W. E.; Stockard, C. R.; Alvarez, R. D.; Zhou, T.; LoBuglio, A. F.; Buchsbaum, D. J. Effect of TRA-8 anti-death receptor 5 antibody in combination

with chemotherapy in an ex vivo human ovarian cancer model. *International journal of gynecological cancer : official journal of the International Gynecological Cancer Society* **2009,** *19* (5), 814–819. DOI: 10.1111/IGC.0b013e3181a2a003.

Friedman, L. S.; Ostermeyer, E. A.; Szabo, C. I.; Dowd, P.; Lynch, E. D.; Rowell, S. E.; King, M. C. Confirmation of BRCA1 by analysis of germline mutations linked to breast and ovarian cancer in ten families. *Nature genetics* **1994,** *8* (4), 399–404. DOI: 10.1038/ng1294-399.

Friedrich, J.; Seidel, C.; Ebner, R.; Kunz-Schughart, L. A. Spheroid-based drug screen: considerations and practical approach. *Nature protocols* **2009,** *4* (3), 309–324. DOI: 10.1038/nprot.2008.226.

Gadea, G.; Toledo, M. de; Anguille, C.; Roux, P. Loss of p53 promotes RhoA-ROCK-dependent cell migration and invasion in 3D matrices. *The Journal of cell biology* **2007,** *178* (1), 23–30. DOI: 10.1083/jcb.200701120.

Gentilin, E.; Simoni, E.; Candito, M.; Cazzador, D.; Astolfi, L. Cisplatin-Induced Ototoxicity: Updates on Molecular Targets. *Trends in molecular medicine* **2019,** *25* (12), 1123–1132. DOI: 10.1016/j.molmed.2019.08.002.

Gerlach, M. M.; Merz, F.; Wichmann, G.; Kubick, C.; Wittekind, C.; Lordick, F.; Dietz, A.; Bechmann, I. Slice cultures from head and neck squamous cell carcinoma: a novel test system for drug susceptibility and mechanisms of resistance. *British journal of cancer* **2014,** *110* (2), 479–488. DOI: 10.1038/bjc.2013.700.

Gerlinger, M.; Rowan, A. J.; Horswell, S.; Math, M.; Larkin, J.; Endesfelder, D.; Gronroos, E.; Martinez, P.; Matthews, N.; Stewart, A.; Tarpey, P.; Varela, I.; Phillimore, B.; Begum, S.; McDonald, N. Q.; Butler, A.; Jones, D.; Raine, K.; Latimer, C.; Santos, C. R.; Nohadani, M.; Eklund, A. C.; Spencer-Dene, B.; Clark, G.; Pickering, L.; Stamp, G.; Gore, M.; Szallasi, Z.; Downward, J.; Futreal, P. A.; Swanton, C. Intratumor heterogeneity and branched evolution revealed by multiregion sequencing. *The New England journal of medicine* **2012,** *366* (10), 883–892. DOI: 10.1056/NEJMoa1113205.

Gey, G. O.; Coffman, W. D.; Kubicek, M. T. Tissue culture studies of the proliferative capacity of cervical carcinoma and normal epithelium. *Cancer Res* [Online] **1952,** *12*, 264–265. https://ci.nii.ac.jp/naid/10006432514/.

Gonzalez, V. D.; Samusik, N.; Chen, T. J.; Savig, E. S.; Aghaeepour, N.; Quigley, D. A.; Huang, Y.-W.; Giangarrà, V.; Borowsky, A. D.; Hubbard, N. E.; Chen, S.-Y.; Han, G.; Ashworth, A.; Kipps, T. J.; Berek, J. S.; Nolan, G. P.; Fantl, W. J. Commonly

Occurring Cell Subsets in High-Grade Serous Ovarian Tumors Identified by Single-Cell Mass Cytometry. *Cell reports* **2018,** *22* (7), 1875–1888. DOI: 10.1016/j.celrep.2018.01.053.

Gottesman, M. M. Mechanisms of cancer drug resistance. *Annual review of medicine* **2002,** *53*, 615–627. DOI: 10.1146/annurev.med.53.082901.103929.

Gottesman, M. M.; Pastan, I. H. The Role of Multidrug Resistance Efflux Pumps in Cancer: Revisiting a JNCI Publication Exploring Expression of the MDR1 (P-glycoprotein) Gene. *Journal of the National Cancer Institute* **2015,** *107* (9). DOI: 10.1093/jnci/djv222.

Green, D. R.; Kroemer, G. Cytoplasmic functions of the tumour suppressor p53. *Nature* **2009,** *458* (7242), 1127–1130. DOI: 10.1038/nature07986.

Grosso, S. H. G.; Katayama, M. L. H.; Roela, R. A.; Nonogaki, S.; Soares, F. A.; Brentani, H.; Lima, L.; Folgueira, M. A. A. K.; Waitzberg, A. F. L.; Pasini, F. S.; Góes, J. C. G. S.; Brentani, M. M. Breast cancer tissue slices as a model for evaluation of response to rapamycin. *Cell and tissue research* **2013,** *352* (3), 671–684. DOI: 10.1007/s00441-013-1608-8.

Gudmundsdottir, K.; Ashworth, A. The roles of BRCA1 and BRCA2 and associated proteins in the maintenance of genomic stability. *Oncogene* **2006,** *25* (43), 5864–5874. DOI: 10.1038/sj.onc.1209874.

Haber, D. A.; Settleman, J. Cancer: drivers and passengers. *Nature* **2007,** *446* (7132), 145–146. DOI: 10.1038/446145a.

Hamilton, J. A. GM-CSF in inflammation and autoimmunity. *Trends in immunology* **2002,** *23* (8), 403–408. DOI: 10.1016/S1471-4906(02)02260-3.

Hammond, E. M.; Asselin, M.-C.; Forster, D.; O'Connor, J. P. B.; Senra, J. M.; Williams, K. J. The meaning, measurement and modification of hypoxia in the laboratory and the clinic. *Clinical oncology (Royal College of Radiologists (Great Britain))* **2014,** *26* (5), 277–288. DOI: 10.1016/j.clon.2014.02.002.

Hanahan, D.; Weinberg, R. A. Hallmarks of cancer: the next generation. *Cell* **2011,** *144* (5), 646–674. DOI: 10.1016/j.cell.2011.02.013.

Harding, H. P.; Zhang, Y.; Zeng, H.; Novoa, I.; Lu, P. D.; Calfon, M.; Sadri, N.; Yun, C.; Popko, B.; Paules, R.; Stojdl, D. F.; Bell, J. C.; Hettmann, T.; Leiden, J. M.; Ron, D. An Integrated Stress Response Regulates Amino Acid Metabolism and Resistance to Oxidative Stress. *Molecular cell* **2003,** *11* (3), 619–633. DOI: 10.1016/S1097-2765(03)00105-9.

Haupt, Y.; Rowan, S.; Shaulian, E.; Vousden, K. H.; Oren, M. Induction of apoptosis in HeLa cells by trans-activation-deficient p53. *Genes & development* **1995,** *9* (17), 2170–2183. DOI: 10.1101/gad.9.17.2170.

Hickman, J. A.; Graeser, R.; Hoogt, R. de; Vidic, S.; Brito, C.; Gutekunst, M.; van der Kuip, H. Three-dimensional models of cancer for pharmacology and cancer cell biology: capturing tumor complexity in vitro/ex vivo. *Biotechnology journal* **2014,** *9* (9), 1115–1128. DOI: 10.1002/biot.201300492.

Hinton, T. J.; Jallerat, Q.; Palchesko, R. N.; Park, J. H.; Grodzicki, M. S.; Shue, H.-J.; Ramadan, M. H.; Hudson, A. R.; Feinberg, A. W. Three-dimensional printing of complex biological structures by freeform reversible embedding of suspended hydrogels. *Science advances* **2015,** *1* (9), e1500758. DOI: 10.1126/sciadv.1500758.

Hirschberg, E. Tissue Culture in Cancer Chemotherapy Screening. *Cancer Res* [Online] **1958,** *18* (8 Part 1), 869–878. https://cancerres.aacrjournals.org/content/18/8_part_1/869.short.

Holliday, D. L.; Moss, M. A.; Pollock, S.; Lane, S.; Shaaban, A. M.; Millican-Slater, R.; Nash, C.; Hanby, A. M.; Speirs, V. The practicalities of using tissue slices as preclinical organotypic breast cancer models. *Journal of clinical pathology* **2013,** *66* (3), 253–255. DOI: 10.1136/jclinpath-2012-201147.

Hotary, K.; Li, X.-Y.; Allen, E.; Stevens, S. L.; Weiss, S. J. A cancer cell metalloprotease triad regulates the basement membrane transmigration program. *Genes & development* **2006,** *20* (19), 2673–2686. DOI: 10.1101/gad.1451806.

Hou, S.; Tiriac, H.; Sridharan, B. P.; Scampavia, L.; Madoux, F.; Seldin, J.; Souza, G. R.; Watson, D.; Tuveson, D.; Spicer, T. P. Advanced Development of Primary Pancreatic Organoid Tumor Models for High-Throughput Phenotypic Drug Screening. *SLAS discovery : advancing life sciences R & D* **2018,** *23* (6), 574–584. DOI: 10.1177/2472555218766842.

Huang, X.; Li, X.; Guo, B. KLF6 induces apoptosis in prostate cancer cells through up-regulation of ATF3. *The Journal of biological chemistry* **2008,** *283* (44), 29795–29801. DOI: 10.1074/jbc.M802515200.

HUB Organoids. Organoid Biobank. https://huborganoids.nl/organoid-biobank/ (accessed September 17, 2020).

Hunt, N. C.; Grover, L. M. Cell encapsulation using biopolymer gels for regenerative medicine. *Biotechnology letters* **2010,** *32* (6), 733–742. DOI: 10.1007/s10529-010-0221-0.

Indivumed GmbH. http://indivumed.com/ (accessed August 19, 2020).

Inoue, A.; Omoto, Y.; Yamaguchi, Y.; Kiyama, R.; Hayashi, S.-I. Transcription factor EGR3 is involved in the estrogen-signaling pathway in breast cancer cells. *Journal of molecular endocrinology* **2004,** *32* (3), 649–661. DOI: 10.1677/jme.0.0320649.

Ison, G.; Howie, L. J.; Amiri-Kordestani, L.; Zhang, L.; Tang, S.; Sridhara, R.; Pierre, V.; Charlab, R.; Ramamoorthy, A.; Song, P.; Li, F.; Yu, J.; Manheng, W.; Palmby, T. R.; Ghosh, S.; Horne, H. N.; Lee, E. Y.; Philip, R.; Dave, K.; Chen, X. H.; Kelly, S. L.; Janoria, K. G.; Banerjee, A.; Eradiri, O.; Dinin, J.; Goldberg, K. B.; Pierce, W. F.; Ibrahim, A.; Kluetz, P. G.; Blumenthal, G. M.; Beaver, J. A.; Pazdur, R. FDA Approval Summary: Niraparib for the Maintenance Treatment of Patients with Recurrent Ovarian Cancer in Response to Platinum-Based Chemotherapy. *Clinical cancer research : an official journal of the American Association for Cancer Research* **2018,** *24* (17), 4066–4071. DOI: 10.1158/1078-0432.CCR-18-0042.

Iwata, H.; Kobayashi, K.; Takagi, T.; Oka, T.; Yang, H.; Amemiya, H.; Tsuji, T.; Ito, F. Feasibility of agarose microbeads with xenogeneic islets as a bioartificial pancreas. *Journal of biomedical materials research* **1994,** *28* (9), 1003–1011. DOI: 10.1002/jbm.820280905.

Jeppsson, J. O.; Laurell, C. B.; Franzén, B. Agarose gel electrophoresis. *Clinical chemistry* **1979,** *25* (4), 629–638.

Jiang, H.-Y.; Wek, S. A.; McGrath, B. C.; Lu, D.; Hai, T.; Harding, H. P.; Wang, X.; Ron, D.; Cavener, D. R.; Wek, R. C. Activating transcription factor 3 is integral to the eukaryotic initiation factor 2 kinase stress response. *Molecular and cellular biology* **2004,** *24* (3), 1365–1377. DOI: 10.1128/MCB.24.3.1365-1377.2004.

Jo, H. J.; Yang, J. W.; Park, J. H.; Choi, E. S.; Lim, C.-S.; Lee, S.; Han, C. Y. Endoplasmic Reticulum Stress Increases DUSP5 Expression via PERK-CHOP Pathway, Leading to Hepatocyte Death. *International journal of molecular sciences* **2019,** *20* (18). DOI: 10.3390/ijms20184369.

Junttila, M. R.; Sauvage, F. J. de. Influence of tumour micro-environment heterogeneity on therapeutic response. *Nature* **2013,** *501* (7467), 346–354. DOI: 10.1038/nature12626.

Kaern, M.; Elston, T. C.; Blake, W. J.; Collins, J. J. Stochasticity in gene expression: from theories to phenotypes. *Nature reviews. Genetics* **2005,** *6* (6), 451–464. DOI: 10.1038/nrg1615.

Kallendrusch, S.; Koerfer, J.; Lordick, F.; Benchmann, I. Human tumor slice cultures for cancer research and drug' ' testing. *ICST* [Online] **2017,** No. 4, 1–5.

Kamb, A. What's wrong with our cancer models? *Nature reviews. Drug discovery* **2005,** *4* (2), 161–165. DOI: 10.1038/nrd1635.

Kanjilal, S.; Pierceall, W. E.; Cummings, K. K.; Kripke, M. L.; Ananthaswamy, H. N. High frequency of p53 mutations in ultraviolet radiation-induced murine skin tumors: evidence for strand bias and tumor heterogeneity. *Cancer research* **1993,** *53* (13), 2961–2964.

Katano, K.; Kondo, A.; Safaei, R.; Holzer, A.; Samimi, G.; Mishima, M.; Kuo, Y.-M.; Rochdi, M.; Howell, S. B. Acquisition of resistance to cisplatin is accompanied by changes in the cellular pharmacology of copper. *Cancer research* **2002,** *62* (22), 6559–6565.

Kelm, J. M.; Timmins, N. E.; Brown, C. J.; Fussenegger, M.; Nielsen, L. K. Method for generation of homogeneous multicellular tumor spheroids applicable to a wide variety of cell types. *Biotechnology and bioengineering* **2003,** *83* (2), 173–180. DOI: 10.1002/bit.10655.

Kendrick, J. E.; Straughn, J. M.; Oliver, P. G.; Wang, W.; Nan, L.; Grizzle, W. E.; Stockard, C. R.; Alvarez, R. D.; Buchsbaum, D. J. Anti-tumor activity of the TRA-8 anti-DR5 antibody in combination with cisplatin in an ex vivo human cervical cancer model. *Gynecologic oncology* **2008,** *108* (3), 591–597. DOI: 10.1016/j.ygyno.2007.11.039.

Kern, M. A.; Haugg, A. M.; Eiteneuer, E.; Konze, E.; Drebber, U.; Dienes, H. P.; Breuhahn, K.; Schirmacher, P.; Kasper, H. U. Ex vivo analysis of antineoplastic agents in precision-cut tissue slices of human origin: effects of cyclooxygenase-2 inhibition in hepatocellular carcinoma. *Liver international : official journal of the International Association for the Study of the Liver* **2006,** *26* (5), 604–612. DOI: 10.1111/j.1478-3231.2006.01268.x.

Kibbey, M. C. Maintenance of the EHS sarcoma and Matrigel preparation. *Journal of Tissue Culture Methods* **1994,** *16* (3-4), 227–230. DOI: 10.1007/BF01540656.

Kim, G.; Ison, G.; McKee, A. E.; Zhang, H.; Tang, S.; Gwise, T.; Sridhara, R.; Lee, E.; Tzou, A.; Philip, R.; Chiu, H.-J.; Ricks, T. K.; Palmby, T.; Russell, A. M.; Ladouceur,

G.; Pfuma, E.; Li, H.; Zhao, L.; Liu, Q.; Venugopal, R.; Ibrahim, A.; Pazdur, R. FDA Approval Summary: Olaparib Monotherapy in Patients with Deleterious Germline BRCA-Mutated Advanced Ovarian Cancer Treated with Three or More Lines of Chemotherapy. *Clinical cancer research : an official journal of the American Association for Cancer Research* **2015,** *21* (19), 4257–4261. DOI: 10.1158/1078-0432.CCR-15-0887.

King, M.-C.; Marks, J. H.; Mandell, J. B. Breast and ovarian cancer risks due to inherited mutations in BRCA1 and BRCA2. *Science (New York, N.Y.)* **2003,** *302* (5645), 643–646. DOI: 10.1126/science.1088759.

Kiviharju-af Hällström, T. M.; Jäämaa, S.; Mönkkönen, M.; Peltonen, K.; Andersson, L. C.; Medema, R. H.; Peehl, D. M.; Laiho, M. Human prostate epithelium lacks Wee1A-mediated DNA damage-induced checkpoint enforcement. *Proceedings of the National Academy of Sciences of the United States of America* **2007,** *104* (17), 7211–7216. DOI: 10.1073/pnas.0609299104.

Kleih, M.; Böpple, K.; Dong, M.; Gaißler, A.; Heine, S.; Olayioye, M. A.; Aulitzky, W. E.; Essmann, F. Direct impact of cisplatin on mitochondria induces ROS production that dictates cell fate of ovarian cancer cells. *Cell death & disease* **2019,** *10* (11), 851. DOI: 10.1038/s41419-019-2081-4.

Kleinman, H. K.; Martin, G. R. Matrigel: basement membrane matrix with biological activity. *Seminars in cancer biology* **2005,** *15* (5), 378–386. DOI: 10.1016/j.semcancer.2005.05.004.

Kohen, R.; Barlev, J.; Hornung, G.; Stelzer, G.; Feldmesser, E.; Kogan, K.; Safran, M.; Leshkowitz, D. UTAP: User-friendly Transcriptome Analysis Pipeline. *BMC bioinformatics* **2019,** *20* (1), 154. DOI: 10.1186/s12859-019-2728-2.

Kredel, F. E. Tissue Culture of Intracranial Tumors with a Note on the Meningiomas. *The American journal of pathology* **1928,** *4* (4), 337-340.3.

Kreis, N.-N.; Friemel, A.; Ritter, A.; Roth, S.; Rolle, U.; Louwen, F.; Yuan, J. Function of p21 (Cip1/Waf1/CDKN1A) in Migration and Invasion of Cancer and Trophoblastic Cells. *Cancers* **2019,** *11* (7). DOI: 10.3390/cancers11070989.

Krumdieck, C. L.; dos Santos, J.; Ho, K.-J. A new instrument for the rapid preparation of tissue slices. *Analytical Biochemistry* **1980,** *104* (1), 118–123. DOI: 10.1016/0003-2697(80)90284-5.

Kumachev, A.; Greener, J.; Tumarkin, E.; Eiser, E.; Zandstra, P. W.; Kumacheva, E. High-throughput generation of hydrogel microbeads with varying elasticity for cell

encapsulation. *Biomaterials* **2011,** *32* (6), 1477–1483. DOI: 10.1016/j.biomaterials.2010.10.033.

Kunz-Schughart, L. A. Multicellular tumor spheroids: intermediates between monolayer culture and in vivo tumor. *Cell biology international* **1999,** *23* (3), 157–161. DOI: 10.1006/cbir.1999.0384.

Kurman, R. J.; Shih, I.-M. The origin and pathogenesis of epithelial ovarian cancer: a proposed unifying theory. *The American journal of surgical pathology* **2010,** *34* (3), 433–443. DOI: 10.1097/PAS.0b013e3181cf3d79.

LaFleur, M. D.; Kumamoto, C. A.; Lewis, K. Candida albicans biofilms produce antifungal-tolerant persister cells. *Antimicrobial agents and chemotherapy* **2006,** *50* (11), 3839–3846. DOI: 10.1128/AAC.00684-06.

Lahooti, S.; Sefton, M. V. Agarose enhances the viability of intraperitoneally implanted microencapsulated L929 fibroblasts. *Cell transplantation* **2000,** *9* (6), 785–796. DOI: 10.1177/096368970000900605.

Lane, D. P. Cancer. p53, guardian of the genome. *Nature* **1992,** *358* (6381), 15–16. DOI: 10.1038/358015a0.

Lange, P. S.; Chavez, J. C.; Pinto, J. T.; Coppola, G.; Sun, C.-W.; Townes, T. M.; Geschwind, D. H.; Ratan, R. R. ATF4 is an oxidative stress-inducible, prodeath transcription factor in neurons in vitro and in vivo. *The Journal of experimental medicine* **2008,** *205* (5), 1227–1242. DOI: 10.1084/jem.20071460.

Lee, J. M.; Mhawech-Fauceglia, P.; Lee, N.; Parsanian, L. C.; Lin, Y. G.; Gayther, S. A.; Lawrenson, K. A three-dimensional microenvironment alters protein expression and chemosensitivity of epithelial ovarian cancer cells in vitro. *Laboratory investigation; a journal of technical methods and pathology* **2013,** *93* (5), 528–542. DOI: 10.1038/labinvest.2013.41.

Lee, K. Y.; Mooney, D. J. Alginate: properties and biomedical applications. *Progress in polymer science* **2012,** *37* (1), 106–126. DOI: 10.1016/j.progpolymsci.2011.06.003.

Lewis, K. Persister cells, dormancy and infectious disease. *Nature reviews. Microbiology* **2007,** *5* (1), 48–56. DOI: 10.1038/nrmicro1557.

Lewis, K. Persister cells. *Annual review of microbiology* [Online] **2010,** *64*, 357–372. https://journals.sagepub.com/doi/pdf/10.4137/CGM.S11333.

Liang, C.-C.; Park, A. Y.; Guan, J.-L. In vitro scratch assay: a convenient and inexpensive method for analysis of cell migration in vitro. *Nat Protoc* **2007,** *2* (2), 329–333. DOI: 10.1038/nprot.2007.30.

Lin, R.-Z.; Chou, L.-F.; Chien, C.-C. M.; Chang, H.-Y. Dynamic analysis of hepatoma spheroid formation: roles of E-cadherin and beta1-integrin. *Cell and tissue research* **2006,** *324* (3), 411–422. DOI: 10.1007/s00441-005-0148-2.

Lin, R.-Z.; Lin, R.-Z.; Chang, H.-Y. Recent advances in three-dimensional multicellular spheroid culture for biomedical research. *Biotechnology journal* **2008,** *3* (9-10), 1172–1184. DOI: 10.1002/biot.200700228.

Ling, K.-S.; Chen, G.-D.; Tsai, H.-J.; Lee, M.-S.; Wang, P.-H.; Liu, F.-S. Mechanisms Involved in Chemoresistance in Ovarian Cancer. *Taiwanese Journal of Obstetrics and Gynecology* **2005,** *44* (3), 209–217. DOI: 10.1016/S1028-4559(09)60143-1.

Liu, Y.; Lang, F.; Xie, X.; Prabhu, S.; Xu, J.; Sampath, D.; Aldape, K.; Fuller, G.; Puduvalli, V. K. Efficacy of adenovirally expressed soluble TRAIL in human glioma organotypic slice culture and glioma xenografts. *Cell death & disease* **2011,** *2*, e121. DOI: 10.1038/cddis.2010.95.

Lu, Y.; Liang, F.-X.; Wang, X. A synthetic biology approach identifies the mammalian UPR RNA ligase RtcB. *Molecular cell* **2014,** *55* (5), 758–770. DOI: 10.1016/j.molcel.2014.06.032.

Ma, Y.; Hendershot, L. M. The role of the unfolded protein response in tumour development: friend or foe? *Nature reviews. Cancer* **2004,** *4* (12), 966–977. DOI: 10.1038/nrc1505.

Mak, I. W.; Evaniew, N.; Ghert, M. Lost in translation: animal models and clinical trials in cancer treatment. *American journal of translational research* **2014,** *6* (2), 114–118.

Mandal, B. B.; Kundu, S. C. Calcium alginate beads embedded in silk fibroin as 3D dual drug releasing scaffolds. *Biomaterials* **2009,** *30* (28), 5170–5177. DOI: 10.1016/j.biomaterials.2009.05.072.

Marullo, R.; Werner, E.; Degtyareva, N.; Moore, B.; Altavilla, G.; Ramalingam, S. S.; Doetsch, P. W. Cisplatin induces a mitochondrial-ROS response that contributes to cytotoxicity depending on mitochondrial redox status and bioenergetic functions. *PloS one* **2013,** *8* (11), e81162. DOI: 10.1371/journal.pone.0081162.

Marusyk, A.; Polyak, K. Tumor heterogeneity: causes and consequences. *Biochimica et biophysica acta* **2010,** *1805* (1), 105–117. DOI: 10.1016/j.bbcan.2009.11.002.

Masters, J. R. Human cancer cell lines: fact and fantasy. *Nature reviews. Molecular cell biology* **2000,** *1* (3), 233–236. DOI: 10.1038/35043102.

Maytin, E. V.; Ubeda, M.; Lin, J. C.; Habener, J. F. Stress-inducible transcription factor CHOP/gadd153 induces apoptosis in mammalian cells via p38 kinase-dependent and -independent mechanisms. *Experimental Cell Research* [Online] **2001,** *267* (2). https://pubmed.ncbi.nlm.nih.gov/11426938/.

McMillin, D. W.; Negri, J. M.; Mitsiades, C. S. The role of tumour-stromal interactions in modifying drug response: challenges and opportunities. *Nature reviews. Drug discovery* **2013,** *12* (3), 217–228. DOI: 10.1038/nrd3870.

Meijer, A.; Kruyt, F. A. E.; van der Zee, A. G. J.; Hollema, H.; Le, P.; Hoor, K. A. ten; Groothuis, G. M. M.; Quax, W. J.; Vries, E. G. E. de; Jong, S. de. Nutlin-3 preferentially sensitises wild-type p53-expressing cancer cells to DR5-selective TRAIL over rhTRAIL. *British journal of cancer* **2013,** *109* (10), 2685–2695. DOI: 10.1038/bjc.2013.636.

Merz, F.; Gaunitz, F.; Dehghani, F.; Renner, C.; Meixensberger, J.; Gutenberg, A.; Giese, A.; Schopow, K.; Hellwig, C.; Schäfer, M.; Bauer, M.; Stöcker, H.; Taucher-Scholz, G.; Durante, M.; Bechmann, I. Organotypic slice cultures of human glioblastoma reveal different susceptibilities to treatments. *Neuro-oncology* **2013,** *15* (6), 670–681. DOI: 10.1093/neuonc/not003.

Merz, F.; Müller, M.; Taucher-Scholz, G.; Rödel, F.; Stöcker, H.; Schopow, K.; Laprell, L.; Dehghani, F.; Durante, M.; Bechmann, I. Tissue slice cultures from humans or rodents: a new tool to evaluate biological effects of heavy ions. *Radiation and environmental biophysics* **2010,** *49* (3), 457–462. DOI: 10.1007/s00411-010-0293-1.

Metsalu, T.; Vilo, J. ClustVis: a web tool for visualizing clustering of multivariate data using Principal Component Analysis and heatmap. *Nucleic acids research* **2015,** *43* (W1), W566-70. DOI: 10.1093/nar/gkv468.

Mihailidou, C.; Papazian, I.; Papavassiliou, A. G.; Kiaris, H. CHOP-dependent regulation of p21/waf1 during ER stress. *Cellular physiology and biochemistry : international journal of experimental cellular physiology, biochemistry, and pharmacology* **2010,** *25* (6), 761–766. DOI: 10.1159/000315096.

Miki, Y.; Swensen, J.; Shattuck-Eidens, D.; Futreal, P. A.; Harshman, K.; Tavtigian, S.; Liu, Q.; Cochran, C.; Bennett, L. M.; Ding, W. A strong candidate for the breast and

ovarian cancer susceptibility gene BRCA1. *Science (New York, N.Y.)* **1994,** *266* (5182), 66–71. DOI: 10.1126/science.7545954.

Milani, C.; Welsh, J.; Katayama, M. L. H.; Lyra, E. C.; Maciel, M. S.; Brentani, M. M.; Folgueira, M. A. A. K. Human breast tumor slices: a model for identification of vitamin D regulated genes in the tumor microenvironment. *The Journal of steroid biochemistry and molecular biology* **2010,** *121* (1-2), 151–155. DOI: 10.1016/j.jsbmb.2010.03.051.

Milburn, M. V.; Hassell, A. M.; Lambert, M. H.; Jordan, S. R.; Proudfoot, A. E.; Graber, P.; Wells, T. N. A novel dimer configuration revealed by the crystal structure at 2.4 A resolution of human interleukin-5. *Nature* **1993,** *363* (6425), 172–176. DOI: 10.1038/363172a0.

Minchinton, A. I.; Tannock, I. F. Drug penetration in solid tumours. *Nature reviews. Cancer* **2006,** *6* (8), 583–592. DOI: 10.1038/nrc1893.

Mira-y-Lopez, R.; Ossowski, L. Preservation of steroid hormone receptors in organ cultures of human breast carcinomas. *Cancer Res* **1990,** *50* (1), 78–83.

Mirchandani, D.; Zheng, J.; Miller, G. J.; Ghosh, A. K.; Shibata, D. K.; Cote, R. J.; Roy-Burman, P. Heterogeneity in intratumor distribution of p53 mutations in human prostate cancer. *The American journal of pathology* **1995,** *147* (1), 92–101.

Mishima, M.; Samimi, G.; Kondo, A.; Lin, X.; Howell, S.B. The cellular pharmacology of oxaliplatin resistance. *European Journal of Cancer* **2002,** *38* (10), 1405–1412. DOI: 10.1016/S0959-8049(02)00096-5.

Mootha, V. K.; Lindgren, C. M.; Eriksson, K.-F.; Subramanian, A.; Sihag, S.; Lehar, J.; Puigserver, P.; Carlsson, E.; Ridderstråle, M.; Laurila, E.; Houstis, N.; Daly, M. J.; Patterson, N.; Mesirov, J. P.; Golub, T. R.; Tamayo, P.; Spiegelman, B.; Lander, E. S.; Hirschhorn, J. N.; Altshuler, D.; Groop, L. C. PGC-1alpha-responsive genes involved in oxidative phosphorylation are coordinately downregulated in human diabetes. *Nature genetics* **2003,** *34* (3), 267–273. DOI: 10.1038/ng1180.

Moynahan, M. E.; Jasin, M. Mitotic homologous recombination maintains genomic stability and suppresses tumorigenesis. *Nature reviews. Molecular cell biology* **2010,** *11* (3), 196–207. DOI: 10.1038/nrm2851.

Muller, P. A. J.; Vousden, K. H.; Norman, J. C. p53 and its mutants in tumor cell migration and invasion. *The Journal of cell biology* **2011,** *192* (2), 209–218. DOI: 10.1083/jcb.201009059.

Nagy, Á.; Lánczky, A.; Menyhárt, O.; Győrffy, B. Validation of miRNA prognostic power in hepatocellular carcinoma using expression data of independent datasets. *Scientific reports* **2018,** *8* (1), 9227. DOI: 10.1038/s41598-018-27521-y.

National Center for Biotechnology Information. PubChem Compound Summary for CID 40473141, beta-D-Mannuronate. https://pubchem.ncbi.nlm.nih.gov/compound/beta-D-Mannuronate (accessed August 11, 2020).

National Center for Biotechnology Information. PubChem Compound Summary for CID 439353, beta-D-Galactose. https://pubchem.ncbi.nlm.nih.gov/compound/beta-D-Galactose (accessed September 9, 2020).

National Center for Biotechnology Information. PubChem Compound Summary for CID 446401, alpha-L-Guluronate. https://pubchem.ncbi.nlm.nih.gov/compound/alpha-L-Guluronate (accessed August 11, 2020).

National Center for Biotechnology Information. PubChem Compound Summary for CID 448931, 3,6-Anhydro-alpha-L-galactopyranose. https://pubchem.ncbi.nlm.nih.gov/compound/3_6-Anhydro-alpha-L-galactopyranose (accessed September 9, 2020).

Neal, J. T.; Li, X.; Zhu, J.; Giangarra, V.; Grzeskowiak, C. L.; Ju, J.; Liu, I. H.; Chiou, S.-H.; Salahudeen, A. A.; Smith, A. R.; Deutsch, B. C.; Liao, L.; Zemek, A. J.; Zhao, F.; Karlsson, K.; Schultz, L. M.; Metzner, T. J.; Nadauld, L. D.; Tseng, Y.-Y.; Alkhairy, S.; Oh, C.; Keskula, P.; Mendoza-Villanueva, D.; La Vega, F. M. de; Kunz, P. L.; Liao, J. C.; Leppert, J. T.; Sunwoo, J. B.; Sabatti, C.; Boehm, J. S.; Hahn, W. C.; Zheng, G. X. Y.; Davis, M. M.; Kuo, C. J. Organoid Modeling of the Tumor Immune Microenvironment. *Cell* **2018,** *175* (7), 1972-1988.e16. DOI: 10.1016/j.cell.2018.11.021.

Niibe, Y.; Hayakawa, K. Oligometastases and oligo-recurrence: the new era of cancer therapy. *Japanese journal of clinical oncology* **2010,** *40* (2), 107–111. DOI: 10.1093/jjco/hyp167.

Oikawa, T.; Kamiya, A.; Zeniya, M.; Chikada, H.; Hyuck, A. D.; Yamazaki, Y.; Wauthier, E.; Tajiri, H.; Miller, L. D.; Wang, X. W.; Reid, L. M.; Nakauchi, H. Sal-like protein 4 (SALL4), a stem cell biomarker in liver cancers. *Hepatology (Baltimore, Md.)* **2013,** *57* (4), 1469–1483. DOI: 10.1002/hep.26159.

Olivier, M.; Hollstein, M.; Hainaut, P. TP53 mutations in human cancers: origins, consequences, and clinical use. *Cold Spring Harbor perspectives in biology* **2010,** *2* (1), a001008. DOI: 10.1101/cshperspect.a001008.

Paszek, M. J.; Zahir, N.; Johnson, K. R.; Lakins, J. N.; Rozenberg, G. I.; Gefen, A.; Reinhart-King, C. A.; Margulies, S. S.; Dembo, M.; Boettiger, D.; Hammer, D. A.; Weaver, V. M. Tensional homeostasis and the malignant phenotype. *Cancer cell* **2005,** *8* (3), 241–254. DOI: 10.1016/j.ccr.2005.08.010.

Patch, A.-M.; Christie, E. L.; Etemadmoghadam, D.; Garsed, D. W.; George, J.; Fereday, S.; Nones, K.; Cowin, P.; Alsop, K.; Bailey, P. J.; Kassahn, K. S.; Newell, F.; Quinn, M. C. J.; Kazakoff, S.; Quek, K.; Wilhelm-Benartzi, C.; Curry, E.; Leong, H. S.; Hamilton, A.; Mileshkin, L.; Au-Yeung, G.; Kennedy, C.; Hung, J.; Chiew, Y.-E.; Harnett, P.; Friedlander, M.; Quinn, M.; Pyman, J.; Cordner, S.; O'Brien, P.; Leditschke, J.; Young, G.; Strachan, K.; Waring, P.; Azar, W.; Mitchell, C.; Traficante, N.; Hendley, J.; Thorne, H.; Shackleton, M.; Miller, D. K.; Arnau, G. M.; Tothill, R. W.; Holloway, T. P.; Semple, T.; Harliwong, I.; Nourse, C.; Nourbakhsh, E.; Manning, S.; Idrisoglu, S.; Bruxner, T. J. C.; Christ, A. N.; Poudel, B.; Holmes, O.; Anderson, M.; Leonard, C.; Lonie, A.; Hall, N.; Wood, S.; Taylor, D. F.; Xu, Q.; Fink, J. L.; Waddell, N.; Drapkin, R.; Stronach, E.; Gabra, H.; Brown, R.; Jewell, A.; Nagaraj, S. H.; Markham, E.; Wilson, P. J.; Ellul, J.; McNally, O.; Doyle, M. A.; Vedururu, R.; Stewart, C.; Lengyel, E.; Pearson, J. V.; Waddell, N.; deFazio, A.; Grimmond, S. M.; Bowtell, D. D. L. Whole-genome characterization of chemoresistant ovarian cancer. *Nature* **2015,** *521* (7553), 489–494. DOI: 10.1038/nature14410.

Pelaez, D.; Huang, C.-Y. C.; Cheung, H. S. Cyclic compression maintains viability and induces chondrogenesis of human mesenchymal stem cells in fibrin gel scaffolds. *Stem cells and development* **2009,** *18* (1), 93–102. DOI: 10.1089/scd.2008.0030.

Pelzer, A. E.; Bektic, J.; Haag, P.; Berger, A. P.; Pycha, A.; Schäfer, G.; Rogatsch, H.; Horninger, W.; Bartsch, G.; Klocker, H. The Expression of Transcription Factor Activating Transcription Factor 3 in the Human Prostate and its Regulation by Androgen in Prostate Cancer. *Journal of Urology* **2006,** *175* (4), 1517–1522. DOI: 10.1016/S0022-5347(05)00651-8.

Perumal, N. B.; Kaplan, M. H. Regulating Il9 transcription in T helper cells. *Trends in immunology* **2011,** *32* (4), 146–150. DOI: 10.1016/j.it.2011.01.006.

Pietras, K.; Ostman, A. Hallmarks of cancer: interactions with the tumor stroma. *Experimental Cell Research* **2010,** *316* (8), 1324–1331. DOI: 10.1016/j.yexcr.2010.02.045.

Poulos, R. C.; Wong, J. W. H. Finding cancer driver mutations in the era of big data research. *Biophysical reviews* **2019,** *11* (1), 21–29. DOI: 10.1007/s12551-018-0415-6.

Quail, D. F.; Joyce, J. A. Microenvironmental regulation of tumor progression and metastasis. *Nature medicine* **2013,** *19* (11), 1423–1437. DOI: 10.1038/nm.3394.

Ramirez, M.; Rajaram, S.; Steininger, R. J.; Osipchuk, D.; Roth, M. A.; Morinishi, L. S.; Evans, L.; Ji, W.; Hsu, C.-H.; Thurley, K.; Wei, S.; Zhou, A.; Koduru, P. R.; Posner, B. A.; Wu, L. F.; Altschuler, S. J. Diverse drug-resistance mechanisms can emerge from drug-tolerant cancer persister cells. *Nature communications* **2016,** *7*, 10690. DOI: 10.1038/ncomms10690.

Ramos, P.; Bentires-Alj, M. Mechanism-based cancer therapy: resistance to therapy, therapy for resistance. *Oncogene* **2015,** *34* (28), 3617–3626. DOI: 10.1038/onc.2014.314.

Reyes-Aldasoro, C. C. The proportion of cancer-related entries in PubMed has increased considerably; is cancer truly "The Emperor of All Maladies"? *PloS one* **2017,** *12* (3), e0173671. DOI: 10.1371/journal.pone.0173671.

Riley, T.; Sontag, E.; Chen, P.; Levine, A. Transcriptional control of human p53-regulated genes. *Nature reviews. Molecular cell biology* **2008,** *9* (5), 402–412. DOI: 10.1038/nrm2395.

Robert Koch-Institute. Krebsarten: Krebs gesamt. https://www.krebsdaten.de/Krebs/DE/Content/Krebsarten/Krebs_gesamt/krebs_gesamt_node.html (accessed August 19, 2020).

Röller, M. R.; Owen, S. P.; Heidelberger, C. Studies on the organ culture of human tumors. *Cancer Res* **1966,** *26* (4), 626–637.

Saggar, J. K.; Yu, M.; Tan, Q.; Tannock, I. F. The tumor microenvironment and strategies to improve drug distribution. *Frontiers in oncology* **2013,** *3*, 154. DOI: 10.3389/fonc.2013.00154.

Sakuragi, N.; Salah-eldin, A.-e.; Watari, H.; Itoh, T.; Inoue, S.; Moriuchi, T.; Fujimoto, S. Bax, Bcl-2, and p53 expression in endometrial cancer. *Gynecologic oncology* **2002,** *86* (3), 288–296. DOI: 10.1006/gyno.2002.6742.

Salmon, H.; Franciszkiewicz, K.; Damotte, D.; Dieu-Nosjean, M.-C.; Validire, P.; Trautmann, A.; Mami-Chouaib, F.; Donnadieu, E. Matrix architecture defines the preferential localization and migration of T cells into the stroma of human lung

tumors. *The Journal of clinical investigation* **2012,** *122* (3), 899–910. DOI: 10.1172/JCI45817.

Sassone-Corsi, P.; Sisson, J. C.; Verma, I. M. Transcriptional autoregulation of the proto-oncogene fos. *Nature* **1988,** *334* (6180), 314–319. DOI: 10.1038/334314a0.

Sato, T.; Stange, D. E.; Ferrante, M.; Vries, R. G. J.; van Es, J. H.; van den Brink, S.; van Houdt, W. J.; Pronk, A.; van Gorp, J.; Siersema, P. D.; Clevers, H. Long-term expansion of epithelial organoids from human colon, adenoma, adenocarcinoma, and Barrett's epithelium. *Gastroenterology* **2011,** *141* (5), 1762–1772. DOI: 10.1053/j.gastro.2011.07.050.

Sato, T.; Vries, R. G.; Snippert, H. J.; van de Wetering, M.; Barker, N.; Stange, D. E.; van Es, J. H.; Abo, A.; Kujala, P.; Peters, P. J.; Clevers, H. Single Lgr5 stem cells build crypt-villus structures in vitro without a mesenchymal niche. *Nature* **2009,** *459* (7244), 262–265. DOI: 10.1038/nature07935.

Schmid, J. O.; Dong, M.; Haubeiss, S.; Friedel, G.; Bode, S.; Grabner, A.; Ott, G.; Mürdter, T. E.; Oren, M.; Aulitzky, W. E.; van der Kuip, H. Cancer cells cue the p53 response of cancer-associated fibroblasts to cisplatin. *Cancer Res* **2012,** *72* (22), 5824–5832. DOI: 10.1158/0008-5472.CAN-12-1201.

Schneider, S.; Feilen, P.; Cramer, H.; Hillgärtner, M.; Brunnenmeier, F.; Zimmermann, H.; Weber, M. M.; Zimmermann, U. Beneficial effects of human serum albumin on stability and functionality of alginate microcapsules fabricated in different ways. *Journal of microencapsulation* **2003,** *20* (5), 627–636. DOI: 10.3109/02652040309178351.

Schrezenmeir, J.; Hering, B. J.; Gerö, L.; Wiegand-Dressler, J.; Solhdju, M.; Velten, F.; Kirchgessner, J.; Laue, C.; Beyer, J.; Bretzel, R. Long-term function of porcine islets and single cells embedded in barium-alginate matrix. *Hormone and metabolic research = Hormon- und Stoffwechselforschung = Hormones et metabolisme* **1993,** *25* (4), 204–209. DOI: 10.1055/s-2007-1002077.

Scully, R. E. Pathology of ovarian cancer precursors. *Journal of cellular biochemistry. Supplement* **1995,** *23*, 208–218. DOI: 10.1002/jcb.240590928.

Séveno, C.; Loussouarn, D.; Bréchet, S.; Campone, M.; Juin, P.; Barillé-Nion, S. γ-Secretase inhibition promotes cell death, Noxa upregulation, and sensitization to BH3 mimetic ABT-737 in human breast cancer cells. *Breast cancer research : BCR* **2012,** *14* (3), R96. DOI: 10.1186/bcr3214.

Sharma, S. V.; Lee, D. Y.; Li, B.; Quinlan, M. P.; Takahashi, F.; Maheswaran, S.; McDermott, U.; Azizian, N.; Zou, L.; Fischbach, M. A.; Wong, K.-K.; Brandstetter, K.; Wittner, B.; Ramaswamy, S.; Classon, M.; Settleman, J. A chromatin-mediated reversible drug-tolerant state in cancer cell subpopulations. *Cell* **2010,** *141* (1), 69–80. DOI: 10.1016/j.cell.2010.02.027.

Shi, B.; Yan, W.; Liu, G.; Guo, Y. MicroRNA-488 inhibits tongue squamous carcinoma cell invasion and EMT by directly targeting ATF3. *Cellular & molecular biology letters* **2018,** *23*, 28. DOI: 10.1186/s11658-018-0094-0.

Shi, Y.; Wang, Y.; Huang, W.; Wang, Y.; Wang, R.; Yuan, Y. Integration of Metabolomics and Transcriptomics To Reveal Metabolic Characteristics and Key Targets Associated with Cisplatin Resistance in Nonsmall Cell Lung Cancer. *Journal of proteome research* **2019,** *18* (9), 3259–3267. DOI: 10.1021/acs.jproteome.9b00209.

Shoichet, M. S.; Li, R. H.; White, M. L.; Winn, S. R. Stability of hydrogels used in cell encapsulation: An in vitro comparison of alginate and agarose. *Biotechnol. Bioeng.* **1996,** *50* (4), 374–381. DOI: 10.1002/(SICI)1097-0290(19960520)50:4%3C374:AID-BIT4%3E3.0.CO;2-I.

Siegel, R. L.; Miller, K. D.; Jemal, A. Cancer statistics, 2019. *CA: a cancer journal for clinicians* **2019,** *69* (1), 7–34. DOI: 10.3322/caac.21551.

Simeone, D. M.; Ji, B.; Banerjee, M.; Arumugam, T.; Li, D.; Anderson, M. A.; Bamberger, A. M.; Greenson, J.; Brand, R. E.; Ramachandran, V.; Logsdon, C. D. CEACAM1, a novel serum biomarker for pancreatic cancer. *Pancreas* **2007,** *34* (4), 436–443. DOI: 10.1097/MPA.0b013e3180333ae3.

Smith, B. H.; Gazda, L. S.; Conn, B. L.; Jain, K.; Asina, S.; Levine, D. M.; Parker, T. S.; Laramore, M. A.; Martis, P. C.; Vinerean, H. V.; David, E. M.; Qiu, S.; Cordon-Cardo, C.; Hall, R. D.; Gordon, B. R.; Diehl, C. H.; Stenzel, K. H.; Rubin, A. L. Three-dimensional culture of mouse renal carcinoma cells in agarose macrobeads selects for a subpopulation of cells with cancer stem cell or cancer progenitor properties. *Cancer Res* **2011,** *71* (3), 716–724. DOI: 10.1158/0008-5472.CAN-10-2254.

Sölétormos, G.; Duffy, M. J.; Othman Abu Hassan, S.; Verheijen, R. H. M.; Tholander, B.; Bast, R. C.; Gaarenstroom, K. N.; Sturgeon, C. M.; Bonfrer, J. M.; Petersen, P. H.; Troonen, H.; CarloTorre, G.; Kanty Kulpa, J.; Tuxen, M. K.; Molina, R. Clinical Use of Cancer Biomarkers in Epithelial Ovarian Cancer: Updated Guidelines From the European Group on Tumor Markers. *International journal of gynecological*

cancer : official journal of the International Gynecological Cancer Society **2016,** *26* (1), 43–51. DOI: 10.1097/IGC.0000000000000586.

Somerville, G. A.; Proctor, R. A. Cultivation conditions and the diffusion of oxygen into culture media: the rationale for the flask-to-medium ratio in microbiology. *BMC microbiology* **2013,** *13*, 9. DOI: 10.1186/1471-2180-13-9.

Sonnenberg, M.; van der Kuip, H.; Haubeis, S.; Fritz, P.; Schroth, W.; Friedel, G.; Simon, W.; Mürdter, T. E.; Aulitzky, W. E. Highly variable response to cytotoxic chemotherapy in carcinoma-associated fibroblasts (CAFs) from lung and breast. *BMC cancer* **2008,** *8*, 364. DOI: 10.1186/1471-2407-8-364.

Stoff-Khalili, M. A.; Stoff, A.; Rivera, A. A.; Mathis, J. M.; Everts, M.; Wang, M.; Kawakami, Y.; Waehler, R.; Mathews, Q. L.; Yamamoto, M.; Rocconi, R. P.; Siegal, G. P.; Richter, D. F.; Dall, P.; Zhu, Z. B.; Curiel, D. T. Gene transfer to carcinoma of the breast with fiber-modified adenoviral vectors in a tissue slice model system. *Cancer biology & therapy* **2005,** *4* (11), 1203–1210. DOI: 10.4161/cbt.4.11.2084.

Straussman, R.; Morikawa, T.; Shee, K.; Barzily-Rokni, M.; Qian, Z. R.; Du, J.; Davis, A.; Mongare, M. M.; Gould, J.; Frederick, D. T.; Cooper, Z. A.; Chapman, P. B.; Solit, D. B.; Ribas, A.; Lo, R. S.; Flaherty, K. T.; Ogino, S.; Wargo, J. A.; Golub, T. R. Tumour micro-environment elicits innate resistance to RAF inhibitors through HGF secretion. *Nature* **2012,** *487* (7408), 500–504. DOI: 10.1038/nature11183.

Strehl, R.; Schumacher, K.; Minuth, W. W. Controlled respiratory gas delivery to embryonic renal epithelial explants in perfusion culture. *Tissue engineering* **2004,** *10* (7-8), 1196–1203. DOI: 10.1089/ten.2004.10.1196.

Subramanian, A.; Tamayo, P.; Mootha, V. K.; Mukherjee, S.; Ebert, B. L.; Gillette, M. A.; Paulovich, A.; Pomeroy, S. L.; Golub, T. R.; Lander, E. S.; Mesirov, J. P. Gene set enrichment analysis: a knowledge-based approach for interpreting genome-wide expression profiles. *Proceedings of the National Academy of Sciences of the United States of America* **2005,** *102* (43), 15545–15550. DOI: 10.1073/pnas.0506580102.

Sugimoto, S.; Harada, K.; Shiotani, T.; Ikeda, S.; Katsura, N.; Ikai, I.; Mizuguchi, T.; Hirata, K.; Yamaoka, Y.; Mitaka, T. Hepatic organoid formation in collagen sponge of cells isolated from human liver tissues. *Tissue engineering* **2005,** *11* (3-4), 626–633. DOI: 10.1089/ten.2005.11.626.

Sutherland, R. M. Cell and environment interactions in tumor microregions: the multicell spheroid model. *Science (New York, N.Y.)* **1988,** *240* (4849), 177–184. DOI: 10.1126/science.2451290.

Swanton, C. Intratumor heterogeneity: evolution through space and time. *Cancer Res* **2012,** *72* (19), 4875–4882. DOI: 10.1158/0008-5472.CAN-12-2217.

Syed, V.; Mukherjee, K.; Lyons-Weiler, J.; Lau, K.-M.; Mashima, T.; Tsuruo, T.; Ho, S.-m. Identification of ATF-3, caveolin-1, DLC-1, and NM23-H2 as putative antitumorigenic, progesterone-regulated genes for ovarian cancer cells by gene profiling. *Oncogene* **2005,** *24* (10), 1774–1787. DOI: 10.1038/sj.onc.1207991.

Takahashi, T. Organoids for Drug Discovery and Personalized Medicine. *Annual review of pharmacology and toxicology* **2019,** *59*, 447–462. DOI: 10.1146/annurev-pharmtox-010818-021108.

Tapia, G.; Diaz-Padill, I. Molecular Mechanisms of Platinum Resistance in Ovarian Cancer. In *Ovarian Cancer - A Clinical and Translational Update*; Diaz-Padilla, I., Ed.; InTech, 2013. DOI: 10.5772/55562.

Tentori, L.; Graziani, G. Chemopotentiation by PARP inhibitors in cancer therapy. *Pharmacological research* **2005,** *52* (1), 25–33. DOI: 10.1016/j.phrs.2005.02.010.

Thissen, D.; Steinberg, L.; Kuang, D. Quick and Easy Implementation of the Benjamini-Hochberg Procedure for Controlling the False Positive Rate in Multiple Comparisons. *Journal of Educational and Behavioral Statistics* **2002,** *27* (1), 77–83. DOI: 10.3102/10769986027001077.

Tian, C.; Di Huang; Yu, Y.; Zhang, J.; Fang, Q.; Xie, C. ABCG1 as a potential oncogene in lung cancer. *Experimental and therapeutic medicine* **2017,** *13* (6), 3189–3194. DOI: 10.3892/etm.2017.4393.

Tomasetti, C.; Marchionni, L.; Nowak, M. A.; Parmigiani, G.; Vogelstein, B. Only three driver gene mutations are required for the development of lung and colorectal cancers. *Proceedings of the National Academy of Sciences of the United States of America* **2015,** *112* (1), 118–123. DOI: 10.1073/pnas.1421839112.

Tone, A. A.; Salvador, S.; Finlayson, S. J.; Tinker, A. V.; Kwon, J. S.; Lee, C.-H.; Cohen, T.; Ehlen, T.; Lee, M.; Carey, M. S.; Heywood, M.; Pike, J.; Hoskins, P. J.; Stuart, G. C.; Swenerton, K. D.; Huntsman, D. G.; Gilks, C. B.; Miller, D. M.; McAlpine, J. N. The role of the fallopian tube in ovarian cancer. *Clinical advances in hematology & oncology : H&O* **2012,** *10* (5), 296–306.

Torre, L. A.; Trabert, B.; DeSantis, C. E.; Miller, K. D.; Samimi, G.; Runowicz, C. D.; Gaudet, M. M.; Jemal, A.; Siegel, R. L. Ovarian cancer statistics, 2018. *CA: a cancer journal for clinicians* **2018,** *68* (4), 284–296. DOI: 10.3322/caac.21456.

Vaira, V.; Fedele, G.; Pyne, S.; Fasoli, E.; Zadra, G.; Bailey, D.; Snyder, E.; Faversani, A.; Coggi, G.; Flavin, R.; Bosari, S.; Loda, M. Preclinical model of organotypic culture for pharmacodynamic profiling of human tumors. *Proceedings of the National Academy of Sciences of the United States of America* **2010,** *107* (18), 8352–8356. DOI: 10.1073/pnas.0907676107.

van der Kuip, H.; Mürdter, T. E.; Sonnenberg, M.; McClellan, M.; Gutzeit, S.; Gerteis, A.; Simon, W.; Fritz, P.; Aulitzky, W. E. Short term culture of breast cancer tissues to study the activity of the anticancer drug taxol in an intact tumor environment. *BMC cancer* **2006,** *6*, 86. DOI: 10.1186/1471-2407-6-86.

Vanacker, J.; Luyckx, V.; Dolmans, M.-M.; Des Rieux, A.; Jaeger, J.; van Langendonckt, A.; Donnez, J.; Amorim, C. A. Transplantation of an alginate-matrigel matrix containing isolated ovarian cells: first step in developing a biodegradable scaffold to transplant isolated preantral follicles and ovarian cells. *Biomaterials* **2012,** *33* (26), 6079–6085. DOI: 10.1016/j.biomaterials.2012.05.015.

Venkitaraman, A. R. Cancer Susceptibility and the Functions of BRCA1 and BRCA2. *Cell* **2002,** *108* (2), 171–182. DOI: 10.1016/S0092-8674(02)00615-3.

Vinci, M.; Gowan, S.; Boxall, F.; Patterson, L.; Zimmermann, M.; Court, W.; Lomas, C.; Mendiola, M.; Hardisson, D.; Eccles, S. A. Advances in establishment and analysis of three-dimensional tumor spheroid-based functional assays for target validation and drug evaluation. *BMC Biol* **2012,** *10* (1), 1–21. DOI: 10.1186/1741-7007-10-29.

Vogelstein, B.; Papadopoulos, N.; Velculescu, V. E.; Zhou, S.; Diaz, L. A.; Kinzler, K. W. Cancer genome landscapes. *Science (New York, N.Y.)* **2013,** *339* (6127), 1546–1558. DOI: 10.1126/science.1235122.

Vousden, K. H.; Prives, C. Blinded by the Light: The Growing Complexity of p53. *Cell* **2009,** *137* (3), 413–431. DOI: 10.1016/j.cell.2009.04.037.

Vukicevic, S.; Kleinman, H. K.; Luyten, F. P.; Roberts, A. B.; Roche, N. S.; Reddi, A. H. Identification of multiple active growth factors in basement membrane matrigel suggests caution in interpretation of cellular activity related to extracellular matrix components. *Experimental Cell Research* **1992,** *202* (1), 1–8. DOI: 10.1016/0014-4827(92)90397-Q.

Walter, P.; Ron, D. The unfolded protein response: from stress pathway to homeostatic regulation. *Science (New York, N.Y.)* **2011,** *334* (6059), 1081–1086. DOI: 10.1126/science.1209038.

Wang, Y.; Niu, X. L.; Qu, Y.; Wu, J.; Zhu, Y. Q.; Sun, W. J.; Li, L. Z. Autocrine production of interleukin-6 confers cisplatin and paclitaxel resistance in ovarian cancer cells. *Cancer letters* **2010,** *295* (1), 110–123. DOI: 10.1016/j.canlet.2010.02.019.

Warburg, O. Versuche am überlebenden Karzinomgewebe. *Biochemische Zeitung* [Online] **1923,** No. 142, 317–333.

Warburg, O.; Negelein, E.; Posener, K. Versuche an Überlebendem Carcinomgewebe. *Klin Wochenschr* **1924,** *3* (24), 1062–1064. DOI: 10.1007/BF01736087.

Weissinger, D.; Tagscherer, K. E.; Macher-Göppinger, S.; Haferkamp, A.; Wagener, N.; Roth, W. The soluble Decoy Receptor 3 is regulated by a PI3K-dependent mechanism and promotes migration and invasion in renal cell carcinoma. *Molecular cancer* **2013,** *12* (1), 120. DOI: 10.1186/1476-4598-12-120.

Weisz, L.; Oren, M.; Rotter, V. Transcription regulation by mutant p53. *Oncogene* **2007,** *26* (15), 2202–2211. DOI: 10.1038/sj.onc.1210294.

Wilding, J. L.; Bodmer, W. F. Cancer cell lines for drug discovery and development. *Cancer Res* **2014,** *74* (9), 2377–2384. DOI: 10.1158/0008-5472.can-13-2971.

Wolfgang, C. D.; Chen, B. P.; Martindale, J. L.; Holbrook, N. J.; Hai, T. gadd153/Chop10, a potential target gene of the transcriptional repressor ATF3. *Molecular and cellular biology* **1997,** *17* (11), 6700–6707. DOI: 10.1128/MCB.17.11.6700.

Wooster, R.; Bignell, G.; Lancaster, J.; Swift, S.; Seal, S.; Mangion, J.; Collins, N.; Gregory, S.; Gumbs, C.; Micklem, G. Identification of the breast cancer susceptibility gene BRCA2. *Nature* **1995,** *378* (6559), 789–792. DOI: 10.1038/378789a0.

Wright, W. D.; Shah, S. S.; Heyer, W.-D. Homologous recombination and the repair of DNA double-strand breaks. *The Journal of biological chemistry* **2018,** *293* (27), 10524–10535. DOI: 10.1074/jbc.TM118.000372.

Wu, X.; Peters-Hall, J. R.; Bose, S.; Peña, M. T.; Rose, M. C. Human bronchial epithelial cells differentiate to 3D glandular acini on basement membrane matrix. *American journal of respiratory cell and molecular biology* **2011,** *44* (6), 914–921. DOI: 10.1165/rcmb.2009-0329OC.

Wu, X.; Zhao, J.; Ruan, Y.; Sun, L.; Xu, C.; Jiang, H. Sialyltransferase ST3GAL1 promotes cell migration, invasion, and TGF-β1-induced EMT and confers paclitaxel resistance in ovarian cancer. *Cell death & disease* **2018,** *9* (11), 1102. DOI: 10.1038/s41419-018-1101-0.

Xu, Y.; Miao, C.; Jin, C.; Qiu, C.; Li, Y.; Sun, X.; Gao, M.; Lu, N.; Kong, B. SUSD2 promotes cancer metastasis and confers cisplatin resistance in high grade serous ovarian cancer. *Experimental Cell Research* **2018,** *363* (2), 160–170. DOI: 10.1016/j.yexcr.2017.12.029.

Yuki, K.; Cheng, N.; Nakano, M.; Kuo, C. J. Organoid Models of Tumor Immunology. *Trends in immunology* **2020,** *41* (8), 652–664. DOI: 10.1016/j.it.2020.06.010.

Zhang, K.; Erkan, E. P.; Dai, J.; Andersson, N.; Kaipio, K.; Lamminen, T.; Mansuri, N.; Huhtinen, K.; Carpén, O.; Hynninen, J.; Hietanen, S.; Oikkonen, J.; Häkkinen, A.; Hautaniemi, S.; Vähärautio, A. *Analysis of single-cell RNA-seq data from ovarian cancer samples before and after chemotherapy links stress-related transcriptional profile with chemotherapy resistance* 6, 2020.

Zhang, X.; Yuan, X.; Zhu, W.; Qian, H.; Xu, W. SALL4: an emerging cancer biomarker and target. *Cancer letters* **2015,** *357* (1), 55–62. DOI: 10.1016/j.canlet.2014.11.037.

Zhao, Y.; Yao, R.; Ouyang, L.; Ding, H.; Zhang, T.; Zhang, K.; Cheng, S.; Sun, W. Three-dimensional printing of Hela cells for cervical tumor model in vitro. *Biofabrication* **2014,** *6* (3), 35001. DOI: 10.1088/1758-5082/6/3/035001.

Zimmermann, M.; Lampe, J.; Lange, S.; Smirnow, I.; Königsrainer, A.; Hann-von-Weyhern, C.; Fend, F.; Gregor, M.; Bitzer, M.; Lauer, U. M. Improved reproducibility in preparing precision-cut liver tissue slices. *Cytotechnology* **2009,** *61* (3), 145–152. DOI: 10.1007/s10616-009-9246-4.

Zinszner, H.; Kuroda, M.; Wang, X.; Batchvarova, N.; Lightfoot, R. T.; Remotti, H.; Stevens, J. L.; Ron, D. CHOP is implicated in programmed cell death in response to impaired function of the endoplasmic reticulum. *Genes & development* **1998,** *12* (7), 982–995. DOI: 10.1101/gad.12.7.982.

9 Acknowledgements

I am truly grateful to those who were involved in the process of my doctoral thesis and made this thesis possible in the past years.

First and foremost, I would like to express my deepest gratitude to Prof. Dr. Walter E. Aulitzky for the opportunity to perform my PhD study under his supervision. Without your support and advice in numerous discussions, this dissertation would not have been possible, and you have contributed significantly to the success of this work.

I would like to specially thank Prof. Dr. Roland Kontermann for his willingness to take over the supervision of the dissertation on the part of the university and for his support especially in times when it was most needed.

I would also like to thank Prof. Dr. Hans-Georg Kopp for his support and his scientific contributions to my work.

Many thanks to Prof. Dr. Matthias Schwab for the opportunity to conduct this work at the Dr. Margarete Fischer-Bosch Institute of Clinical Pharmacology and University Tübingen and for his support in all matters.

Certainly, very special thanks are directed to Dr. Heiko van der Kuip. I cannot adequately express my appreciation for his time and patience as a mentor. I will always be grateful for his help, and I am very sorry that he cannot watch me graduating. I would have loved to share this moment with you.

My special thanks go to PD Dr. Frank Eßmann for his guidance during my PhD study. Thanks a lot for your helpful advices, the share of scientific knowledge, and nice memories of our working trips to Israel.

I do not think I can ever thank Dr. Meng Dong enough for her untiring willingness to help, discuss and her skills as a patient mentor. This dissertation would not have been possible without you. This makes it even more wonderful that a friendship has developed out of a professional relationship.

My warm and sincere thanks also go to Prof. Dr. Georg Sauer and Dr. Bernd Winkler from the Department of Gynecology and Obstetrics of the Robert Bosch Hospital for kindly supplying us with patient material of ovarian cancer. In this context, I also want to express my deepest appreciation to Dr. Svitlana Igel for her willingness to help us handling the documentation of patient data and ethical concerns. Special thanks go to Prof. Dr. Heike Walles for the kind support of the cell-free porcine intestine scaffold, which made it possible to test the scaffold in our system. My gratitude also goes to

Dr. Julia Schüler from Charles River and to Dr. Emma Davies from AstraZeneca for providing us with the CDXs.
Without the help of Dr. Nicole Janssen, the organoid culture in this work would not have been feasible. Many thanks for the scientific and emotional support during my PhD student time and beyond.
Many thanks to Tauno Metsalu, PhD, from the Institute of Computer Science (University of Tartu, Estonia) for his bioinformatics support in the analysis of tumor tissue slices. Also, I would like to thank Dr. Stefan Winter, Siarhei Kandabarau and Dr. Florian Büttner for their patience in answering all my questions and their help about bioinformatics.
I would like to express my appreciation to Prof. Dr. Moshe Oren and all members of his laboratory from the Weizmann Institute of Science in Rehovot, especially Dr. Yael Aylon, for a great time as a visiting student. Thank you so much for giving me the opportunity to learn new techniques, benefit from your scientific knowledge and enjoy science!
Many thanks also to the whole AG Aulitzky and Kopp (and alumni): Markus Kleih, Kerstin Willecke, Sandra Weller, Benjamin Schäfer, Tobias Beigl, Damaris Zipperer, Lenke Schröder, Simon Heine and Andrea Gaißler. Without our coffee rounds, mutual support and constructive discussions, the time would never have been as enjoyable as it has been!
Furthermore, I would like to thank all colleagues at the IKP for the pleasant working atmosphere and their constant willingness to help.
A lot of thanks are addressed to my friends at the IKP and outside of it. You have supported me; you have gone through good and bad moods with me and have built me up repeatedly. I am infinitely grateful for this. In this context, I would like to specifically thank Martina, Vroni, Caro, Nadja, Nicole, Doro and Vero and all the others that are not named.
Last but not least, I owe my deepest thanks to my family. The never-ending support, motivating words and faith in me has inspired me. I thank you from the bottom of my heart and I am very glad that I have you by my side. As well I cannot put my appreciation for the support and help, I received from Chris into words. Thank you for always being there for me.

10 Conference contributions and publications

10.1 Conference contributions

Date	Conference name	Contribution
Jun/2020	American Association for Cancer Research (AACR) - Annual Meeting 2020 *Virtual Meeting*	Poster presentation
Feb/2020	Personalized and Precision Medicine International Conference 2020	Selected abstract presentation
Nov/2019	The European Association for Cancer Research (EACR) Conferences - Goodbye Flat Biology	Poster presentation
Mar-Apr/2019	AACR - Annual Meeting 2019	Poster presentation
Sept/2018	EACR Conferences - Goodbye Flat Biology	Poster presentation
Apr/2018	AACR - Annual Meeting 2018	Poster presentation

10.2 Publications

Year	Publication
2020	Miguel Fuentes-Chandía, Andreas Vierling, Melanie Kappelman-Fenzl, Lucas Höne, Gaelle Letort, Mahshid Monavari, Özlem Ertekin, Philipp Tripal, Meng Dong, **Kathrin Böpple**, Aldo Boccaccini, Anja Bosserhoff & Aldo Leal-Egaña. *Confinement and mechanical stress may lead to the expression of malignant responses in cancer cells.* Advanced Healthcare Materials (2020) → submitted
2019	Markus Kleih, **Kathrin Böpple**, Meng Dong, Andrea Gaißler, Simon Heine, Monilola A. Olayioye, Walter E. Aulitzky & Frank Essmann. *Direct Impact of Cisplatin on Mitochondria Induces ROS Production That Dictates Cell Fate of Ovarian Cancer Cells.* Cell Death & Disease
2018	Simon Heine, Markus Kleih, Neus Giménez, **Kathrin Böpple**, German Ott, Dolors Colomer, Walter E. Aulitzky, Heiko van der Kuip & Elisabeth

	Silkenstedt. *Cyclin D1-CDK4 Activity Drives Sensitivity to Bortezomib in Mantle Cell Lymphoma by Blocking Autophagy-mediated Proteolysis of NOXA*. Journal of Hematology & Oncology
2017	Annina Huser, Melanie Eschment, Nazli Güllü, Katharina A. N. Collins, **Kathrin Böpple**, et al. *Anatomy and Behavioral Function of Serotonin Receptors in Drosophila melanogaster Larvae*. PLoS ONE
2016	Annekathrin Widmann, Marc Artinger, Lukas Biesinger, **Kathrin Boepple**, et al. *Genetic Dissection of Aversive Associative Olfactory Learning and Memory in Drosophila Larvae.* PLoS Genetics

11 Curriculum vitae

The CV has been removed due to data protection.

12 Appendix

A1: List of transcripts analyzed in high through-put qPCR and their functional classification (Davies et al., 2015).

Gene name	Assay (applied)	Functional gene grouping
ABCB1	Hs00184500_m1	drug transporter
ACTB	Hs03023943_g1	housekeeping gene
AIFM2	Hs01097299_m1	apoptosis
APAF1	Hs00559440_m1	apoptosis
ATF2	Hs01099617_m1	UPR/ER stress
ATF3	Hs00231069_m1	UPR/ER stress
ATF4	Hs00909569_g1	UPR/ER stress
ATF6	Hs00232586_m1	UPR/ER stress
ATG12	Hs01047860_g1	necrosis/autophagy
ATG5	Hs01555465_m1	necrosis/autophagy
ATG7	Hs00197348_m1	necrosis/autophagy
ATM	Hs00175892_m1	DNA damage and repair
ATR	Hs00992132_m1	DNA damage and repair
BAK1	Hs00832876_g1	apoptosis
BCL2	Hs01048932_g1	apoptosis
BCL2A1	Hs03405589_m1	apoptosis
BCL2L1	Hs01067345_g1	apoptosis
BCL2L11	Hs01083836_m1	apoptosis
BCL2L13	Hs00209787_m1	apoptosis
BCL2L14	Hs00373302_m1	apoptosis
BECN1	Hs01011594_g1	necrosis/autophagy
BID	Hs00609632_m1	apoptosis
BIK	Hs00154189_m1	apoptosis
BIRC2	Hs01112284_m1	apoptosis
BLM	Hs01119886_g1	DNA damage and repair
BNIP3	Hs00969289_m1	apoptosis
BOK	Hs00261296_m1	apoptosis
BRCA1	Hs01556185_m1	DNA damage and repair
BTG2	Hs00198887_m1	proliferation / cell cycle regulation
CCNA2	Hs00153138_m1	proliferation / cell cycle regulation
CCNB1	Hs01030097_m1	proliferation / cell cycle regulation
CCNG1	Hs00171112_m1	proliferation / cell cycle regulation
CCNK	Hs01083210_m1	proliferation / cell cycle regulation
CDC25C	Hs00156411_m1	proliferation / cell cycle regulation
CDK1	Hs00364293_m1	proliferation / cell cycle regulation

CDKN1A	Hs99999142_m1	proliferation / cell cycle regulation
CDKN1B	Hs00153277_m1	proliferation / cell cycle regulation
CFLAR	Hs01116281_m1	apoptosis
CHEK1	Hs00967510_g1	proliferation / cell cycle regulation
DDB2	Hs03044953_m1	DNA damage and repair
DNAJC3	Hs00534489_m1	UPR/ER stress
EDEM1	Hs00976004_m1	UPR/ER stress
EDEM2	Hs01076556_m1	UPR/ER stress
EGFR	Hs01076078_m1	proliferation / cell cycle regulation
EGR1	Hs00152928_m1	p38/JNK
EPHB1	Hs01057855_m1	UPR/ER stress
ERCC1	Hs01012156_m1	DNA damage and repair
ETS1	Hs00901423_m1	p38/JNK
FANCA	Hs01116661_m1	DNA damage and repair
FANCD2	Hs00395700_m1	DNA damage and repair
FANCG	Hs00184947_m1	DNA damage and repair
FANCM	Hs00913609_m1	DNA damage and repair
FAS	Hs00531110_m1	apoptosis
FASLG	Hs00181226_g1	apoptosis
FEN1	Hs01099393_g1	DNA damage and repair
FOS	Hs01119266_g1	p38/JNK
FOSL1	Hs04187685_m1	p38/JNK
FTH1	Hs01000476_g1	ROS
GRB2	Hs00257910_s1	necrosis/autophagy
GSTP1	Hs00168310_m1	ROS
HERPUD1	Hs01124265_m1	UPR/ER stress
HGF	Hs00900067_m1	proliferation / cell cycle regulation
HIF1A	Hs00936368_m1	ROS
HMOX1	Hs01110250_m1	ROS
HRK	Hs01388767_g1	apoptosis
HSP90AA1	Hs00743767_sH	UPR/ER stress
HSPA5	Hs00946084_g1	UPR/ER stress
IER3	Hs04187506_g1	apoptosis
IGFBP3	Hs00426287_m1	proliferation / cell cycle regulation
JUN	Hs00277190_s1	p38/JNK
JUND	Hs02330233_u1	p38/JNK
KLF6	Hs00296661_s1	p38/JNK
MAFF	Hs00202412_m1	p38/JNK
MAPK8	Hs01548508_m1	p38/JNK
MCL1	Hs00172036_m1	apoptosis

MDM2	Hs00234753_m1	proliferation / cell cycle regulation
MDM4	Hs00159092_m1	proliferation / cell cycle regulation
MET	Hs01565584_m1	proliferation / cell cycle regulation
MLH1	Hs00179866_m1	DNA damage and repair
MSH2	Hs00954125_m1	DNA damage and repair
MYC	Hs00905030_m1	proliferation / cell cycle regulation
NLRP2	Hs01546932_m1	DNA damage and repair
NOS2A	Hs01075523_m1	apoptosis
NQO1	Hs00168547_m1	ROS
OAS1	Hs00242943_m1	p38/JNK
P2RY13	Hs01090437_g1	UPR/ER stress
PARP1	Hs00911377_g1	necrosis/autophagy
PCNA	Hs00696862_m1	proliferation / cell cycle regulation
PGK1	Hs00943178_g1	housekeeping gene
PHLDA1	Hs00378285_g1	p38/JNK
PIDD	Hs01076855_g1	apoptosis
PLA2G6	Hs00895666_m1	UPR/ER stress
PMAIP1	Hs00560402_m1	apoptosis
POL2RB	Hs00265358_m1	housekeeping gene
PPP1R15A	Hs00921550_g1	UPR/ER stress
PRDX1	Hs03044568_g1	ROS
PVR	Hs00197846_m1	necrosis/autophagy
RAD51	Hs00947964_m1	DNA damage and repair
RB1	Hs01078075_m1	proliferation / cell cycle regulation
RIPK1	Hs00169407_m1	necrosis/autophagy
RPA1	Hs01556877_m1	proliferation / cell cycle regulation
RPLP0	Hs02992885_s1	housekeeping gene
RRM2B	Hs00968427_m1	DNA damage and repair
SENP2	Hs00989703_m1	apoptosis
SESN1	Hs00902782_m1	DNA damage and repair
SFN	Hs00968567_s1	proliferation / cell cycle regulation
SHISA5	Hs00429977_m1	apoptosis
SIRT1	Hs01009000_m1	DNA damage and repair
SOD1	Hs00916176_m1	ROS
SOD2	Hs04260076_g1	ROS
SQSTM1	Hs01061917_g1	ROS
SUMO1	Hs00830844_g1	DNA damage and repair
TAp73	Hs01056228_m1	proliferation / cell cycle regulation
TBP	Hs00427621_m1	housekeeping gene

TERT	Hs00972656_m1	proliferation / cell cycle regulation
TNFRSF10A	Hs00269492_m1	apoptosis
TNFRSF10B	Hs00366278_m1	apoptosis
TNFRSF10C	Hs00182570_m1	apoptosis
TNFRSF10D	Hs04187502_m1	apoptosis
TP53	Hs99999147_m1	proliferation / cell cycle regulation
TP53AIP1	Hs00986095_m1	apoptosis
TP53I3	Hs00936520_m1	DNA damage and repair
TP53INP1	Hs00264502_m1	DNA damage and repair
TP63	Hs00978342_m1	proliferation / cell cycle regulation
TP73	Hs01056230_m1	proliferation / cell cycle regulation
TRAF1	Hs01090167_g1	apoptosis
TRAF2	Hs00184192_m1	apoptosis
TRPM3	Hs01558432_m1	p38/JNK
TXN	Hs00828652_m1	ROS
XBP1	Hs00231936_m1	UPR/ER stress
XBP1(U)	Hs02856596_m1	UPR/ER stress
XIAP	Hs00745222_s1	apoptosis
XPA	Hs00166045_m1	DNA damage and repair
XPC	Hs01104213_m1	DNA damage and repair
XRCC1	Hs00959834_m1	DNA damage and repair
XRCC3	Hs00193725_m1	DNA damage and repair
ZFP36	Hs00185658_m1	p38/JNK
ZMAT3	Hs00536976_m1	apoptosis

A2: List of 33 differentially expressed genes (DEG) of bioinformatical analyses naïve versus DTP (FC>2, p_{adj}<0.05).

Gene name	**log2FoldChange**	**p_{adj}**
EMILIN3	-5.47142	2.02E-12
ARHGAP6	-5.24081	0.012957
PKD1L1	-4.78962	2.02E-12
CPA4	-4.35602	0.028009
RIMBP3	-4.16563	0.000286
SALL4	-2.85681	2.4E-05
ZNF648	-2.55788	0.011146
TGM5	-2.43572	0.000481
CRISPLD1	-2.2573	0.006075
DTX1	-2.02333	0.001767
HGD	-1.84828	0.00574

CDKN1A	-1.77351	0.029461
ME1	-1.74682	0.008228
SLC16A7	-1.66131	0.002784
TMEM18	1.047817	0.002937
GTF2IRD1	1.076731	0.00613
KIAA1143	1.093062	3.65E-05
ZNF510	1.104497	0.002829
CUX1	1.14721	0.029461
BCL7B	1.16749	0.000682
MROH6	1.283186	0.026763
GTF2IRD2B	1.335591	0.006748
ISYNA1	1.807485	0.012382
KLHL35	1.844685	0.026362
STOX1	1.88497	0.017689
GSTO2	2.000893	0.022705
CIART	2.045316	0.023415
LOC730102	2.708514	0.012246
RRAD	2.75764	0.025621
HCG11	3.231459	4.5E-06
MMP14	3.852188	0.000162
IRAK3	4.011849	0.006292
XAGE2	4.435588	0.039489

A3: List of 55 differentially expressed genes (DEG) of bioinformatical analyses naïve versus DTP (FC>1.5, p_{adj}<0.05).

Gene name	**log2FoldChange**	**p_{adj}**
EMILIN3	-5.47142476	2.02E-12
ARHGAP6	-5.240814604	0.012957113
PKD1L1	-4.789618546	2.02E-12
CPA4	-4.356016496	0.028009129
RIMBP3	-4.165631279	2.86E-04
SALL4	-2.85681472	2.40E-05
ZNF648	-2.557883343	0.011145816
TGM5	-2.435718059	4.81E-04
CRISPLD1	-2.257298475	0.006075109
DTX1	-2.02333065	0.001767426

HGD	-1.848279022	0.005739596
CDKN1A	-1.773507048	0.029461066
ME1	-1.746824879	0.008228171
SLC16A7	-1.661310171	0.002783723
SVIL-AS1	-0.964553621	0.003698371
CUL2	-0.88952765	0.036194694
ARPC5	-0.673861112	0.026362135
ACP1	0.593324849	0.043507832
LSM8	0.595527541	4.89E-05
CPSF4	0.602795769	0.003555484
ZKSCAN1	0.61250155	0.036194694
ZSCAN25	0.643794935	0.00880565
GTF2I	0.66660305	0.028571372
ZNF655	0.696639966	0.04928602
RNASEH1-AS1	0.712637061	0.011869102
LRCH4	0.726207834	0.001767426
LMTK2	0.794529359	4.25E-04
POM121	0.850971014	4.36E-05
WBSCR16	0.854936654	0.013929394
NSUN5	0.861344807	0.038295171
STYXL1	0.883530649	0.036194694
POM121C	0.914968075	6.82E-06
ZNF382	0.932855577	0.002936535
TYW1B	0.956877377	0.002783723
ZNF181	0.986459216	0.029461066
SH3YL1	0.99379597	0.003698371
TMEM18	1.047816631	0.002936535
GTF2IRD1	1.076730977	0.006129845
KIAA1143	1.093062236	3.65E-05
ZNF510	1.104497444	0.002829031
CUX1	1.147210417	0.029461066
BCL7B	1.167489901	6.82E-04
MROH6	1.283186451	0.026763046
GTF2IRD2B	1.335591311	0.006747641
ISYNA1	1.807485447	0.01238162
KLHL35	1.844685137	0.026362135

STOX1	1.884970444	0.017689298
GSTO2	2.000892902	0.022705298
CIART	2.045315755	0.023414852
LOC730102	2.708513587	0.012245723
RRAD	2.757639834	0.025621479
HCG11	3.231458664	4.50E-06
MMP14	3.852188179	1.62E-04
IRAK3	4.011848855	0.006292492
XAGE2	4.43558783	0.0394894

A4: List of 334 DEG of bioinformatical analyses naControl versus sDTP (FC>1.5, p_{adj}<0.05).

Gene name	**log2FoldChange**	**p_{adj}**
ITIH5	-21.72336596	3.32E-09
AFF2	-21.6730702	4.27E-09
PTPRD	-12.33664753	4.32E-07
MME	-11.83084738	6.28E-18
SMOC1	-11.10919789	2.46E-04
ZNF423	-10.53678137	0.020620512
CHST1	-10.5101711	1.13E-13
JAKMIP2	-10.09797671	0.011392653
CADM1	-9.638692056	3.03E-06
C17orf77	-9.521858071	4.00E-13
ZNF385D	-9.425269503	1.50E-05
CACNA2D1	-9.146292741	4.27E-09
HLA-DRB1	-8.788770294	8.81E-04
LINC01467	-8.713878848	1.36E-06
GAS7	-8.355727271	3.65E-16
APCDD1	-8.331355099	7.97E-08
LSAMP	-8.281648927	0.013084272
LINC01553	-8.211775248	4.88E-05
ADGRD1	-8.163757871	0.013338142
PLCL2	-8.160684344	1.97E-11
TRPC7	-8.129717099	0.00264306
SATB1	-8.032547799	2.32E-10
ZNF737	-8.011692578	2.88E-04
SPIN2A	-7.977648673	0.002857436

EVC	-7.9737668	0.002407568
BACE2	-7.931315673	3.73E-05
LOC101927136	-7.930069595	0.020531133
EBF1	-7.865893321	1.53E-04
HLA-DQB1	-7.831231366	0.044412085
S100A9	-7.723052251	0.018186249
SLC5A1	-7.653229645	3.01E-04
FFAR4	-7.485489835	1.23E-48
PDE1B	-7.426764937	0.00545473
PTPRD-AS1	-7.302661856	0.02612516
GABRQ	-7.297193256	0.025148629
RBP4	-7.258311124	4.50E-27
S100A8	-7.110765683	0.030805734
GRIK2	-7.090887084	0.010022801
PHKA1	-6.989503546	1.73E-04
HLA-DRA	-6.978714621	1.61E-06
CDYL2	-6.972961786	0.045076823
CASP14	-6.912142297	0.035066806
EDA	-6.735380231	2.06E-08
CFAP46	-6.674232647	5.60E-05
CALB2	-6.634069633	3.01E-09
ST6GALNAC3	-6.630195434	1.12E-04
GPC3	-6.608169392	0.001132772
HOXA10	-6.423627711	3.69E-06
PCDHAC2	-6.388341743	4.85E-04
SORCS1	-6.341411534	0.01709604
CALCB	-6.314106736	9.68E-04
HS6ST2	-6.265616396	2.05E-11
GSC	-6.127292851	0.00180693
HLA-DPB1	-5.996907228	0.009838945
VSTM4	-5.791057005	0.00767445
EMILIN3	-5.714151347	1.84E-08
LGALS17A	-5.707764367	3.11E-05
OSTCP1	-5.652694744	0.009295784
SLC24A3	-5.576538037	0.00883444
RARB	-5.457842982	0.006320136

SPP1	-5.40654099	0.029756635
PRODH	-5.388941768	0.00105055
LRRC4B	-5.360406432	0.038092837
ST3GAL1	-5.342499343	1.87E-08
SFRP2	-5.260498361	0.003694207
GPR37	-5.203988118	0.010339115
GHR	-5.104249487	0.043979592
KRT77	-5.02563947	0.002475777
ABCG1	-5.012941134	1.73E-05
HLA-DPA1	-5.003169213	0.027042159
BEND5	-4.978673636	2.02E-07
HOXA13	-4.96078697	0.001127618
G0S2	-4.955243172	0.006571311
NEURL1	-4.918526401	0.016035135
PPP1R1A	-4.898784248	7.32E-04
ZNF750	-4.824403457	0.006912657
SNED1	-4.695539333	0.026800294
MYEOV	-4.684341549	3.73E-05
KRT4	-4.606546966	3.11E-07
DGCR6	-4.606036912	0.010287284
ADGRB3	-4.439685879	0.043046494
KCNK1	-4.324253015	6.90E-05
DOC2B	-4.303719137	6.68E-04
MAB21L1	-4.267213321	0.02710914
WDFY4	-4.248623681	0.00180693
CP	-4.163752411	1.03E-04
ZNF711	-4.158752499	0.010287284
CH25H	-4.137891829	0.012389571
PTGER3	-4.100152661	0.036445446
MAP6	-3.999369375	0.003440944
PTPRM	-3.948830919	4.26E-12
CEND1	-3.938087282	0.018007757
NKD1	-3.909687504	0.011185307
BEX5	-3.882127971	0.001455993
DCHS2	-3.87667076	1.05E-04
PKD1L1	-3.822724068	2.66E-05

C10orf128	-3.779628089	2.62E-08
FABP5	-3.723808591	0.007284489
DHRS9	-3.692961183	0.001343317
HMCN2	-3.649351279	1.73E-05
LGALS14	-3.594172441	0.002258302
ST3GAL6-AS1	-3.585485678	0.032188657
UBXN10	-3.571477238	0.031569532
ALDOC	-3.549952872	3.11E-07
OPLAH	-3.524565716	1.14E-05
HSPA12A	-3.523659892	5.63E-04
EGR3	-3.459105865	4.36E-09
IRX5	-3.408308354	0.020744862
RGS11	-3.39765297	1.03E-04
HTR6	-3.340082939	2.74E-05
TEKT4	-3.315859133	0.018748007
LINC00659	-3.284546189	0.02448492
PAK3	-3.204210753	0.045444059
TNS4	-3.201020551	8.99E-04
CFAP74	-3.170620285	0.003385617
CDH23	-3.150352495	0.029834711
PDE4B	-3.146968473	3.11E-07
AKR1C2	-3.132816399	0.001013141
FZD8	-3.086983408	0.044346831
CFAP45	-3.018882791	0.005951536
SSX8	-3.011050366	0.031170404
SLFN11	-2.994760728	0.043046494
GNAZ	-2.971984548	7.14E-04
CAMK2N1	-2.962816525	8.64E-04
SLC2A13	-2.959629979	6.76E-08
LOC102723854	-2.958093794	0.026792131
LRAT	-2.930994856	0.036445446
AKR1C1	-2.926551189	0.002856719
SEMA5B	-2.884619482	1.62E-04
C15orf59	-2.878403787	8.81E-04
THSD7B	-2.851018417	8.21E-10
MT1F	-2.815082674	0.024043411

STAC2	-2.793141051	3.09E-04
SYT12	-2.785410024	0.021141453
LAMA2	-2.743906807	3.29E-05
PTN	-2.736879581	0.02505006
ADCY1	-2.657239104	0.012882144
KRT23	-2.634379594	0.009042475
LOC105375734	-2.627031741	0.010080909
KLF9	-2.606654668	2.58E-04
MID2	-2.589351511	0.017113329
SLC2A9	-2.574424154	0.009295784
LINC00488	-2.565524105	0.003797571
GRM1	-2.532419886	0.015787028
DNAH11	-2.525012542	0.035363075
AKR1C3	-2.503431018	1.25E-05
OSBP2	-2.492089013	0.016576831
RNF223	-2.481956935	0.035363075
CDKN1A	-2.472154732	2.02E-07
ST3GAL6	-2.469234603	0.022638967
TGM5	-2.407198985	0.00767445
KRT86	-2.404937646	0.016638066
PTPRU	-2.375075569	1.24E-08
COL23A1	-2.365744688	2.92E-11
IL4R	-2.325727733	0.010610307
SALL4	-2.323055481	8.81E-04
DUSP5	-2.319844575	1.06E-06
EML1	-2.287353454	0.002412157
SLC16A2	-2.270798045	0.043450381
ZNF438	-2.268168632	5.59E-04
ANKRD45	-2.255727059	3.96E-11
HES2	-2.247519168	0.027473695
CYP2R1	-2.216635117	6.12E-09
TNFRSF1B	-2.17818921	0.022638967
CIITA	-2.136524037	0.018086058
PRKG1	-2.134501826	0.007284489
TPPP	-2.108775251	0.002287785
IL6	-2.102996051	0.035363075

HGD	-2.057319026	0.02415684
CEACAM1	-2.050280797	0.039060981
MT1X	-2.049123914	0.001880987
SNPH	-2.033678945	0.006771132
ZIC2	-2.016985651	0.003771217
HECW2	-2.008803097	4.53E-04
CRNDE	-2.004067203	0.022638967
ATF3	-1.982328198	4.46E-04
SLC29A4	-1.980122406	0.02448492
SPTLC3	-1.968535875	1.03E-06
RASD1	-1.930331428	0.018608897
SUSD2	-1.912929031	0.004050315
TRIM29	-1.900424563	5.29E-11
GPR153	-1.871543228	0.029805793
ZNF585B	-1.856905128	0.006771132
SLC19A3	-1.826069719	0.001180905
KLHDC8A	-1.814970724	0.027254853
DLX2	-1.772210973	0.046077055
CCDC113	-1.752859959	0.00264306
TAOK3	-1.748084265	0.014456783
CHST15	-1.743251242	5.60E-09
ARHGAP40	-1.739803708	0.011527892
SLC6A11	-1.732955411	0.006320136
C3	-1.695440585	0.036437443
SPSB1	-1.68121084	0.007400727
PANX2	-1.676494898	0.00104214
RAB36	-1.67011757	2.07E-05
DNAH7	-1.549141873	0.019250605
PER2	-1.54379521	0.022622881
ME1	-1.531217339	0.032248608
RAB39B	-1.524974477	0.016398124
PCSK1N	-1.472245264	0.017147805
SLC16A7	-1.467414044	0.016638066
HYDIN	-1.428805609	0.007159154
LRP1B	-1.41767482	0.036437443
FAM101B	-1.398797605	0.029763099

IL1R2	-1.341086503	0.043450381
SMARCD3	-1.326288211	0.04944575
DUSP18	-1.290164338	0.021799186
MAPK15	-1.266340964	0.002407568
STK17B	-1.257114525	8.64E-04
ELF3	-1.254178704	0.028364921
LINC00346	-1.237767536	8.12E-04
SEC24D	-1.233633588	5.75E-05
ITPR1	-1.2200278	0.028311443
INVS	-1.186638275	0.011559858
RXRA	-1.183381139	0.002112166
OXTR	-1.150061697	1.08E-04
MAPRE3	-1.147262721	0.001271399
SVIL-AS1	-1.142191039	0.015560057
DAAM1	-1.136259148	0.010610307
SNHG19	-1.129628658	0.021048927
CRISPLD1	-1.118243705	0.029329235
KCNAB2	-1.088533691	0.045872976
EPB41L4B	-1.068846729	0.028364921
CUL2	-1.034148981	0.048463153
CCNY	-1.025272312	0.01664581
ATG4B	-1.001558578	0.010022801
SLC2A12	-0.979847222	0.038630797
FHAD1	-0.976337833	0.024273852
BTG2	-0.972347329	0.003771217
FAM110A	-0.937856161	0.014016278
XRRA1	-0.879207504	0.018007757
ITM2C	-0.866940405	0.048657988
KLHL20	-0.858915676	0.043450381
MYEOV2	-0.844989555	0.023830882
CRELD2	-0.844280506	0.04014748
ZNF585A	-0.834975503	0.001150649
NDUFS1	-0.826997464	0.00104214
CARS2	-0.821131086	0.030329048
C2orf69	-0.813624192	0.030805734
HSPE1	-0.801493407	0.046122142

FAM213B	-0.791389404	0.009295784
SYAP1	-0.765223443	0.022638967
SCARA3	-0.679346923	0.031722843
RBBP7	-0.619495972	0.030805734
CERS6	0.600184862	0.047237936
FNBP1L	0.617089464	0.030122841
TLK1	0.667030033	0.041253226
KTN1	0.676413764	0.011527892
WDR6	0.70472028	0.048311347
USP10	0.724551545	0.012616266
ZCCHC14	0.729723858	0.04997499
DCP2	0.743278007	0.043450381
ZNF260	0.764350879	0.04366587
POM121	0.766542166	0.028616834
PMS1	0.780329308	0.024273852
OLFML2A	0.792313671	0.036445446
GTF2I	0.797915221	0.037938865
TRRAP	0.800792877	0.011753918
ANKRD11	0.844268887	0.002179571
LMTK2	0.858341319	0.010022801
BRPF3	0.862801358	0.010083041
POM121C	0.882387612	7.35E-04
GTF2IRD1	0.884128797	0.004621701
TFCP2	0.890356699	0.018608897
PDAP1	0.904655784	5.63E-04
ZNF197	0.904737448	0.013042606
STAT6	0.907567654	0.030805734
NASP	0.907655079	0.011527892
STK11	0.908261657	0.001013141
SMURF1	0.919094425	0.011138905
IQCH-AS1	0.93237411	0.048010862
ZNF382	1.007323918	0.040792035
C19orf25	1.030752372	0.019388059
GSE1	1.035462546	8.99E-04
NEMP2	1.051065384	3.62E-04
KIAA1143	1.067544351	4.98E-04

BAZ1B	1.067824477	0.016542111
HMHA1	1.108268409	0.032922366
AMOT	1.127075664	0.02451976
LOC100133091	1.145634048	0.049121108
CDCP1	1.155692228	3.06E-06
CIRBP	1.159515072	0.008817714
ATF5	1.184241468	0.022622881
CELSR3	1.194379247	0.010164144
CRIP1	1.203409909	1.05E-04
MYEF2	1.210848651	0.002835554
SHISA9	1.226736982	7.08E-04
UBASH3B	1.23180199	3.43E-04
CUX1	1.239773274	0.00729209
NELL2	1.261810987	0.03545136
RTKN2	1.266125642	0.003235188
LOC729970	1.2973984	0.047169168
ZNF181	1.313886898	0.022606123
DCDC2	1.316187128	0.005893193
FER1L4	1.425410133	0.027355865
DNAJC6	1.480202372	0.035742541
B3GALNT1	1.528071066	0.010080909
RCOR2	1.576395783	0.027473695
GUCY1A2	1.634678203	0.006876226
ZFP69	1.668331805	0.013711089
ST6GAL2	1.697749536	2.26E-04
FGF18	1.714953706	4.17E-04
PHLDB2	1.758345582	3.01E-05
MARVELD1	1.843729287	0.001180221
STAT5A	1.994645561	0.00105055
SEC16B	2.013741631	0.005677236
GSTO2	2.023390285	0.036445446
HCN2	2.033171584	6.25E-05
LOC730102	2.135426295	6.42E-07
CDK6	2.186630785	0.002049744
NAPRT	2.18667097	0.020531133
CA3	2.243188487	0.024196293

IL18R1	2.247752608	2.50E-05
RARRES2	2.317264414	0.002407568
OR2B6	2.641093438	0.049241875
DHX58	2.797139531	0.010610307
MMP24	2.843432599	0.036564673
PRKCG	2.887646517	7.32E-04
ITGB6	2.898060558	0.018186249
ZNF662	2.927558655	5.51E-04
CNGB1	2.980764688	6.12E-09
SHC3	3.218626963	0.011113077
LTF	3.367730821	0.028616834
ADAMTS5	3.384749632	0.031722843
ZNF763	3.439295798	0.01813936
AQP5	3.562090415	0.001591947
NUPR1	3.66478481	0.001095392
CST6	3.68677964	0.01759062
CACNG6	3.85047991	6.34E-04
MMP14	3.978482012	1.58E-20
HCG11	4.039164195	8.21E-10
KLK11	4.171400898	0.026800294
NXPH2	5.282812135	7.51E-05
CNTNAP4	8.854181072	3.57E-08